The University Of Sheffield.

An investigation of drug release from granules linking structure, process and performance

The University of Sheffield

Faculty of Engineering
Department of Chemical and Biological Engineering

By Faraj Shmam

Supervisors: Rachel Smith and Kate Pitt

A thesis submitted to The University of Sheffield in partial fulfilment of the requirement for the degree of Doctor of Philosophy

December 2022

Acknowledgments

I would like to thank my supervisors, Dr. Rachel Smith and Dr. Kate Pitt for all their kind guidance and support throughout my PhD project. I am really thankful of Rachel's assistance, directions for giving me the opportunity to travel with this research project. Thank you Kate for your invaluable advice on my doctoral development program and the feedback on my writing.

Thanks must also be extended to the outstanding members of the Particle Technology Group. Thank you for all of your input, your support, for providing a great working environment, and for all of the fun things we have done together.

Special thanks go to Bilal Ahmed for his support especially an organizing Strathclyde lab visit for doing experimental work. Special thanks go to Suruthi Gnanenthiran and Victoria Kitching for giving feedback on my thesis writing. I would also like to thank Mario Dorna for sharing his knowledge and time in the workshop at the University of Sheffield.

From the University of Sheffield, I would like to thank Dr. Daniel Markl for sharing his time and knowledge during Strathclyde lab experiments.

I am grateful to the ministry of education in Libya for providing the funding of my study.

Finally, but most essentially, my deepest gratitude also goes to my mother, wife, brothers, and sisters for their moral love and support.

Publications

Main publications

F. Shmam, K. Pitt, R. Smith “An investigation into drug release from granule linking to the granulation process, structure and granule performance” [In preparation].

F. Shmam, K. Pitt, B. Ahmed R. Smith “An investigation of individual granule swelling performance in relation to the granule structure” [In preparation].

Conference presentations

F. Shmam, K. Pitt, R. Smith “Effect of granulation process on the granule structure and drug release” presented at the InterPore online conference, Berlin, 2021.

F. Shmam “9th International Granulation Workshop (2019)” 8th - 10th July 2019, Sir Robert Hadfield Building, University of Sheffield.

Abstract

For any formulated product designed to perform a specific function, the impact of the intrinsic product microstructure displays a crucial role to the performance characteristics. In pharmaceutical manufacturing, this function relates to the amount of drug particles released, i.e., the dissolution profile, during patient administration. Wet granulation is the most popular choice for the production of oral solid dosage forms due to its capacity to accommodate a wide variety of active pharmaceutical ingredient (API) properties and to transform API into granules with superior properties. Whilst the majority of research has focussed on the performance of tablets, there remains a clear need to examine how the granule product performs across different length scales. Moreover, establishing and understanding the links between formulation and process parameters to the granule structure is limited.

High shear granulation is a key particle engineering technique which is used for particle size enlargement and was chosen for this work. The most influential and controlling parameters are liquid to solid mass ratio and granulation time, wherein these parameters were selected and varied with a fixed granule formulation to carefully study and examine the links between process conditions and the granule microstructure. The microstructure was quantified in terms of porosity by using several advanced characterization techniques and was found to be greatly dependent on the liquid to solid mass ratio. The results established that extended granulation times increased granule porosity which formed voids, and cracks were observed from 3D-imaging.

Granules of different microstructures were then subjected to dissolution rate studies. To establish the relationship between product to performance, a range of granule porosities were investigated on the amount of active ingredient released. An online sampling method was implemented to track the evolving concentration profiles where it was shown that lower porous granules displayed a slower dissolution rate compared to higher porous granules. The results indicated that depending on the porosity, the granule dissolution mechanism either followed a diffusion-controlled dissolution process or de-aggregation to finer particles to then dissolution of the active ingredient in solution.

For a deeper insight into the granule performance mechanisms, an individual granule study of varying porosity was then designed for mechanistic understanding of the disintegration mechanisms. By coupling imaging techniques with a purpose-built small scale device, granule

size and swelling behaviour were both quantified and tracked over time. More porous granules prompted faster swelling kinetics compared to denser granules which exhibited slower and longer swelling behaviour. The swelling phenomena was accompanied by additional mechanisms such as loosening of the particulate structure, crack and void formation. This work demonstrated the importance of disintegration and how the swelling kinetics influences the amount of active ingredient released from the microstructure during dissolution as well as presenting the link between process conditions, granule microstructure and granule dissolution.

Table of Contents

List of Figures

List of Tables

Nomenclature

Symbol	Definition	Quantity
C_s	Solute particles concentration	Mass*Volume^{-1}
D	Diffusion Coefficient	Length^2 * Time^{-1}
D_c	Pore Diameter	Length
H	Granule Liquid to Solid mass ratio	-
L/S	Liquid to Solid mass ratio	Mass * mass^{-1}
L	Liquid Penetration Length into capillary pore	Length
S	Liquid Saturation	Volume
S	Surface area of exposed solid	Area
h	Diffusion Layer Thickness	Length
t	Time	Time
η	Liquid Viscosity	Time*length-1
γ	Liquid Surface Tension	Force/Length
ε	Granule Porosity	Percent
θ	Contact Angle	Angle
ρ	Particle Density	Density

Abbreviations

Abbreviation	Definition
APAP	Acetaminophen
API	Active Pharmaceutical Ingredient
CCS	Croscarmellose Sodium
IUPAC	International Union of Pure and Applied Chemistry
LM	Lactose Monohydrate
MCC	Microcrystalline Cellulose
MRI	Magnetic Resonance Imaging
OCT	Optical Coherence Tomography
PEG	Polyethylene Glycol
PSD	Particle Size Distribution
PVP	Polyvinylpyrrolidone
SSG	Sodium Starch Glycolate
TSG	Twin Screw Granulator
XPVP	Crospovidone
HPMC	Hydroxy propyl methyl cellulose
XRCT	X-ray computed tomography
TPI	Terahertz pulse imaging
LCI	Low coherence interferometry
FFT	Fast Fourier transform

CHAPTER 1 - Introduction

1.1 Background

Granulation is an important process in the production of pharmaceutical dosage forms which involves particle enlargement by agglomeration, where coarse or fine particles are transformed into large granules (Litster, 2016a). Generally, granulation in the pharmaceutical industry starts by blending of the active pharmaceutical ingredient (API) along with other required ingredients (excipients) to reach a uniform distribution of whole powder ingredients. In general, the particle size range of the granules is around 0.2-4.0 mm. Granules are usually packed as a dosage form (capsules) or mixed with other excipients and tabletted (Swarbrick *et al.*, 2005).

Prior to tableting, granulation is used to enhance product handling, reduce dust, change the bulk density and improve dissolution or dispersion. The design of particles with an appropriate combination of formulation and process parameters that regulate product characteristics can help to achieve these desired properties (Knight, 2001). Granules can improve the content uniformity of the API within the dosage form. Also, they enhance compaction and compression properties and improve powder flow, which makes the production process much easier and consistent (Krishnaiah, 2010).

The most common granulation technique is wet granulation, in particular, high shear wet granulation. This has many advantages over the other methods such as producing dense granules suitable for tableting, uniform size distribution of granules and short granulation time (Hansuld and Briens, 2014). However, the high shear wet granulation process is complicated and multivariate and it is crucial to obtain desirable granule quality and tablet properties. In a high shear granulator, both granule size and structure can be changed by varying the granulation time and the amount of liquid binder added (Meng *et al.*, 2019). The relationships between formulation, process, and granule structure and performance require a deep understanding.

Wet massing time and liquid to solid mass ratio are the main process variables in high shear granulation. The wet massing time plays an important role in achieving a uniform distribution of binder into the powder bed. Obtaining granules with particular properties requires selection of an optimum massing time (Thapa *et al.*, 2019). Uneven distribution of liquid binder occurs

in case of inadequate massing time resulting in uncontrolled granule growth. Conversely, a longer massing time produces granules with lower porosity (Rahmanian *et al.*, 2011).

Liquid to solid mass ratio (L/S) is an essential variable in high shear granulation that affects the granule properties. Increasing the quantity of liquid binder increases particle agglomeration, which is enhanced by continuous addition of the liquid in the process (Chitu *et al.*, 2011). In designing a granulation process, the amount of liquid binder required is largely dependent on the formulation properties such as water uptake capacity and solubility. Insufficient amount of liquid binder produces porous and fragile granules with high quantity of fines, whereas a large quantity of liquid binder tends to produce dense, hard or over-wetted granules (Sakr *et al.*, 2012).

Granule structure has a strong influence on the dissolution rate of granules (Ansari and Stepanek, 2008). High density granules may reduce the disintegration and dissolution time of the granules (van den Ban and Goodwin, 2017). Designing granules with the desired dissolution rate requires a clear understanding of the granulation process and the influence of formulation variables on granule size and structure, which affect granule performance.

1.2 Research objectives

This thesis aims to create an understanding of the relationships between process conditions, granule structure and granule performance.

The main objectives are as follows:

- Develop an experimental understanding of the relationship between granulation process parameters and granule structure:
    1- The relationship between different liquid/solid mass ratios on granule porosity.
    2- The effect of granulation time on granule porosity.
    3- A study of the 3D internal structure of product granules.
    4- A systematic study of granule porosity measurement techniques, with comparisons between pycnometry, mercury porosimetry and micro-CT.

- Investigate the relationship between granule structure, granule dissolution and drug release profile.

- Conduct a micro-scale study of the swelling behaviour of single granules comprised of different microstructures, to develop understanding of the micro-scale kinetics of granule swelling and break up, using a purpose-built flow-cell equipped with optical coherence tomography (OCT) and microscopy.

1.3 Thesis outline

Chapter 2 is a literature review starting with an introduction to the general granulation process followed by literature on granule structure and dissolution.

Chapter 3 describes the properties of the raw materials used in this research and methods used for preparation of granules using different granulation parameters. Methods for the determination of granule structure and porosity distribution are described. In addition, the set up for the method of granule dissolution and single granule swelling is presented.

Chapter 4 describes the results obtained from high shear granulation experiments and discusses the effect of liquid to solid mass ratio and granulation time on the granule porosity and structure. The aim is to investigate the change in granule structure using different granulation parameters.

Chapter 5 describes the dynamic drug release performance of the dried granules with various porosities.

Chapter 6 describes the swelling behaviour of single granules during disintegration comprising of different microstructures by using a purpose-built flow-cell equipped with optical coherence tomography (OCT).

Chapter 7 gives conclusions of the effect of different parameters on granule internal microstructure and the performance of these different structure granules. Finally, recommendations for further research in this field are proposed.

An outline of this work is shown in Figure 1.1.

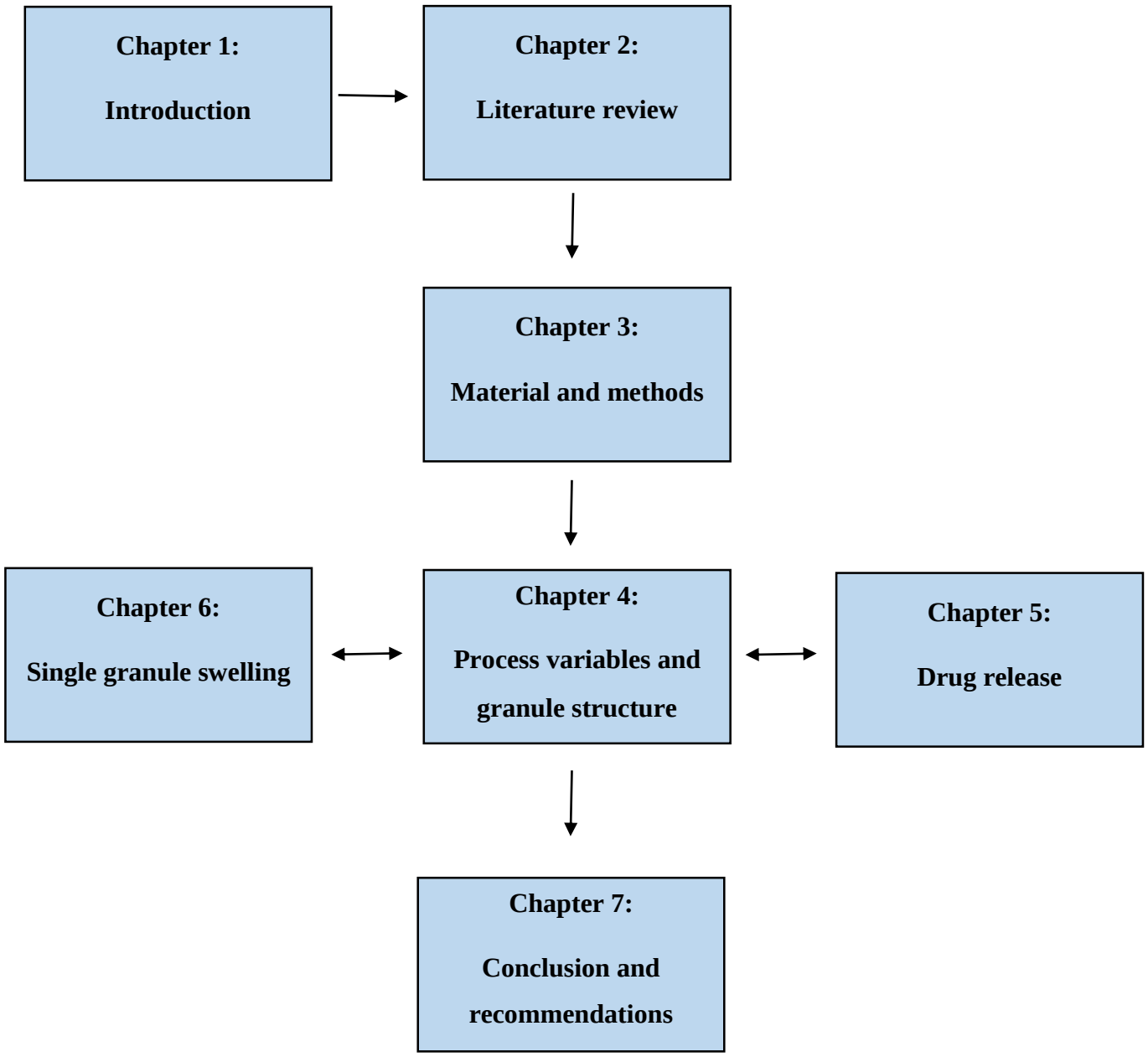

Figure 1.1: Flow chart of the work conducted in this thesis

CHAPTER 2 - Literature review

2.1 Introduction

Granulation is a method of particle size enlargement where coarse or fine particles are converted into large agglomerates called granules, and the original small particles are still distinguishable. This process can be carried out by either wet or dry granulation methods. In case of wet granulation, liquid binders are added onto powder particles and act as linking material (Iveson, *et al.*, 2001; Hapgood *et al*, 2003; Rhodes, 2008). This wet granulation process can be performed by high shear, fluidized bed, granulating in a tumbling drum (low shear), twin screw granulator or similar device (Hapgood *et al.*, 2003; Litster, 2016). Dry granulation can also be used to make granules by pressurization or by the cohesive properties of the particle itself (Kumar *et al*., 2014; Tu *et al*., 2013).

The advantages of granulation in industry can include improved flowability, porosity, and control over the granule dissolution rate. Granules are less likely to separate, therefore granulation in the pharmaceutical industry lowers dust formation (Ennis, 2005). It is essential to use granulation as an intermediary stage in the tableting process to ensure content consistency and particle distribution homogeneity (Chang *et al.*, 2014).

2.2 Steps of granulation

Granulation can be classified according to the method utilised, the binder physical form, and the equipment used in the granulation process. Granulation techniques are classified as dry granulation, wet granulation and melt granulation (Swarbrick *et al.*, 2005; Rhodes, 2008). The most widely used technique is wet granulation which will be covered in Section 2.2.1.

The dry granulation process is suitable for ingredients that are moisture and heat sensitive and involves compression of the powder mixture without the use of liquid and heat. There are two basic procedures, roller compaction and the slugging method. Roller compaction involves forcing a continuous powder stream into the gap between two counter-rotating rollers by using high pressure. The slugging method is more widely used, where powder is compressed to produce slugs (Swarbrick *et al.*, 2005). In both roller compaction and slugging techniques,

milling equipment is used to break the intermediate product to produce granules. The granules are then sieved to different size fractions.

The melt granulation process is used for moisture sensitive drug preparations. Low-melting binders are added to the powder mixture, which usually soften or melt at relatively low temperatures (50-80 °C). During the granulation process, the temperature is kept above the glass transition temperature of the binder and below the melting point of the active ingredient (Weatherley *et al.*, 2013).

2.2.1 Wet granulation

Wet granulation is a widely used technique in the pharmaceutical industry, where all excipients and API are premixed and then wet massed with binder liquid. Wet granulation provides some control of drug content uniformity as well as control of product compatibility and bulk density (Faure *et al.*, 2001). In wet granulation, a liquid binder is added to the powder in order to promote particle growth. Typically, as the particle size grows, the bulk density and flow rate increase, allowing the powder to withstand further tableting processes. In addition, granulation alters the granules' shape and porosity, hence influencing their dissolving behaviour (Oka *et al.*, 2015).

2.2.2 The principle mechanisms of wet granulation

Wet granulation is mechanistically a complicated process that often involves a variety of physical phenomena that compete with one another inside the granulator. Hence, it is increasingly common to see granulation as a mixture of three different rate process; wetting and nucleation, growth and consolidation, and breakage and attrition (Iveson *et al*., 2001), as illustrated in Figure 2.1.

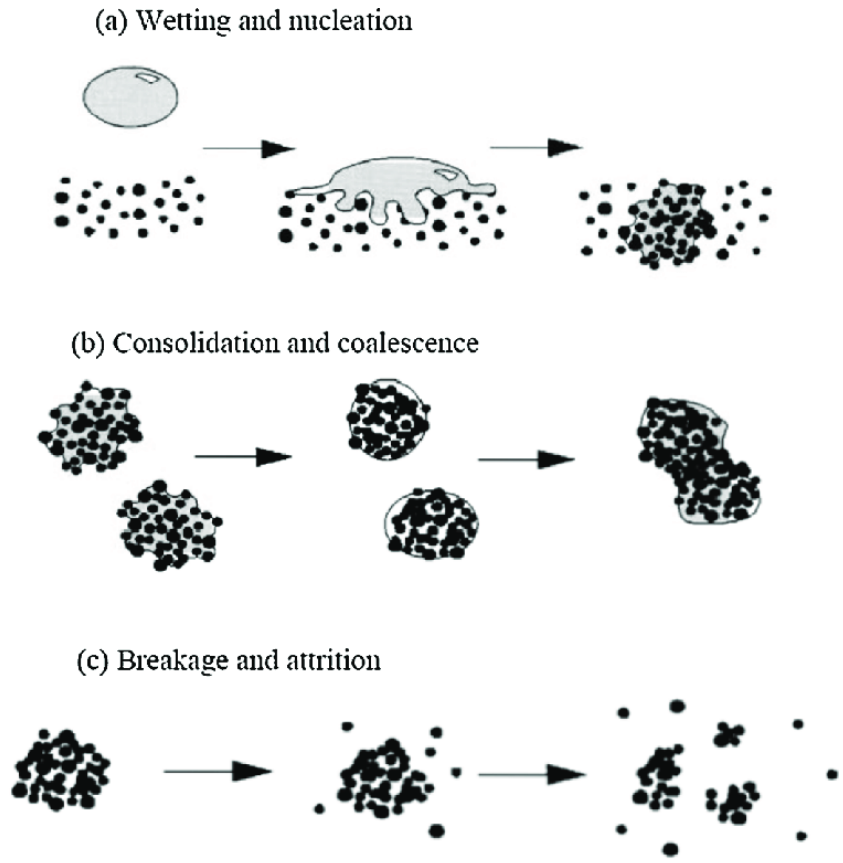

Figure 2.1: Schematic of the wet granulation mechanism (Iveson *et al*., 2001)

2.2.3 Wetting and Nucleation

In the wetting and nucleation step, a liquid binder is used to wet the dry powder bed. This liquid binder is distributed through the bed to create granule nuclei, and the initial aggregates are formed as a result of the powder's interaction with the spray droplets of binder. Because of the surface tension of the liquid binder, the individual particles are held together (Litster, 2016a). Depending on the relative size of the powder particles to the binder droplet, nucleation is formed by two main mechanisms: immersion or distribution (Figure 2.2). Nucleation proceeds by the immersion mechanism when the powder particles are smaller than the binder droplets. When the powder particles are larger than the binder droplets the distribution mechanism will take place by distribution of the binder droplets on a surface of the powder particles. The penetration of a single drop into a porous surface is governed by the Washburn equation, which considers the balance between capillary pressure driving the flow and viscous dissipation opposing it. Therefore, the time it takes for penetration depends on the wetting thermodynamics, which are influenced by the liquid's surface tension and the contact angle

between the solid and the liquid. Additionally, the wetting kinetics are greatly influenced by the viscosity of the liquid and the effective pore size of the powder bed (Iveson *et al.*, 2001; Liu *et al.*, 2021). Reducing surface tension has the effect of decreasing the force that holds particles together, known as capillary pressure, thereby reducing the friction between particles. This allows for easier rearrangement of the particles. However, lowering surface tension also weakens the cohesion of granules, making them more prone to dilation or shearing apart. The segregation of multi-component mixtures during the process of granulation is a prevalent issue, particularly in the pharmaceutical industry, where extensive research has focused on addressing this problem. In the pharmaceutical field, most drugs are hydrophobic and administered in low dosages, requiring a small surface area to ensure controlled dissolution and absorption. Consequently, drugs are typically formulated with small particle sizes, generally less than 30 mm. On the other hand, excipient powders used in the formulation process are usually larger in size to prevent complications associated with the handling and fluidization of extremely fine powders. Various factors contribute to the occurrence of segregation, including differences in solubility, migration of the binder fluid, binder fluid flow rate, and abrasion. One common explanation for segregation is the migration of the binder fluid to the outer layers of the granule during the drying process. As the fluid evaporates, the drug components are transported with the flowing fluid and then redeposited at the surface. Furthermore, abrasion can remove the enriched outer layers of the granule, resulting in the production of drug-enriched fines (Liu *et al.*, 2021).

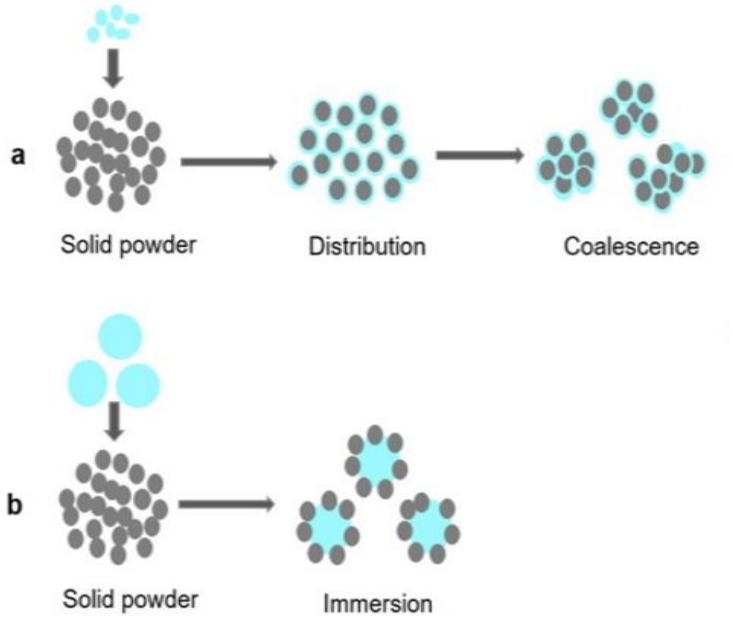

Figure 2.2: Wetting and nucleation mechanism (a) distribution (b) immersion (Liu *et al.*, 2021)

2.2.4 Consolidation and growth

Coalescence and consolidation make up the second stage of wet granulation. As the trapped air and liquid in the granule body is forced out to the surface, the density of the granules increases noticeably and eventually causes the granules to develop to a specified size and strength (Iveson *et al.*, 2001). This process can be carried out either by layering or coalescence (Figure 2.3). During the coalescence process, the granulation powder is sufficiently wet for the granules to stick together and grow larger. Fine material adheres to the surface of granules during layering (Liu *et al.*, 2000). The success of collisions will depend on factors such as particle size, powder and binder properties, mixer granulator speed, and powder velocity (Rajniak *et al.*, 2007). The main mechanism giving strength to the granule is that the particles are held together by liquid bridges at their contact points pendular bonds. The capillary state occurs when a granule is saturated and all the voids are filled with liquid and the surface liquid is drawn back into the pores under capillary action. Liquid-bound granule strength is dominated by two categories of forces: liquid bridge and inter-particle friction. The liquid bridges can generate both static surface tension forces and dynamic forces due to the liquid viscosity.

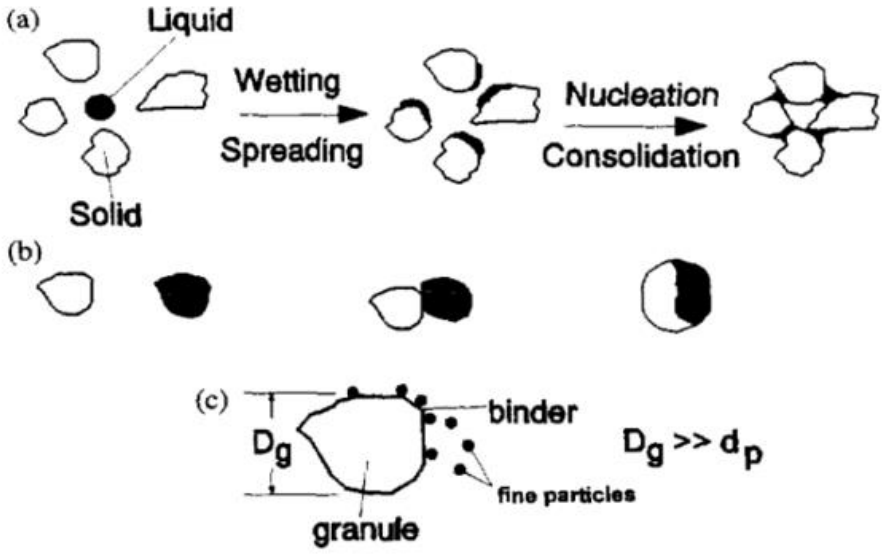

Figure 2.3: Consolidation and growth mechanisms: (a) agglomerate formation by nucleation of particles; (b) granule growth by coalescence; (c) layering of fine particles sticking onto the surface of granules (Tardos *et al.*, 1997)

2.2.5 Attrition and breakage

Attrition and breakage take place when granules impact with other particles or surfaces, or through shear forces in the granulator. Breakage is an important mechanism in high shear granulators due to collisions with the wall or impeller (Cameron *et al.*, 2005). These forces can also lead to high levels of granule densification, creating robust granules able to growth and survive the shear forces (Van Den Dries *et al*., 2003). When breakage occurs, the granules typically fragment into a number of smaller cracks, with a noticeable loss in both size and strength (Figure 2.4).

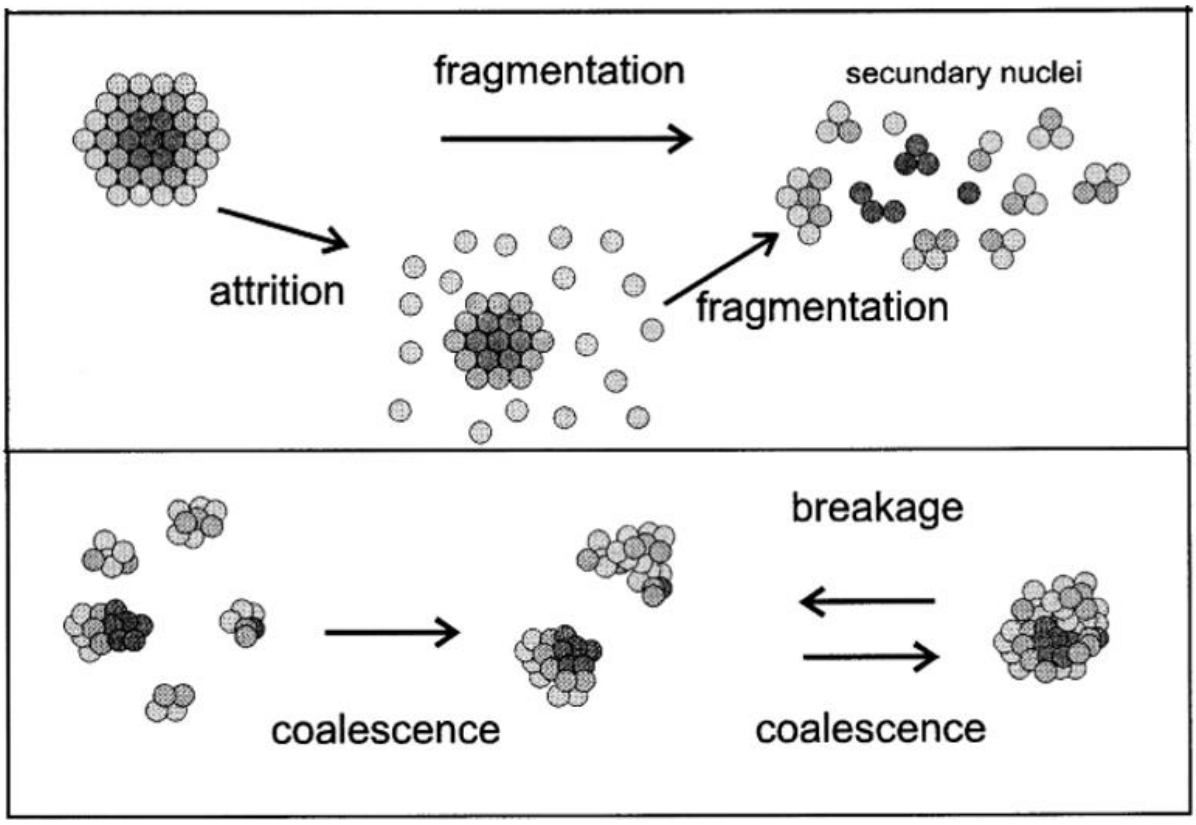

Figure 2.4: Attrition, breakage and coalescence in wet granulation (Vonk *et al.*, 1997)

2.3 Granulation equipment

Different types of equipment have been used for powder granulation, including fluidized bed granulators, twin screw granulators, tumbling drums, and low and high-shear granulators. Operation of these types of equipment in production processes can be continuous or batch-wise. The characteristics of desired granules, e.g. granule density, particle size distribution and dissolution time, determine the use of specific equipment (Flore *et al.*, 2009).

2.3.1 Fluidized bed granulation

Fluidized bed granulation is currently being utilised for wet granulation after previously being used for drying and coating. The use of fluidized beds for continuous production of granules for tabletting was designed and presented by Rankell *et al.*, 1964. Granule characteristics in fluidized bed granulation can be easily changed by both product and process variables. Examples of formulation factors include powder particle size, surface area, water solubility,

binder type, and binder concentration. The process variables are air pressure, intake temperature, granulator air velocity, and binder addition rate (Gao *et al.*, 2002).

Binder is sprayed over a fluidized powder bed during the granulation process in the form of a solution or suspension. The fluidized bed process has been widely used for particle enlargement in the pharmaceutical industry. However, other process industries have adopted this technology to address particle enlargement such as food, agrochemical, and other chemical industries (Hemati *et al.*, 2003). Compared to high shear wet granulation, the fluidized bed granulator produces granules that are more uniform, fine and free-flowing. In addition, after compression, the tablets formed were more robust and disintegrated faster (Litster, 2016a).

2.3.2 Tumbling granulation

In tumbling granulators, the granulation process can be performed when the particles are set in motion by the tumbling or crushing action in presence of a balance between centrifugal forces and gravity. Tumbling granulators are usually not suitable for producing small granules and the produced granules by this technique have high density. Tumbling granulators include drums, pans and discs (Litster & Ennis, 2004).

2.3.3 Twin screw granulation

The twin screw granulator (TSG) has recently become widely used in polymer, food and chemical processing industries as a continuous granulator. Use of TSG in continuous granulation provides high volume production of material with less space required. TSG mainly consists of two intermeshed barrel screws. Powder material is conveyed along the screw length, and liquid binder is added from the top through the liquid binder feeder. Liquid distribution and granulation take place in the mixing zones under a temperature controlled jacket (Seem *et al.*, 2015).

2.3.4 Mixer granulation

In the pharmaceutical, agricultural, and chemical industries, mixer granulators are extensively utilised. Here, the impeller can impart velocity to the particles based on the shear force. There are two types of mixer granulators, which will be detailed in the following sections.

2.3.4.1 Low-shear granulation

Low-shear granulators are characterised by low agitation speed, and consume low energy compared with the high shear granulator. The low shear granulator allows powder movement through both internal agitation and tumbling. Liquid is added through the agitator bar and exits by blades located on a disc assembly into a toroidal void space. The main disadvantages of this technique are that it is time consuming and there can be a considerable loss of material (Chirkot, 2002).

2.3.4.2 High-shear granulation

High-shear granulators have been widely used and a number of studies have intended to demonstrate the growth mechanisms of granules through using a high-shear granulator (Mangwandi *et al.*, 2011). In general, high-shear granulators are composed of a mixing bowl, a multi-bladed impeller and a chopper. The mixing bowl is cylindrical or conical in shape. The contents in the bowl can be heated or cooled through using a mixing bowl jacket. Dry powder and the binder fluid are mixed using an impeller, with a typical impeller speed ranging from approximately 100 to 500 rpm. The chopper rotation speed ranges from 1000 to 3000 rpm. The role of the chopper is to break down very large granules after wetting. Based on the orientation of the impeller, the high shear granulator can be classed as either horizontal or vertical axis (Figure 2.5). The vertical high shear mixer could be a bottom or top-driven unit (Swarbrick *et al.*, 2005).

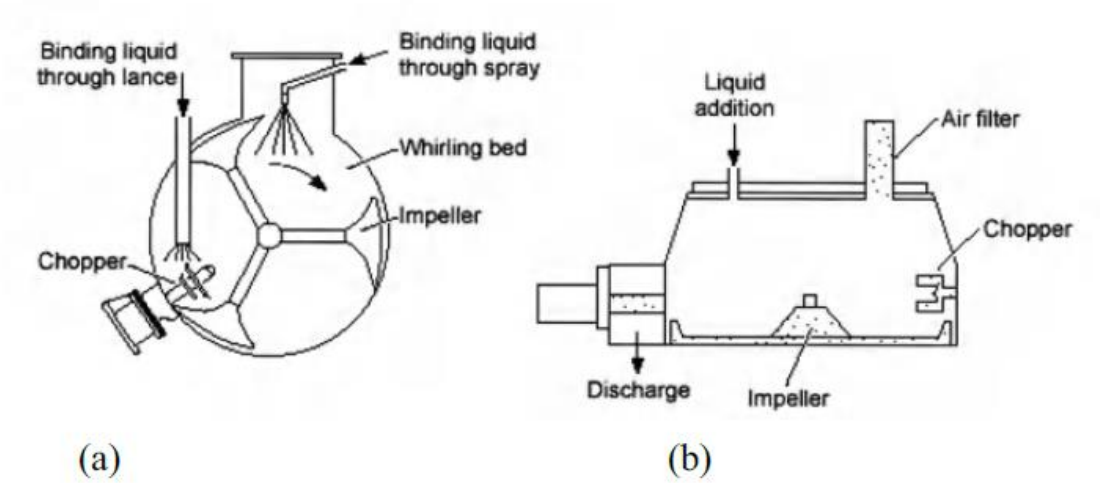

Figure 2.5: Schematic of (a) a horizontal impeller high-shear granulator and (b) a vertical impeller high-shear granulator (Litster, 2016a)

The capacity to mechanically spread the liquid binder and break up material clumps is the main advantage of mixer granulators over tumbling or fluidised bed granulators. This type of equipment can work with a variety of materials, such as very fine cohesive powders and viscous liquid binders (Litster & Ennis, 2004). Mixer granulators produce less spherical, denser, smaller granules (0.2-2 mm) than their tumbling counterparts or fluidised bed granulators (Litster, 2016a).

2.4 Effect of operational and formulation variables on granule properties

Many efforts have been made to understand the mechanisms of granulation through changing operational parameters such as impeller speed, time and liquid binder quantity, and their effect on granule properties. A summary of these is given in Table 2.1. The literature indicates that the liquid to solid mass ratio (L/S) and granulation time will have a significant effect on the structure. These variables will be discussed in more detail in the following sections.

Table 2.1: Review of studies of effect granulation conditions on the granule properties

Author	**Operational Parameters**	**Results**
Effect of operational parameters on the granule structure		
Author	**Formulations**	**Results**
Bouwman *et al*. (2005)	MCC as a powder and water as a liquid binder	At 1.0 L/S ratio, densification was more obvious in the core of the MCC granule. At 1.2 L/S densification was decreased with more fragments of irregular shape.
Ansari *et al.* (2008)	Mannitol as a powder and PVP as binder Sucrose as a filler and PEG as binder	Increasing L/S ratio reduces porosity of both mannitol and sucrose granules.
Eshtiaghi *et al*. (2009)	Fumed silica as a powder and hydroxy propyl cellulose solution as a binder	Increasing L/S ratio → fumed silica granules transformed from spherical to deformed structure. Optimal L/S ratio was found to be between 3:1 and 6:1 range.
Mangwandi *et al*. (2010)	The powder was mixture of lactose monohydrate and potato starch. Hydroxypropyl cellulose solution as a binder	At low viscosities, granule size decreased at high impeller speeds and in highly viscous systems, granule size increased at high impeller speeds.
Limin shi *et al.* (2011)	MCC as a pweder and PEG as a liquid binder	The granule porosity decreased sharply with increasing the massing time for the first 10 min.

		After this, there was little effect on granule porosity.
Rahmanian *et al*. (2011)	Calcium carbonate as a powder and PEG as a liquid binder	Granule densification and strength was higher with increased impeller speed and granulation time.
Badawy *et al.* 2012	MCC as a powder and water as a liquid binder	Increasing wet massing time enhanced density while decreasing porosity.
Van den Ban & Goodwin (2017)	MCC and Lactose monohydrate as a powder and water as a binder	The granule density increased with the increasing of both water quantity and wet massing time.
Meng *et al.* (2019)	MCC and Lactose monohydrate as a powder and dry polyvinylpyrrolidone as binder	High impeller speed and high L/S ratio produced lower porosity and larger size granules.
Effect of porosity and granule structure on the granule and tablet dissolution		
Ansari *et al.* (2008)		The dissolution rate was strongly affected by mannitol granule porosity. However, for sucrose granules, the dissolution rate was found to be independent of porosity.
Badawy *et al.* (2012)		Tablet porosity and dissolution rate decreased with lower granule porosity.
Van den Ban & Goodwin (2017)		The tablet dissolution rate decreased as the granule density increased.
Meng *et al.* (2019)		Decreasing porosity of MCC and lactose monohydrate (LM) granules then showed a slow drug release after tabletting.

2.4.1 Effect of the liquid to solid mass ratio (L/S) and granulation time on the granule microstructure and performance

Granules are multiple component systems and include binder and primary solid particles. The void space within a granule is also important, as it influences the mechanism and rate of dissolution. In recent years, granule microstructure has become an increasingly recognised attribute for quality assurance purposes and this granule microstructure is defined as the spatial arrangement of solid particles, binder and intra particle porosity (Rahmanian *et al.*, 2009). The granule internal structure and porosity is mainly dependent on the granulation process conditions. High binder volume causes a decrease in the granule porosity due to an increase in the fraction of the inter-particle void space which would be occupied by the binder (Ansari and Stepanek, 2008). Increasing the liquid saturation of the granules enhances granule coalescence and makes granules more easily deformable which results in more liquid being available at the granule surface. This increases the probability of successful coalescence with low void space between coalescing particles (Liu *et al.*, 2000). Liquid bonds between primary particles are generated during the wet granulation process, resulting in the formation of semi-permanent aggregates. The amount of energy carried to the powder mass by the mixing intensity during granulation can affect the level of densification and intragranular porosity (van den Ban and Goodwin, 2017).

The influence of the amount of liquid binder on the granule structure during the granulation process has been studied by Bouwman *et al.* (2005) by using microcrystalline cellulose (MCC) and water as the filler and liquid binder, respectively. When using MCC granules with a L/S ratio of 1.0, the densification of generated granules increased with time, and densification was more noticeable in the core of the granule while the outer part remained more porous. On the other hand, when using a L/S of 1.25, densification decreased even after extended granulation time. This is due to an increase in the MCC deformability. These granules upon continued granulation are more easily subjected to breakage and this will reduce the granule core densification. At this time, the breakage and the coalescence of the granule fragments are balanced which results in weak granules with irregular shapes (Bouwman *et al.*, 2005). It is assumed that excipients that swell during the granulation process, for example MCC, need more liquid binder for granulation compared to soluble excipients such as lactose. However, for both systems, increasing L/S ratio resulted in increasing granule densification.

Furthermore, Bouwman *et al.* (2005) also studied the effect of the duration of the granulation process on the MCC granule porosity and structure. X-ray microtomography was used to visualise the granule microstructure and analyse the total granule porosity. It was found that total porosity reduced over time due to the closing up of both small and large pores by the granulation process. By using a fixed liquid to solid mass ratio (1.0 L/S), the total granule porosity decreased from 26 to 9 % by extending the granulation time from 3 min to 15 min respectively (Figure 2.6). This study was in agreement with a subsequent study completed by Ansari and Stepanek (2008), which showed that increasing the liquid binder produced denser granules. In this study, top-spray fluid-bed granulation was used to granulate mannitol primary particles with polyvinylpyrrolidone (PVP) aqueous binder. Furthermore, melt fluid-bed granulation was used to prepare granules from polyethylene glycol (PEG) binder and sucrose primary particles. Granule porosity and microstructure was analysed using X-ray computed micro-tomography. In both granulation cases, increasing the binder to mass ratio produces less porous granules and the dissolution rate of mannitol granules was found to be significantly affected by granule porosity and binder volume (Figure 2.7).

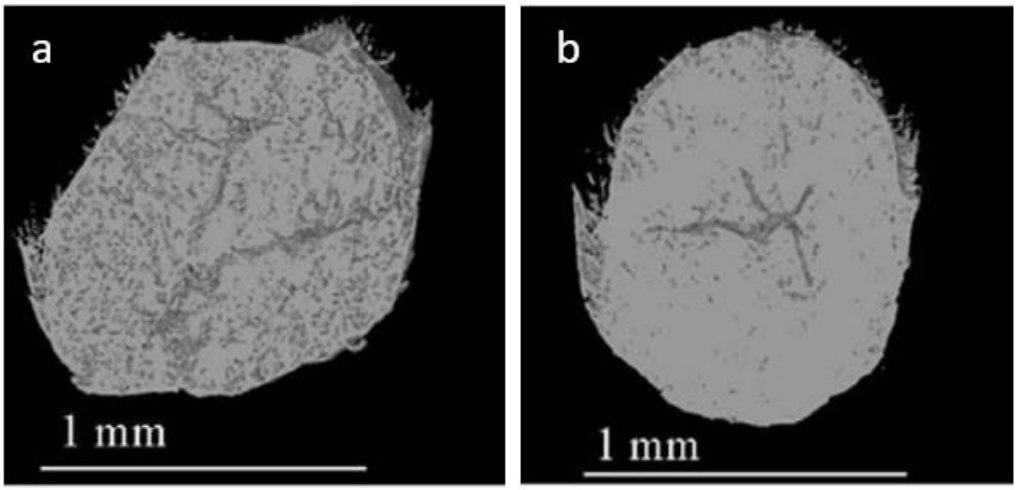

Figure 2.6: Reconstructed X-ray microtomography images showing cross-sections through MCC granules: (a) 3 min and (b) 15 min granulation time (MCC was granulated with water using a high shear granulator with a L/S ratio of 1.0) (Bouwman *et al.*, 2005)

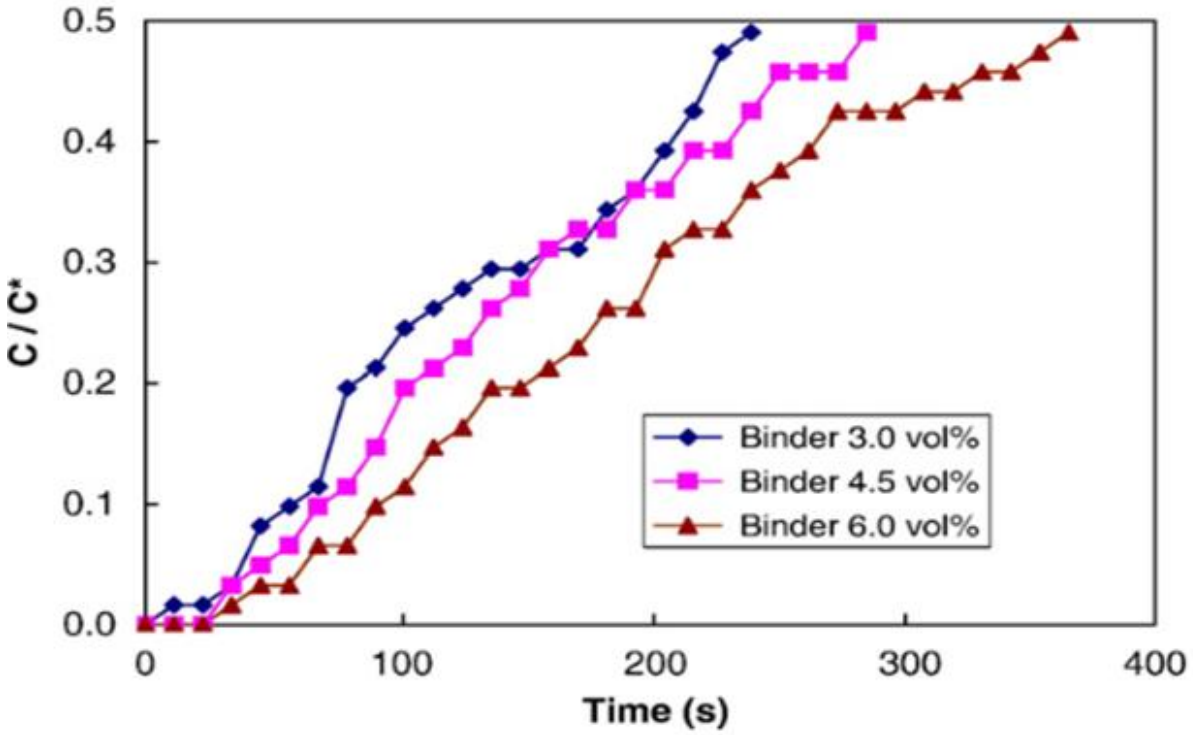

Figure 2.7: The dissolution curves of mannitol granules prepared by different L/S ratios; 0.03 L/S , 0.045 L/S and 0.06 L/S ratio. The Y axis shows mannitol concentration. (Ansari and Stepanek, 2008)

In addition to the previous studies, the effect of liquid binder on granule structure was of interest to many researchers, and in 2009, Eshtiaghi *et al*. studied the structure and morphology of granules prepared by granulating hydrophobic fume silica with 5 % hydroxy propyl cellulose solution as a liquid binder through changing the L/S ratio (0.5 to 15 L/S) and focused on assessing granule morphology. The authors found the structure and morphology of granules changed from spherical to a deformed structure with increasing L/S ratio and illustrated the importance of selecting the optimal L/S ratio. Increasing L/S ratio leads to a decrease in the amount of un-granulated fine particles, however, the quantity of stretched and flattened filament granules increased. As hydrophobic powder was used, the quantity of liquid binder was greater than the powder quantity and the optimal L/S ratio was found to be between 3 and 6. At these ratios, fine particles were granulated and less flattened hollow granules were produced (Eshtiaghi *et al.,* 2009).

The effect of granulation time on granule porosity has also been extensively studied. In general, these studies found that the granule density increased with granulation time, until a plateau was reached. Rahmanian *et al*. (2011) studied the influence of granulation time on granule structure. They found that granule strength was significantly influenced by increasing the granulation time from 6 min until an optimum time was reached at 12 min. Densified granules were produced by increasing the time of granulation, and the granule size distribution increased by increasing the binder concentration (Rahmanian *et al.*, 2011). This study agreed with studies performed by Shi *et al.*, (2011) on the effect of massing time on MCC granule porosity and performance. The massing time was varied from 0 to 40 min while the impeller speed was fixed at 1750 rpm and the binder flow rate was 25 g/min. For the initial 10 min, the granule porosity decreased sharply with increasing massing time (Figure 2.8). However, a further increase in the massing time for longer than 10 min had little effect on the granule porosity (Shi *et al.*, 2011). Figure 2.9 shows that granules with 1 min massing time are expected to deform easily with high fragmentation. The granules are substantially more rounded after 5 min of massing and compared to 1 min massing time, and a significant amount of pores were eliminated. However, the porosity is still high compared to the granules produced after 10 min. Nearly all rough surface features are eliminated after 10, 20, and 40 min massing times, and the quantity of sphere-like granules increases noticeably during longer massing. Additionally, no fractured grains are seen. These findings suggest that extended massing times produce granules that are denser and stronger.

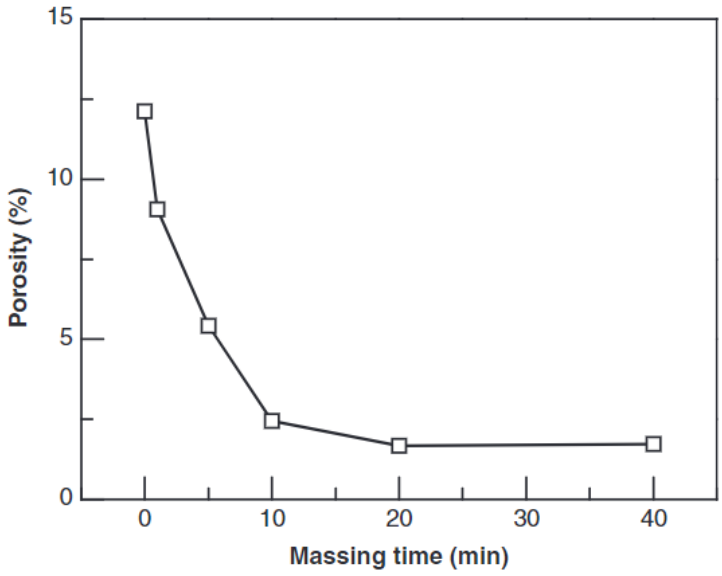

Figure 2.8: Effect of massing time on granule porosity. (Shi *et al.*, 2011)

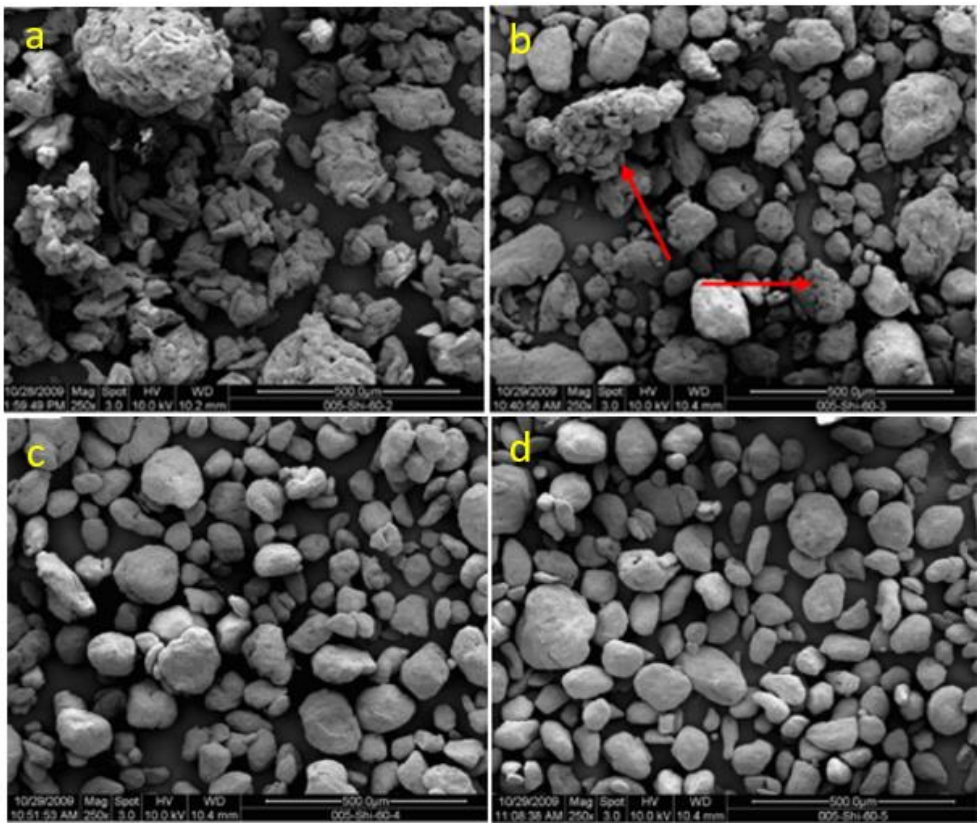

Figure 2.9: Morphology of MCC granules produced using different massing times: (a) 1 min, (b) 5 min, (c) 10 min, (d) 20 min (Shi *et al.*, 2011)

In the previous literature, the granulation time was relatively long. In contrast, Badawy *et al.*, (2012) studied the effect of short massing times on the three different formulations, each containing MCC as an excipient with three different APIs; Brivanib alaninate (Br), Razaxaban (Ra) and Pexacerfont (Pexa). Granule coalescence and growth may occur during wet massing. However, large granules may break until a steady state particle size distribution is attained. Furthermore, during wet massing, granule densification can occur, affecting granule liquid saturation and mechanical characteristics, as well as particle size distribution. The three studies were carried out within 1 min for Br and Pexa, and up to 3 min for Ra which are relatively short wet massing times.

Despite the short massing times (up to 1 min), there was a substantial impact on blend density/porosity for Br and Ra, with increasing wet massing time increasing density while decreasing porosity. For Pexa, the influence of wet massing on blend density was not observed.

This may be due to the longer wet massing time which causes a decrease in the granule size. This smaller granule size causes a reduction in blend density (as a result of trapped air and less granule packing in the powder bed). Therefore, the effect of wet massing on the blend density of Pexa might not have been statistically significant (Badawy *et al.*, 2012).

In this same paper by Badawy *et al.* (2012), the effect of granulation variables on tablet dissolution rate was conducted for the BR formulation. Increasing L/S ratio and granulation time considerably decreased the Br tablet dissolution rate, as measured by the percentage of API dissolved in 10 min. Thus, it appears that the dissolution rate of Br tablets is influenced by granulation parameters in the same direction as granule porosity (mean pore diameter). Porosity of Br granules is reflected in tablet porosity (i.e., granules with smaller pores resulted in tablets with lower porosity and slower drug dissolution rate) (Figure 2.10) (Badawy *et al.*, 2012). Furthermore, the dissolution liquid used in the study conducted by Collins *et al*. (2007) has been shown to influence the pore structure. Their research focused on investigating the impact of water immersion time on the pore structure of placebo and drug-loaded pellets. To analyse the evolving pore structure of the pellets as they absorbed water during the dissolution process, the researchers employed nuclear magnetic resonance (NMR) techniques. The results revealed significant changes in the pore structure of the pellets as water permeated the pellet matrix. With increasing immersion time from 2 minutes to 10 minutes, both the mean pore size and pore size distribution increased. In the case of drug-loaded pellets, a relatively narrow pore size distribution was observed at a short immersion time of 2 minutes, which progressively broadened as the immersion time increased.

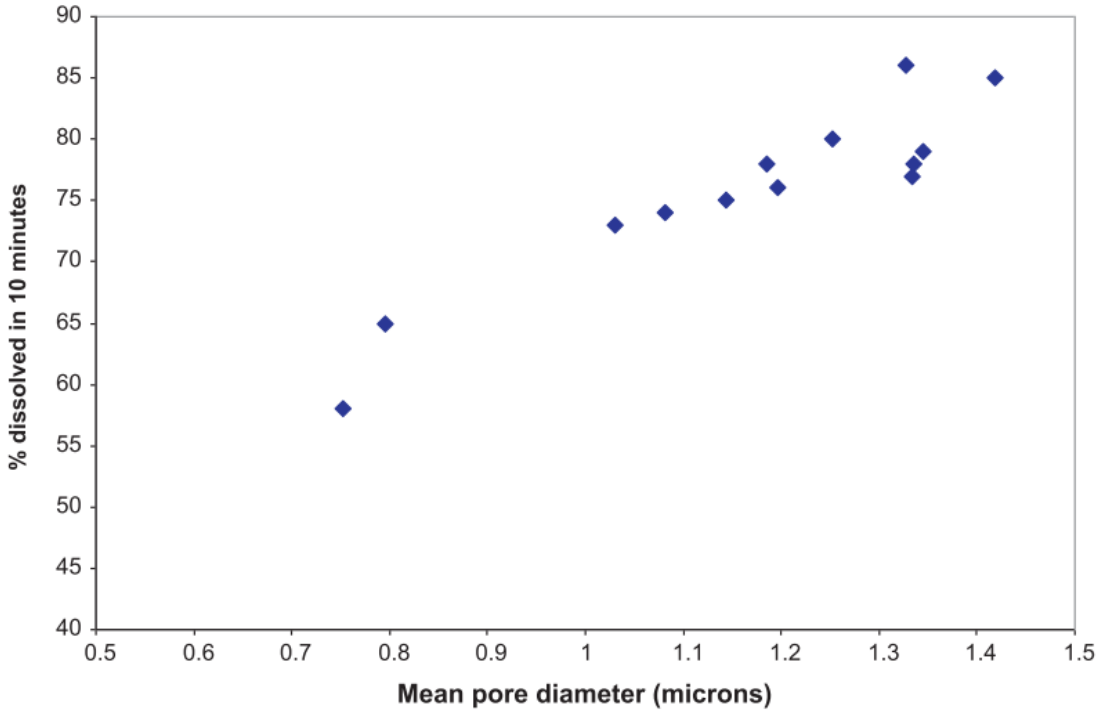

Figure 2.10: Effect of granule pore diameter on dissolution rate of Br tablets (Badawy *et al.*, 2012)

The effect of both L/S and granulation time on the granule porosity has been studied to find out which parameter has the higher effect on the granule porosity. Van den Ban & Goodwin (2017) studied the effect of varying granulation time and binder content on the granule microstructure of mixures of MCC and lactose monohydrate. The granulation times investigated were 2, 4 and 6 min, and the L/S ratios were 0.27, 0.30 and 0.32. The authors found that an increase in water quantity and increase in wet massing time resulted in an increase in granule density (Figure 2.11). This confirms trends found in other studies, however, they found that the L/S ratio has a greater effect on granule porosity than the granulation time. Recently, Meng *et al.* (2019) confirmed these findings and further elucidated the effect of L/S ratio on the granule structure and tablet dissolution. The low-dose formulation comprised 8 % (w/w) acetaminophen (paracetamol) as a model drug. The remainder of the formulation consisted of 44.75 % (w/w) MCC and 44.75 % (w/w) lactose monohydrate, with 2.5 % (w/w) PVP as a liquid binder. The L/S ratios used were 0.35, 0.45 and 0.55. The L/S ratio had a clear influence on the granule properties. Increasing liquid saturation produced larger sized, less porous granules with improved flowability and sphericity. A L/S of 0.55 generated the most densified granules with a small porosity of 33.7 % while a L/S of 0.35 produced the most

porous granules with a porosity of 61.9 %. Furthermore, a L/S of 0.45 produced granules with an intermediate porosity of 46.5 %. These granules after compression generated tablets with different porosity (Figure 2.12). The acetaminophen was slowly released from the tablets that were prepared from denser granules (Figure 2.13) (Meng *et al.*, 2019).

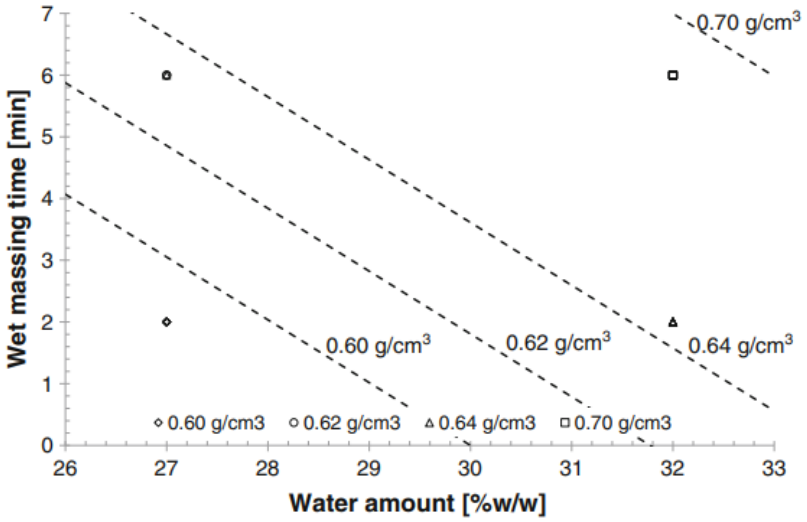

Figure 2.11: The impact of water amount and wet massing time on granule density (van den Ban and Goodwin, 2017)

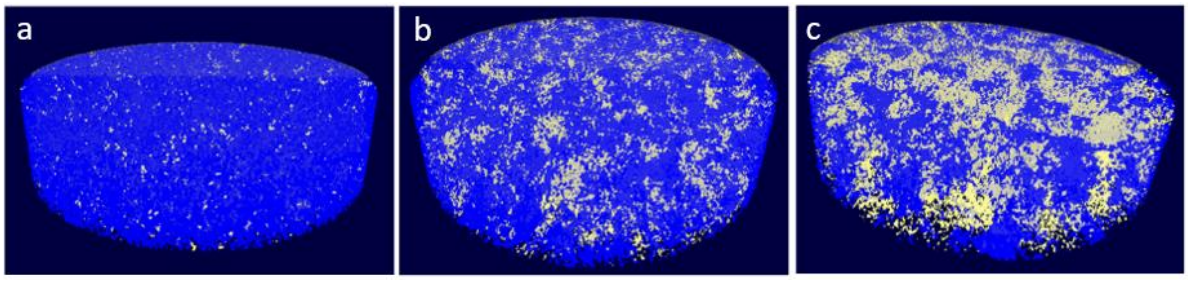

Figure 2.12: 3D images of tablets made from different porosity granules: (a) 0.35 L/S, (b), 0.45 L/S, and (c) 0.55 L/S (Meng *et al.*, 2019)

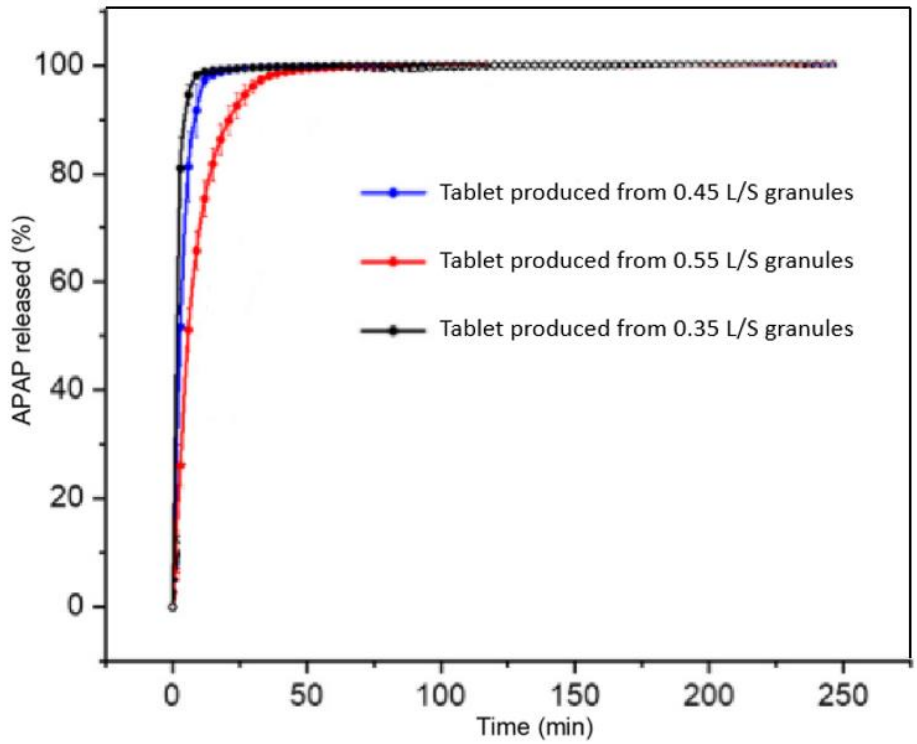

Figure 2.13: Drug release from tablets produced using different L/S ratios (Meng *et al.*, 2019)

2.4.2 Summary

The existing literature on the effect of process parameters (L/S mass ratio & granulation time) on granule structure been reviewed in Section 2.4. Despite the extensive literature on high shear granulation, the effect of granulation parameters on the granule structure is not well defined. The linking of process conditions, granule structure and granule performance is still unclear and requires further work to be fully understood. Furthermore, the ranges of L/S mass ratio and granulation time investigated in the literature were relatively narrow; with only a few studies investigating a wider range of both L/S mass ratios and granulation times.

The main purpose of this thesis is to generate different granule structures, and link these to granule dissolution and disintegration behaviour. From the literature, it is clear that the rate of the drug release from tablets and granules is affected by the granulation process variables. It is proposed that drug release can be affected by changing both granulation time and the quantity of the liquid binder. This is due to a reported decrease in the granule porosity with these two parameters. Decreasing the granule pore size is expected to reduce the time of liquid penetration into the granule pores and hence slow drug dissolution. To study these relationships, it is necessary to review the drug release and the theory of dissolution including the correlations between the liquid penetration time and the granule porosity and surface area. The following sections will review the drug release process including the theory of dissolution and the mechanism of granule dissolution and disintegration.

2.5 Effect of granule structure on drug release

Granule pore structures are characterised by the relative void space in the granule. Porosity is the fraction of the volume of voids divided by the total volume of the granule. The porosity is the most important contributor to granule dissolution and it is directly influenced by the granulation process (Ansari and Stepanek, 2008). Figure 2.14 shows that release of a drug from a porous granule involves the penetration of surrounding liquid into the pores, making the drug dissolve and leach out the granule matrix by the diffusion mechanism**.** The dissolution rate of the drug is related to the porosity that the dissolution liquid can penetrate (Sinko, 2013).

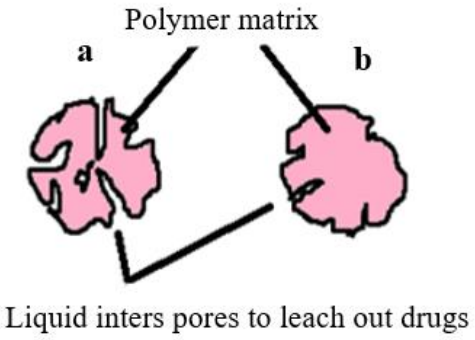

Figure 2.14: Drug leaching from the granule matrix (a) wide pore granule and (b) narrow pore granule. Adapted from (Sinko, 2013)

The key step that plays an important role in the dissolution process of porous granules and the drug release is the liquid penetration. The process of liquid penetration into a porous granule matrix is controlled by the capillary and viscous forces. Capillary forces dominate fluid movement into the granule pores. On the other hand, the viscous forces control the liquid movement out of the pores (Markl *et al*., 2017). In general, narrow pores decrease the ability of the fluid to enter the granule pores and the penetration time of the liquid at depth *L* into porous granules can be calculated using Washburn's Equation (2.1):

$$L^2 = (\frac{\gamma \mathrm{COS}\theta}{2\eta})rt \qquad (2.1)$$

where t is the time of penetration, η is the liquid viscosity, L is the penetration length of a liquid into the capillary pore, r is the pore size, γ is the surface tension of the liquid and θ is the contact angle between penetrating liquid and solid particle. Washburn's equation summaries the essential factors that influence the time for liquid penetration into pores. Wider pores, enhanced surface tension of the liquid and an increase in the contact angle between liquid and granule matrix lead to a decrease in the time required for liquid penetration into the pore. On the other hand, at high liquid viscosity and increasing already partially filled pores, increases the time for liquid penetration (Desai *et al.*, 2016).

In terms of drug release from porous granules, the drug inside granules with wider pores is released faster compared to those with narrow pores. It is important to understand the impact of the high shear granulation process and process parameters (e.g. granulation time and L/S mass ratio) on the structures produced in order to design granules with a required dissolution rate. Relating to the amount of liquid saturation, the separating forces exerted by the impeller of the high shear granulator may be not strong enough to separate the bonding between colliding granules. More free liquid on the granule surface is associated with a higher degree of liquid saturation. Liquid saturation, *S*, of an agglomerate of particles (granule) in this case is given by the following Equation (2.2) (Ritala *et al.*, 1988):

$$S = H(1-\varepsilon)\frac{1-\rho}{\varepsilon} \tag{2.2}$$

where H is the liquid to solid mass ratio in the granule, ε is the granule porosity, and ρ is the density of the initial powder particles. High amounts of water will increase the value of H in the equation causing an increase granule density and hence a decrease the porosity (Badawy *et al.*, 2000).

2.5.1 The theory of dissolution and drug release

Dissolution is defined as a solid phase going into a solution phase, and the dissolution rate is how fast a solid phase takes to dissolve (Smith, 2016). Dissolution of a drug from a solid dosage form takes place in two steps. Firstly, there is separation of drug molecules from the surface of the solid dosage form to form a saturated drug solution at the solid-liquid interface (diffusion layer) (Wang and Flanagan, 1999). The second step is mass transport of the drug from this saturated layer into the bulk solution by the diffusion mechanism (Figure 2.15). The rate of mass transfer of solute particles (drug particles) into the bulk solution was firstly described by Noyes and Whitney as a diffusive process (Equation 2.3) (Seager *et al.*, 2018):

$$\frac{dM}{dt} = \frac{DS}{h}(C_s - C) \tag{2.3}$$

where *dM/dt* is the rate of mass transfer (mass/time), *D* is the diffusion coefficient, *S* is surface area of exposed solid, C is the concentration in the bulk solution, C_s is the concentration of solute particles in the diffusion layer surrounding the solid and *h* is the diffusion layer thickness. The rate of dissolution is directly proportional to the surface area of the exposed solid, diffusion coefficient and the concentration of solute particles present at the diffusion layer. On the other hand, according to the equation, the thickness of the diffusion layer is indirectly proportional to the rate of dissolution, so the greater the thickness of diffusion layer, the lower the rate of dissolution (Smith, 2016). In the case of dissolution of the drug from the granule, the surface area of the exposed solid is related to the size of the granule. Increasing the size of the granule during the granulation process will reduce the surface area of exposed solid which will reduce the rate of mass transfer of drug molecules to the bulk solution.

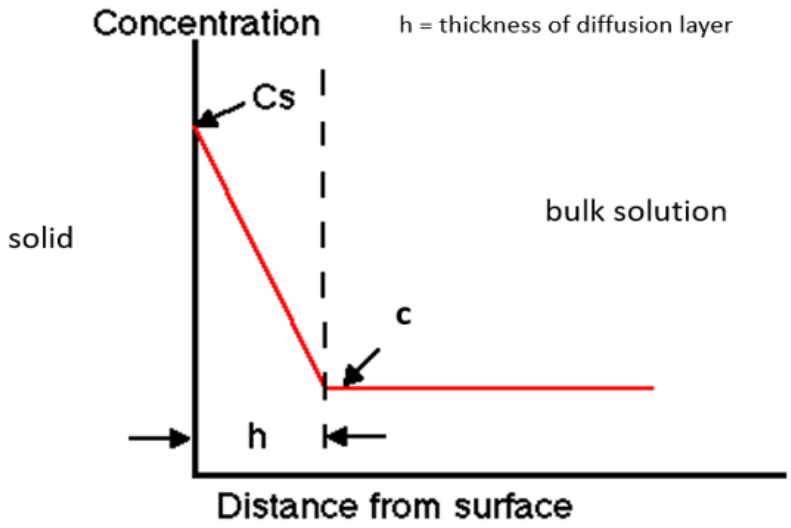

Figure 2.15: Diffusion theory (Baishya, 2017)

Diffusion of drug from the solid dosage form starts when the solid dosage form comes into contact with the dissolution liquid, and the liquid layer close to the solid dosage form surface stays stagnant, forming a diffusion layer (h in the Figure 2.15). A saturated solution is formed at the solid/liquid interface. The rate of dissolution is related to the diffusion of the drug molecules from the stagnant diffusion layer to the bulk solution (Baishya, 2017). The process of removing drug molecules from exposed surfaces of the dosage form is continued until the solubility limit is reached. At this point, the dissolution process and precipitation are in equilibrium and no more drug can be dissolved in the dissolution liquid (Seager *et al.*, 2018).

IUPAC defines dissolution as the blending of two phases to create a single, homogenous phase, which is the solution (Figure 2.16). The two phases are first distinguished from one another and have a distinct boundary between them. As a result of mixing, the boundary gradually fades away until it becomes impossible to distinguish. The formation of a new, homogenous phase known as solution results from the intense molecular mixing of two or more phases during the dissolution process (Siepmann and Peppas, 2011).

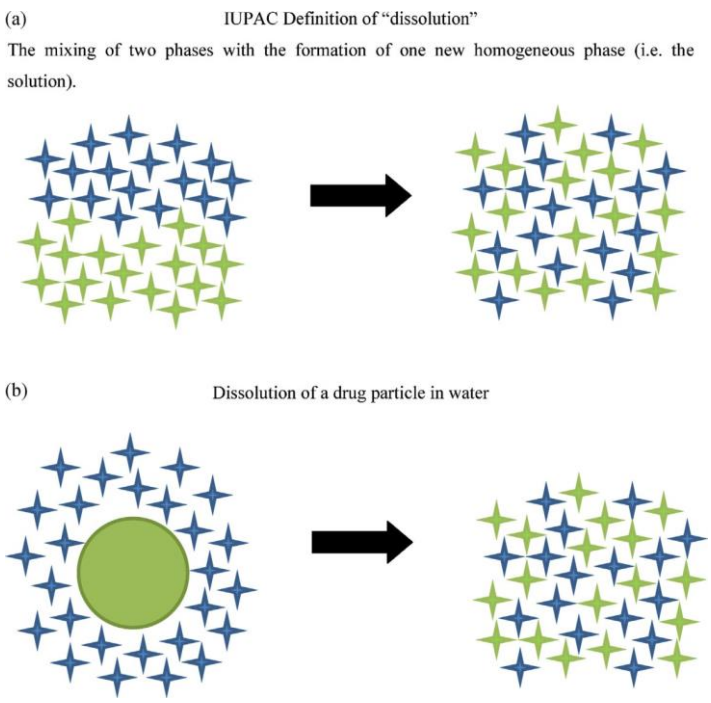

Figure 2.16: Schematic presentation of the: (a) IUPAC definition of the term dissolution, and (b) dissolution of a solid drug particle in an aqueous liquid (Siepmann and Siepmann, 2013)

In the case of a drug-containing polymer matrix agglomerate, one phase is the agglomerate (polymer matrix, drug, and other excipients) and the other phase is a dissolution liquid (which is frequently a fluid containing water). According to Figure 2.17, the following five main physical phenomena take place throughout the dissolution process (Siepmann and Siepmann, 2013):

1. Contact of the solvent with the agglomerate's surface.
2. Each constituent's interparticulate solid state bonds rupture in the agglomerate (e.g. attractive bonds such as hydrogen, electrostatic, van-der Waals).
3. A layer of water molecules surrounds individually isolated molecules.
4. The diffusion of these individualised units across the diffusion boundary layer, an unstirred layer around the agglomerate, into the well-stirred tank. (It is significant to note that this layer, whose thickness depends on the level of agitation, exists even in thoroughly stirred systems due to adhesion force).
5. The convectional movement of the units to the system's well-stirred area. Thermal agitation may also produce diffusion of solvent molecules and other units in this layer, however stirring results in convection as the major transport mechanism.

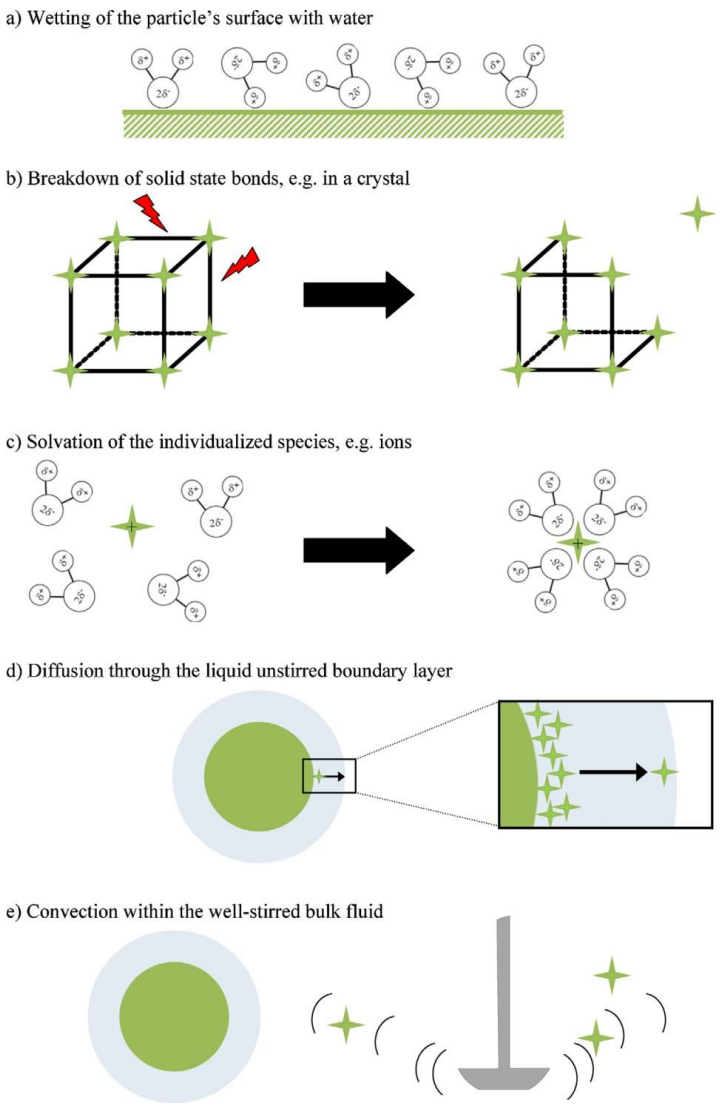

Figure 2.17: Schematic illustration of the 5 steps of the dissolution (Siepmann and Siepmann, 2013)

Despite the phrases drug dissolution rate and drug release rate being frequently used interchangeably in the literature, there is a basic distinction between them. According to the IUPAC's definition of "dissolution," drug dissolution typically entails the five main mass transport processes mentioned above. Contrarily, the word "drug release" typically refers to a considerably more complicated phenomenon that includes a variety of processes, such as drug dissolution (Siepmann and Siepmann, 2013). Figure 2.18 shows that the drug is initially present as solid particles. The solvent entered the system after coming into contact with the release medium and the partially dissolved drug. The drug species is then released from the tablet as a

result of mass transfer brought on by a concentration gradient (Baishya, 2017). Additionally, the polymer may expand significantly, particularly when its concentration at the surface reaches a threshold level that will eventually cause it to dissolve in the medium. Therefore, a variety of events, including drug breakdown, can be implicated in the process of drug release. The solubility and drug dissolution are directly related. This thermodynamic characteristic, which depends on both the drug and the solvent, indicates how well the drug can be dissolved (Siepmann and Siepmann, 2013).

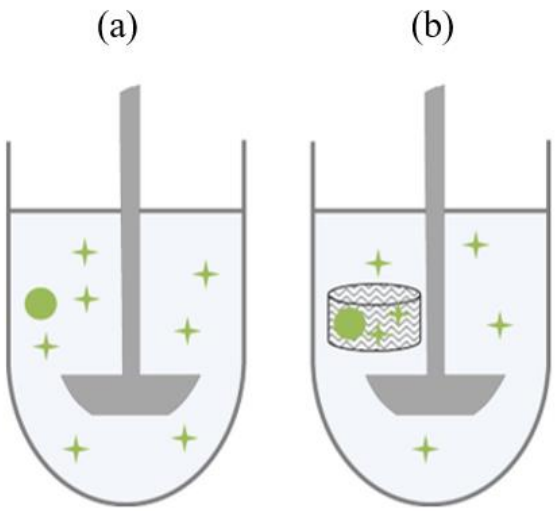

Figure 2.18: The schematic of (a) drug dissolution and (b) drug release. The green stars indicate dissolved drug molecules whereas the green circles represent drug particles (Siepmann and Siepmann, 2013)

2.5.2 Mechanism of tablet and granule disintegration and dissolution

For the active pharmaceutical ingredient to have the desired therapeutic effect, it must be in solution and readily absorbed by the gastrointestinal tract (Swarbrick *et al*., 2005). Due to the limited amount of API in tablets and granules, suitable excipients must be combined with API to achieve the desired volume for tableting processes. By delaying the commencement of dissolution, these excipients may lower API bioavailability, especially in immediate release tablets. In this instance, and where immediate release is required, disintegration agents such as croscarmellose sodium (CCS), sodium starch glycolate (SSG) and crospovidone (XPVP) are commonly included in the formulation to overcome this problem. These disintegration agents work by breaking down tablets into small granules, to enhance the surface area and increase dissolution properties (Figure 2.19) (Markl and Zeitler, 2017). Both tablets and granules undergo similar disintegration and dissolution processes. As tablets are the most common solid oral dosage form, there has been substantially more work performed on tablet disintegration and dissolution than on granules. However, the literature on tablets is very relevant to this thesis and is covered in this literature review.

Disintegration is the breakdown of an aggregate into smaller fragments as a result of internal stress build up. In many instances, this results in the tablet or agglomerate dissolving completely in the solvent. However, there are non-dissolving systems where a suspension is the desired end result (Markl and Zeitler, 2017). The initial cause of disintegration is liquid (solvent) penetration inside the agglomerate, which is caused by the affinity between the solvent and agglomerate components, notably the disintegrant. When the forces within a tablet or granule exceed the total cohesive forces, disintegration and dissolution commence. Hydrogen bonds, van der Waals, capillary, and electrostatic forces are examples of these cohesive forces (Quodbach and Kleinebudde, 2016).

The disruption of particle-particle bonds is one of the most important processes contributing to tablet disintegration and matrix fragmentation. The particles within an agglomerate may be subject to a variety of binding forces. Van der Waals are the most frequent but depending on the materials used to create the component pieces, other intermolecular forces, such as hydrogen bonds, may also occur. Another type of bonding force is mechanical interlocking, which includes the twisting and hooking of components within the agglomerate. This force

only arises when the compaction load is large, as in the case of tablets, and is significantly influenced by the formulation and surface structure. In other words, the amount of contact surface increases the possibility of interlocking (Karehill and Nyström, 1990). The tablet disintegration takes place because of the breaking of these bonds (Desai *et al.,* 2016). Then the following physical changes take place inside the agglomerate:

i) particle rearrangement
ii) agglomerate deformation
iii) new bond formation
iv) fragmentation

All these actions have a significant impact on either weakening or strengthening the agglomerate. Depending on the components and the degree of displacement within the agglomerate, the deformation of the agglomeration may be elastic, plastic, or even viscoelastic. These mechanical and rheological properties may have a significant effect on the drug release mechanism and polymer breakdown (Grassi *et al.,* 2000). Inter-particle bonding forces are dissipated within the agglomerate, but new bonds are also formed. The agglomerates' cohesive force will increase as a result, and the capillary bridges created by liquid capillary force will reinforce it. In other words, there are both positive and negative effects of liquid penetration on the disintegration process. When the tensile strength of these inter-particle links is reached and they can no longer maintain their cohesion, the agglomeration experiences a process known as fragmentation or breakdown. This process of fragmentation continues for smaller agglomerates produced during the disintegration phase until fundamental aggregates are achieved or agglomerates are dissolved away by dissolution (Figure 2.19) (Markl and Zeitler, 2017).

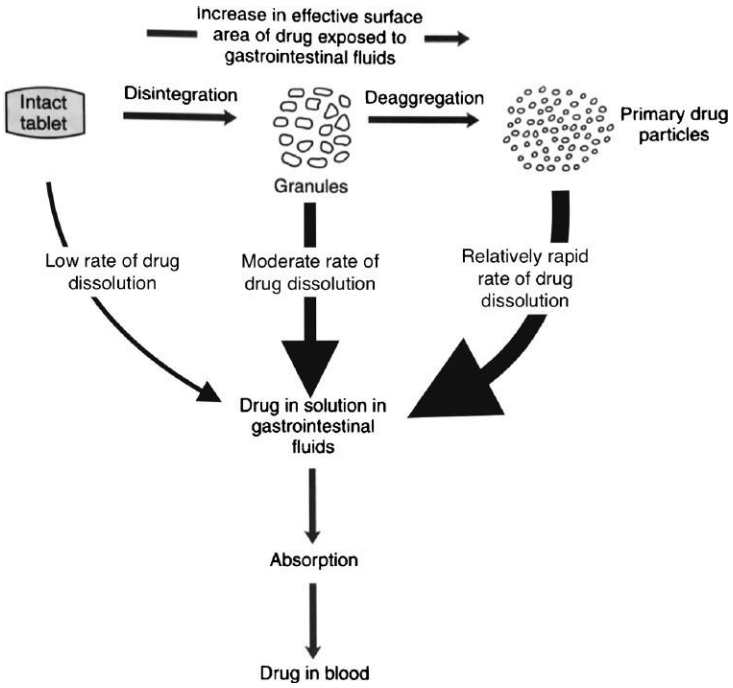

Figure 2.19: Schematic of the drug release process from a tablet (Markl and Zeitler, 2017)

Mechanical interlocking is more likely, and the contact level decreases when particles are more rounded (closer to a spherical shape), whereas twisting and hooking are more common when particles have an irregular shape. Another type of bonding that greatly impacts agglomeration strength is the entanglement of polymer binders. Molecular structures like polymers can have chains that can entangle with one another to form a web of entanglements because of their lengthy chains and local freedom of movement. The strength of agglomeration can be dramatically changed by these interactions with polymeric binders, especially if the polymer's molecular weight reaches a threshold value or if it has a high degree of branching (Li *et al.*, 2011). Additionally, the fourth type of bonding is solid bridges, which function at short distances due to atomic-level interactions. These forces primarily manifest themselves when particles go through chemical or physical changes like melting or crystallisation. The fifth type of force is the capillary force, which is caused by liquid permeating the agglomerate. The fluid-solid interface forces, which can be enhanced by smaller pore diameters, are the main contributions to the capillary force.

2.5.2.1 Wicking or liquid penetration

Wicking is the process of liquid penetration to the porous material which is the first step and rate-determining step in the disintegration process. It plays an essential role in initiating other disintegration mechanisms (Figure 2.20) (Markl and Zeitler, 2017). By itself, liquid penetration weakens the tablet's structure through reduction of interparticulate bonds by decreasing hydrogen, van der Waals, and electrostatic bonds. In the wicking process, the capillary action of the liquid in the pores of the microstructure displaces air into the micro-structure cavities. (Desai, Liew and Heng, 2016). Liquid penetration rate is determined by the equilibrium between capillary and opposing viscous forces (Quodbach and Kleinebudde, 2016).

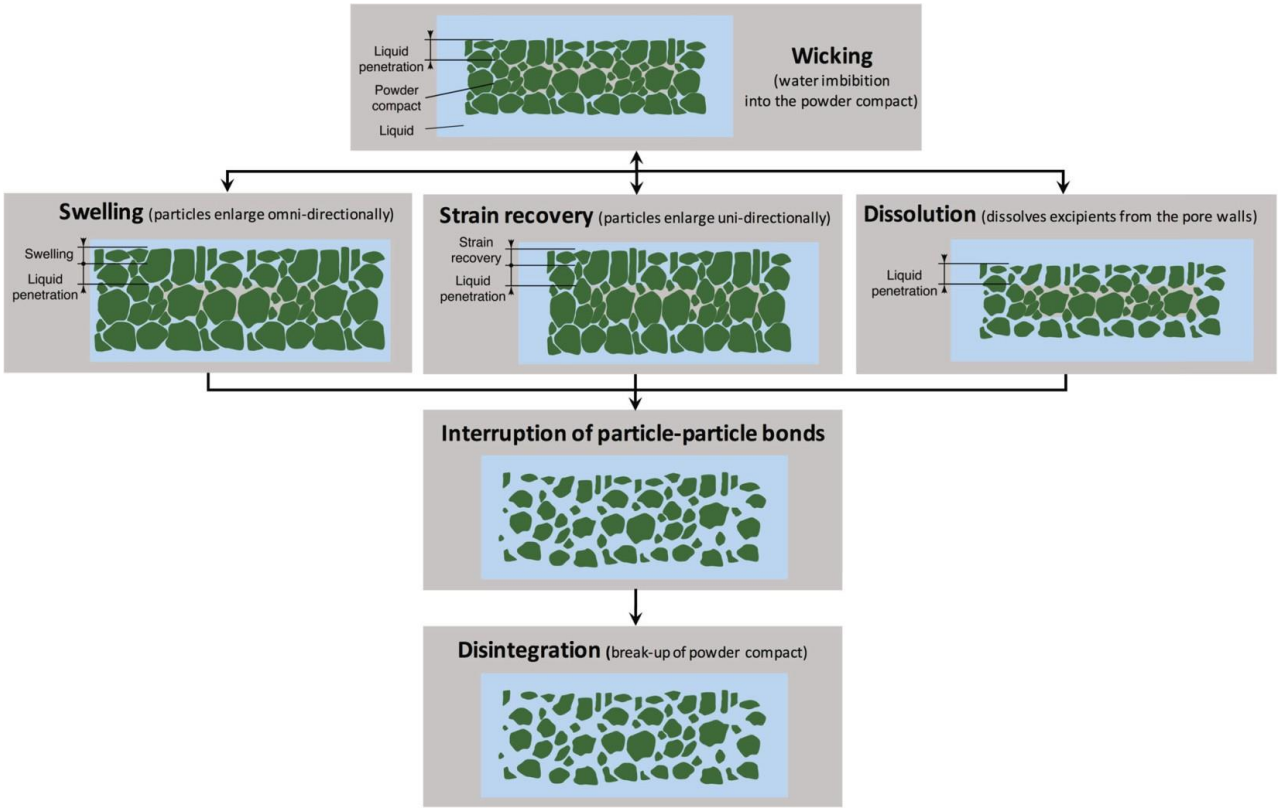

Figure 2.20: Overview of mechanisms involved in the disintegration of pharmaceutical powder compacts (Markl and Zeitler, 2017)

2.5.2.2 Swelling

The most common mechanism involved in disintegration is swelling. Numerous dissolving agents play the role of swelling, which is the expansion of the particle's volume upon contact with dissolution fluid. This volume increase causes a build-up of pressure and stress on the entire system, resulting in its disintegration (Markl and Zeitler, 2017). Several variables, such as the chemical structure and porosity of the tablet matrix, might affect the swelling and disintegration process. Using extremely high compression forces during the tableting process yields tablets with limited porosity. Low porosity can impede liquid ingress and lead to disintegration failure or prolonged disintegration times (Desai *et al.,* 2016). The presence of void spaces in a porous agglomerate allows the polymer chains to relax more quickly. This interferes with the swelling process and makes disintegrants less effective. In rare circumstances, this effect can be great enough to stop the process of disintegration (Diersch *et al.*, 2010).

2.5.2.3 Strain recovery (shape recovery)

Strain recovery is another mechanism of disintegration; it is a reversible viscoelastic deformation process. When in contact with a liquid media, the disintegration polymer becomes hydrated, and polymer chain activation occurs, resulting in the partial return of their original shape. During this process, the recovery of the stressed particles causes the rupture of bonds, and tablet disintegration occurs owing to the production of pressures (Desai *et al.,* 2016).

As a result of the penetrated liquid's plasticising impact, polymer chains become sufficiently mobile to allow for entropy recovery and the restoration of the polymer molecules' original shapes. Shape recovery is therefore considered to be the reversible viscoelastic deformation process (Patel *et al.,* 2007). It is uni-directional and in the opposite direction of the compression force (Figure 2.20). Quodbach *et al.,* (2014) studied the shape recovery mechanism of XPVP using high resolution real-time magnetic resonance imaging (MRI). They examined the expansion behaviour of tablets containing various disintegrants in order to find more evidence for the shape recovery mechanism. They assumed that swelling is responsible for any omnidirectional expansion and strain recovery is responsible for any unidirectional motions, particularly those in the opposite direction of compression.

2.5.2.5 Erosion

Erosion is a significant mechanism that can also contribute to the disintegration process. It is a process in which a stimulus causes a particle to erode. Erosion processes are frequently sub-classified into two categories: chemical and physical controlled erosion. According to Sackett and Narasimhan (2011), the term "chemical erosion of polymers" refers to a combination of diffusion, dissolution and degradation processes (Figure 2.21). Furthermore, polymer erosion can be affected by polymer swelling, pore formation, and gel formation. Erosion is a combination of coupled and simultaneously occurring processes. The erosion rate and behaviour of a particular system may be controlled by one or more of these processes. Swelling and gel formation both can delay the erosion process shown in Figure 2.21 by reducing the ability of water to completely entering into the polymer. Several studies (Kipper and Narasimhan, 2005; Sackett and Narasimhan, 2011) discuss a chemically oriented process where the polymer undergoes a degradation reaction as a result of reactions like hydrolysis. This contrasts with physically controlled erosion, which occurs solely at the surface. Chemically controlled erosion can occur both at the surface and within the bulk. Another study (Scurati *et al.*, 2005) discusses physical erosion caused by hydrodynamic forces imposed by the liquid flow. Physical erosion can occur in nearly any system if there is a shear force between the particle and the surrounding liquid, unlike chemical erosion, which is dependent on the chemical structure of the polymer. It has been reported that in systems containing dry agglomerates, the hydrodynamic forces produced by the viscous flow surrounding the agglomerates can result in phenomena like erosion (wearing) or even fragmentation (rupture), which causes dispersion (Scurati et al., 2005).

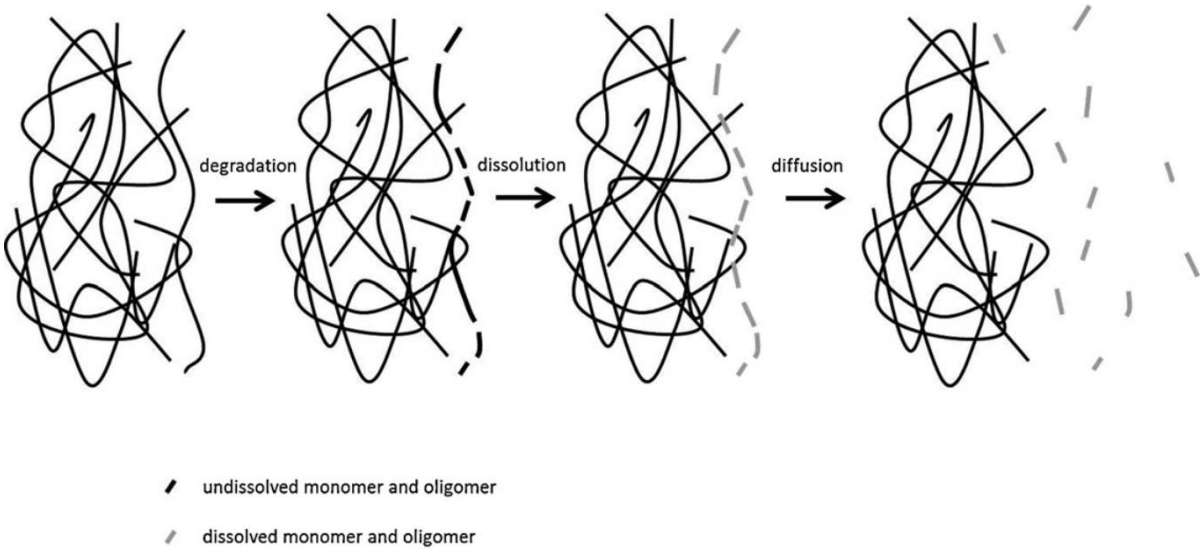

Figure 2.21: The process of polymer erosion, which is a combination of degradation, dissolution and diffusion (Sackett and Narasimhan, 2011)

Disintegration has historically received less attention in the literature than its closest counterpart, dissolution. This may be due in part to the complex mechanisms already mentioned, and the lack of experimental techniques to simultaneously monitor different aspects of disintegration (Markl and Zeitler, 2017). Numerous research projects and papers on the topic of granular materials' disintegration over the past two decades have illustrated the growth of this field of study. These projects and papers were made possible by advances in the theoretical and experimental fields (Sweijen *et al.*, 2017).

Van den Ban and Goodwin (2017) studied tablet disintegration and tablet dissolution as a function of granule filling density. The tablets were made by compressing MCC and lactose monohydrate granules. The tablet disintegration was controlled by tablet porosity; hence the tablet microstructure plays an important role in achieving the required product performance. Tablet dissolution at 15 min and 20 min is affected by porosity and the dissolution was near complete at 25 to 30 min (Figure 2.22). Decreasing tablet porosity (increasing solid fraction) impacts tablet dissolution through an increase in disintegration time. The effect of porosity on the disintigration process was also recently studied by Maclean *et al.*, (2021). Tablets were manufactured by direct compression using two formulations. Each formulation consisted of two fillers (47 % each), MCC/lactose and MCC/dibasic calcium phosphate anhydrous (DCPA) with sodium starch glycolate (SSG) as a disintegrant and magnesium stearate as a lubricant. They reported that for the MCC/lactose tablet, increasing the tablet porosity by 2 % causes

reduction in the dissintigration time by 77 %. For the MCC/dibasic calcium phosphate anhydrous (DCPA), increasing tablet porosity by 2 % reduced dissintegration time by 3 %. These findings illustrate the important influence of tablet formulation and porosity on the disintegration and performance characteristics.

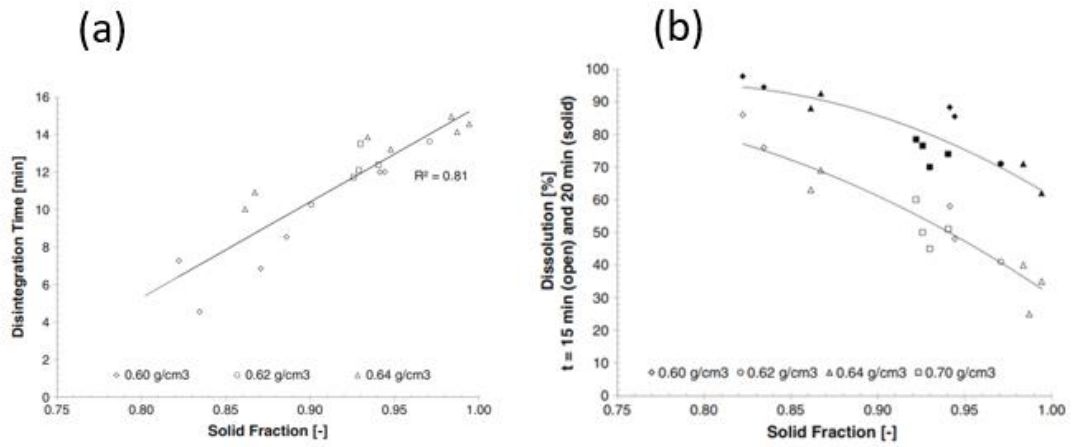

Figure 2.22: (a) Disintegration time as a function of solid fraction (tablet density) and (b) Dissolution at 15 min and 20 min as a function of solid fraction (tablet density) (van den Ban and Goodwin, 2017)

2.5.3 Summary

Despite the disintegration process having a significant impact on drug release, surprisingly little research has been conducted to understand and quantify this crucial process using a mechanistic approach. This might be explained by the disintegration process' intricacy and the challenges associated with observing and measuring it. When attempting to understand and quantify the mechanical breakdown of tablets and agglomerates, Markl and Zeitler (2017) noticed a number of difficult issues:

i) There are many different types of formulations of disintegrating matrices which can interact with chemical and physical properties of API and excipients making each formulation distinctive and difficult to quantify.

ii) The dissolution or erosion process in some formulations can interfere with disintegration, causing a non-linear behaviour over time.

iii) The granulation method (dry/wet) or compaction conditions have a significant effect on the agglomerate/tablet properties such as porosity or tensile strength.

iv) The impact of changing the excipients physical properties on the particle size, disintegration, morphology and distribution have received less attention than the effect of chemical properties. There is a lack of reliable tests to quantify and monitor the disintegration mechanisms. These tests are important to clearly understand the disintegration process in depth. Furthermore, it is essential to know the limitations and capabilities of the experimental tests, and what data they can offer (Markl *et al.*, 2017).

2.6 Summary

This review has summarized the most important studies related to the effect of process parameters on granule structure. Furthermore, the literature studies of the effect of the liquid to solid mass ratio (L/S) and the granulation time on the granule microstructure have been presented. Several studies of tablet dissolution prepared by compression of granules have also been summarised. However, until recently, little experimental data is available for granule dissolution:

- Lack of experimental studies of the effect of the granulation process on both the granule structure and granule performance on the same granule, as most of the previous studies were carried out on the tablet performance.
- No explicit studies on the direct relation between drug release and granule porosity.
- No explicit studies on the effect of a wide range of granulation times (2.5, 5, and 10 min) and a lack of explicit studies of the effect of binder quantity in a wider range (e.g. 0.8, to 1.2 L/S mass ratio).
- Lack of experimental studies on single granule swelling through linking the granule porosity and dissolution profile.

The overarching aims of this work are to further develop the understanding of the relationships between the aforementioned process parameters, granule structure (in particular, pore size), and the effect of these structural properties on dissolution and drug release (Figure 2.23).

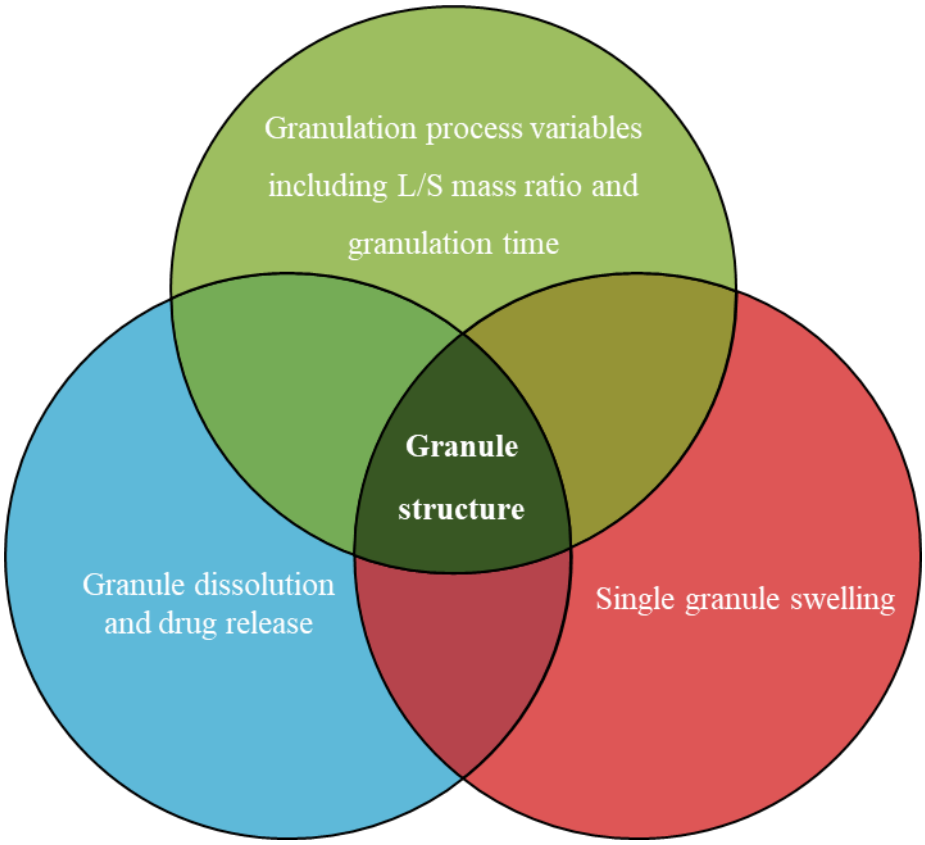

Figure 2.23: Linking drug release to the granulation process

CHAPTER 3 - Materials and Methods

3.1 Background

The aim of this work was to design a suitable experimental methodology to enable a deeper understanding of the scientific relationship between granulation process, granule structure and performance. The methodology can be described in three main steps:

1- High shear granulations: (a) the effect of liquid to solid mass ratio (0.8, 1.0 and 1.2) and (b) granulation time (2.5, 5 and 10 min), on granule structure. An insufficient amount of liquid binder (less than 0.8 L/S) generated under-granulated, fragile granules with a high fraction of fines. Increasing the L/S to more than 1.2 produced lumps and an over-wetted mass. For this reason, a L/S ranging from 0.8 to 1.2 was selected for this study.

2- Dissolution and drug release experiments to relate performance to granule structure.

3- Single granule dissolution experiments to investigate granule swelling and disintegration as a function of granule structure.

3.2 Materials

In this thesis, granules were made from aspirin as the active pharmaceutical ingredient, microcrystalline cellulose (MCC) as the excipient and PEG 4000 as the liquid binder. This formulation was chosen because MCC enables granulation with a range of L/S ratios using aqueous PEG 4000, and due to its ability of absorbing large amounts of water. Moreover, MCC granules can release the drug for a longer duration of time compared to lactose granules.

3.2.1 Acetyl salicylic acid (aspirin)

In these experiments, acetyl salicylic acid (aspirin) was used as a model active component and was purchased from Sigma-Aldrich, Ltd, Germany. Aspirin is a white crystalline substance, slightly soluble in water. This material was ground to specific size (d_{50} = 41.7 μm) to be granulated with MCC.

Grinding of aspirin was performed by placing 300 g of aspirin into a ball mill apparatus (Glen Greston, UK) (5 L mill pot). For the grinding process, 3 kg of different sizes of balls (1 inch, 1/2 inch and ¼ inch diameter**)** were filled in the mill pot with the aspirin crystals. After 10 min of grinding, the mill pot was emptied and balls with the ground aspirin placed in a tray (Figure 3.1). The ground aspirin was collected from balls' surfaces using a brush and passed through a 150 µm mesh sieve (Retsch) (Figure 3.2). This powder with a particle size < 150 µm was used for granulation.

Figure 3.1: Milling balls used to grind aspirin

Figure 3.2: Sieving aspirin powder using 150 µm mesh sieve

3.2.2 Microcrystalline cellulose (MCC)

Microcrystalline cellulose (MCC) (d_{50} = 65.4 μm) was used as excipient and was obtained from HARKE Pharma GmbH, Germany. MCC is widely used as an excipient in pharmaceutical, cosmetic and food industries due to its physical and chemical inactivity, good compressibility during tablet production and lack of toxicity. It is hygroscopic and requires extra liquid binder for granulation compared to other excipients such as lactose (Rowe *et al.*, 2009). MCC enables granulation with different liquid amounts due to its ability of absorbing large amounts of water leading the production of granules with different internal structures (Bouwman *et al.* 2005). Due to the fact that MCC is hygroscopic, it can speed up diffusion and capillary action while improving liquid transport into a tablet matrix (Yassin *et al.*, 2015).

3.2.3 Polyethylene glycol 4000

Polyethylene glycol (PEG 4000) was used as a binder and was purchased from Sigma-Aldrich, Ltd, Germany. PEG is inert, has low toxicity, is available in a range of molecular weights, and can be employed as a liquid or solid binder in wet granulation (Rowe *et al.*, 2009). In these experiments, the liquid binder consisted of 10 % w/w solution of polyethylene glycol (PEG) 4000 in water. Each batch of liquid binder was prepared by dissolving 10 g of PEG powder in 90 g of distilled water, and mechanically stirred until completely dissolved.

3.2.4 Raw material characterisation: particle size distribution

The particle size distributions (PSD) of MCC and ground aspirin were determined by laser diffraction using a Malvern Mastersizer 3000. By detecting the variance in light intensity scattered when a laser beam passes through a dispersed particulate sample, laser diffraction determines the particle size distribution. In relation to the laser beam, small particles scatter light at a large angle while large particles scatter light at a small angle (Figure 3.3). The Mie theory of light scattering is then used to the variation in angular intensity data to determine the particle size responsible for the scattered pattern (Ryzak and Bieganowski, 2011).

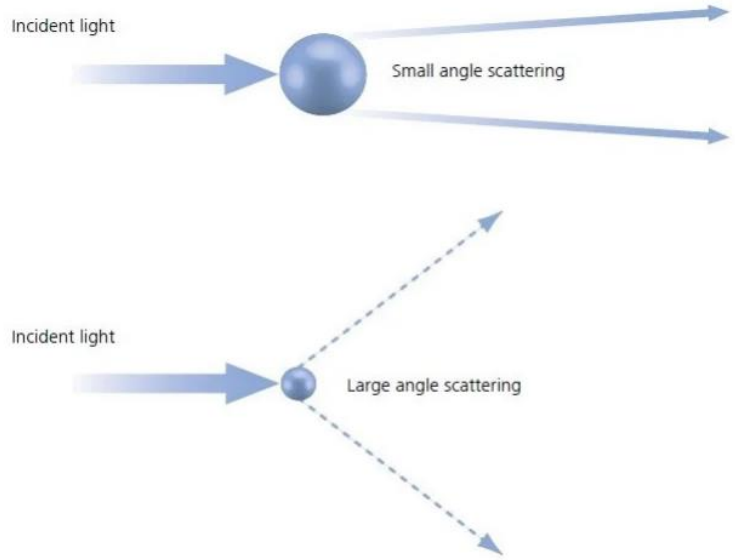

Figure 3.3: Principle of laser diffraction (Panalytical, 2013)

The key factor in the success of laser diffraction is that it is a commonly utilised technology for determining particle size for materials in the nanometer to millimetre particle size range. There are further benefits, including quick measurement, strong repeatability when numerous particles are collected with each measurement, immediate feedback, and high sample throughput.

Three percentile values (d-values) are frequently obtained from the volume frequency distribution plot. The diameter when all particles in a sample are ordered in ascending mass is the d-value, which is the diameter divided by the sample's mass into a defined percentage. The mass percentage below the diameter of interest is indicated by the number after the letter "d." For instance, d_{10} is the diameter when particles less than this size account for 10 % of the sample mass. The d_{50} is the diameter at which 50 % of the mass of a sample is made up of particles with diameters smaller than this. The mass median diameter is another name for the d_{50}. When 90 % of the sample mass is present, the diameter is known as the d_{90} and this means 90 % of the distribution is smaller than this particle size (Allen, 2013).

In this study, the PSD of microcrystalline cellulose and ground acetyl salicylic acid were measured by laser diffraction using the dry method (Figure 3.4). The measurements were performed in triplicate. The analysis was performed and the powder feeder was vibrated at 30 % to ensure smooth movement of the powder and avoid blocking the internal orifices of the

equipment. This gave an obscuration within 2 and 7 % at a pneumatic pressure of 2.5 bar for microcrystalline cellulose and 0.5 bar for ground acetyl salicylic acid.

Figure 3.4: Malvern Mastersizer 3000 (Malvern Instruments Ltd., UK)

Figure 3.5 and 3.6 show the PSD for ground aspirin and MCC respectively. Table 3.1 shows the d_{10}, d_{50} and d_{90} of these materials.

Table 3.1: Particle size of raw material

Material	**Particle size (µm)**			**Span**
	D_{10} (µm)	D_{50} (µm)	D_{90} (µm)	
Ground acetyl salicylic acid	6.98	41.70	156	3.56
Microcrystalline cellulose	19.90	65.40	165	2.21

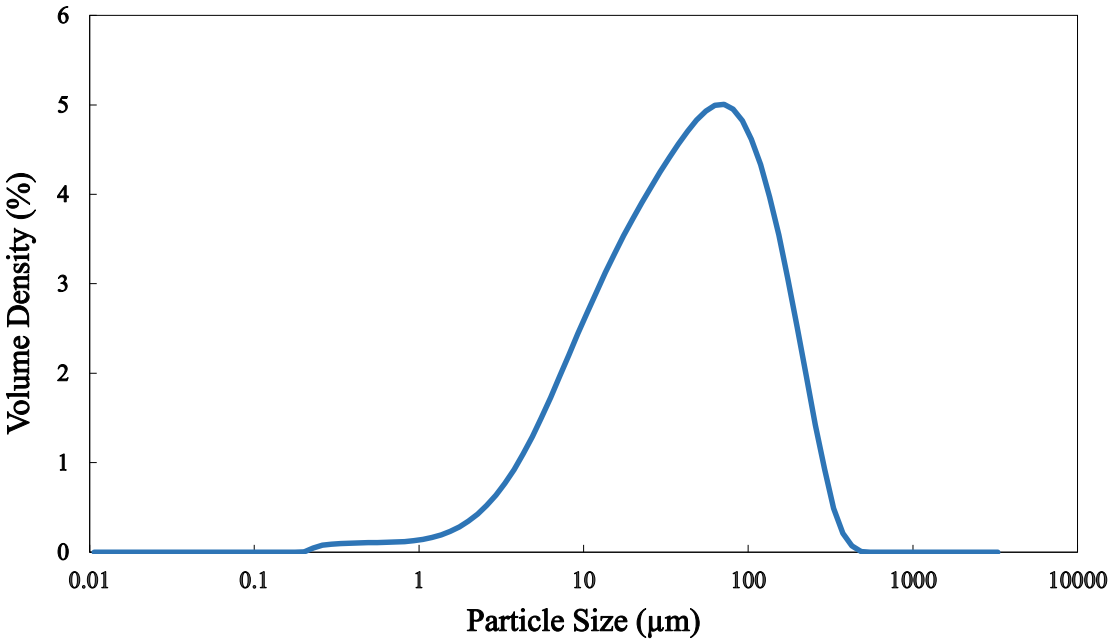

Figure 3.5: Particle size distribution of ground aspirin powder

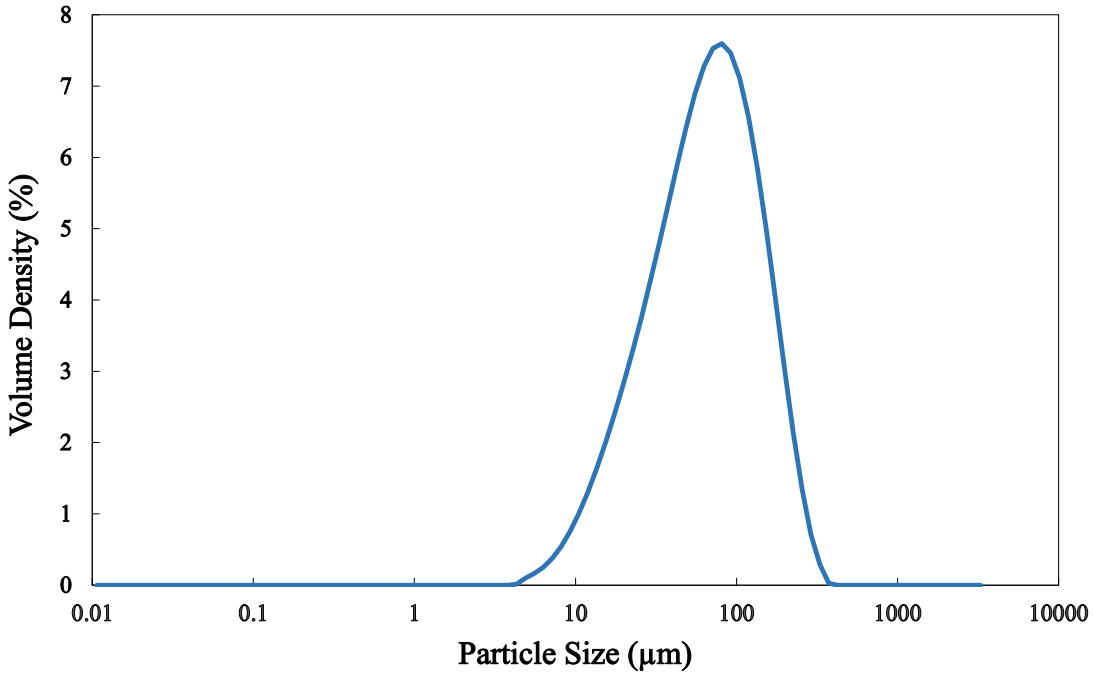

Figure 3.6: Particle size distribution of microcrystalline cellulose

3.3 Production of granules

A Key International laboratory scale high-shear mixer granulator (Englishtown, N.J., USA) (3.7 L bowl, without a chopper) was used to produce granules (Figure 3.7). For all experiments, 90 g of MCC and 10 g of aspirin were added to the granulator. The powder feed was pre-mixed for 2 min at an impeller speed of 250 rpm, at which point the impeller speed was raised to 400 rpm, and the liquid binder was added at a flow rate of 80 ml/min using a syringe pump (Fusion 100 KR Analytical Ltd). For most experiments a post-liquid addition wet massing time of 4 min was used, for a total granulation time of 5 min. For some experiments, the effect of granulation time was investigated, and granulation times of 2.5 and 10 min were used. The liquid binder mass addition was also varied, producing L/S of 0.8, 1.0 and 1.2. In total, five different granulation conditions were performed, and the experimental conditions are summarized in Table 3.2. Granules were dried in ambient conditions (21 °C) overnight (Figure 3.8).

Table 3.2: Summary of experimental conditions

Experiment No.	Mass of Aspirin (g)	Mass of MCC (g)	Mass of PEG (g)	L/S mass ratio	Binder injection time (sec)	Wet massing time (min)	Total Granulation time (min)
1	10	90	80	0.8 L/S	60	4	5
2	10	90	100	1.0 L/S	75	3.75	5
3	10	90	120	1.2 L/S	90	3.5	5
4	10	90	120	1.2 L/S	90	1	2.5
5	10	90	120	1.2 L/S	90	8.5	10

Figure 3.7: High-shear mixer granulator set up

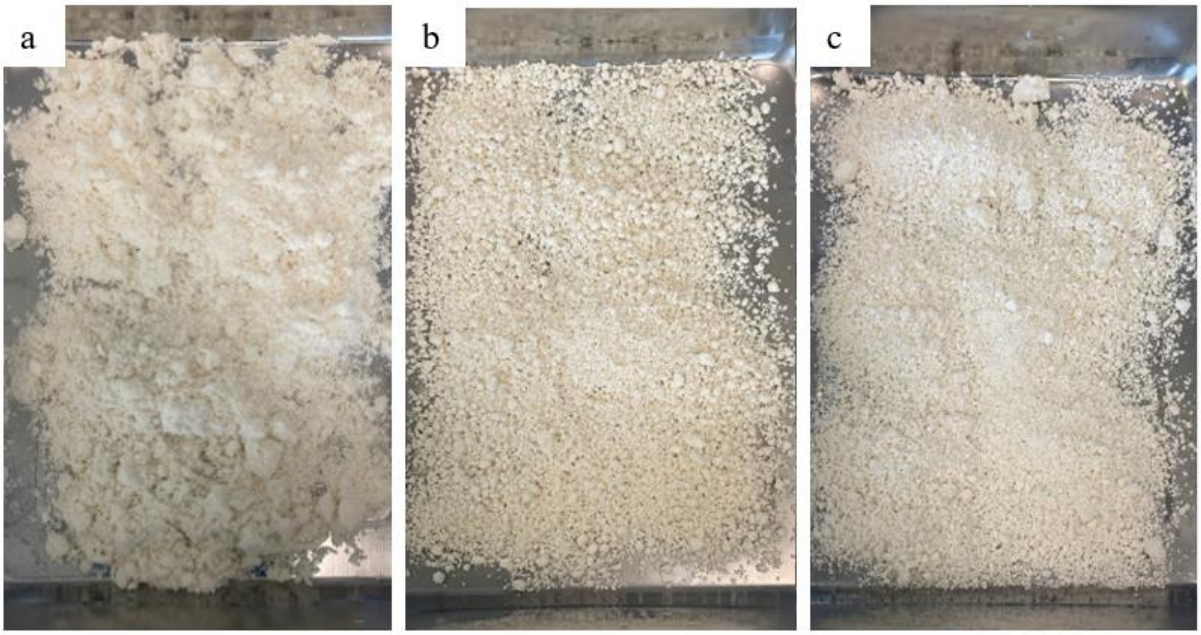

Figure 3.8: Granules drying in trays in ambient conditions (21^{0}C) overnight (a) 0.8 L/S; (b) 1.0 L/S and (c) 1.2 L/S granules

3.4 Granule characterisation

3.4.1. Granule size

In order to consistently measure the release kinetics of the granules produced in this work, a fraction of granules was harvested by sieving between 2000 and 3600 μm (Figure 3.9). This sieve fraction of granules was further characterised for granule porosity, internal structure and release kinetics.

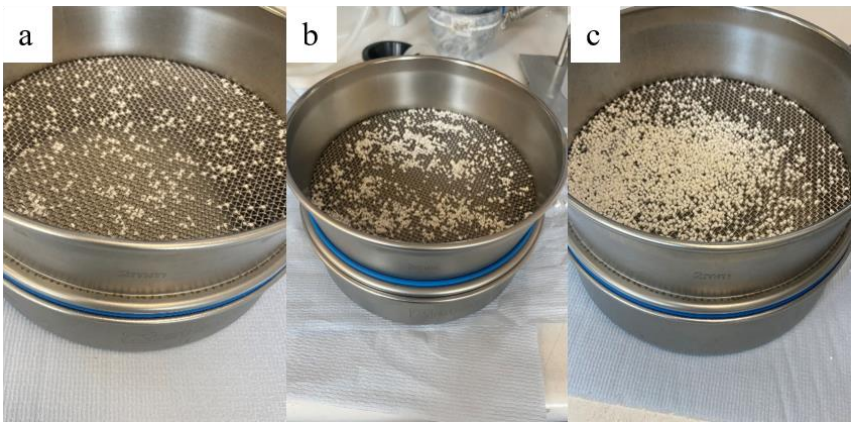

Figure 3.9: Sieve fractions of granules from 2000 to 2360 μm: (a) 0.8 L/S and (b) 1.0 L/S and (c) 1.2 L/S granules

3.4.2 Granule porosity

Porosity is an important property of pharmaceutical granules which can affect their dissolution behaviour. Therefore, it is essential to measure the granule porosity at the initial stage in this study. The granule porosity for the granule size of 2000-2360 μm was measured using three different discrete techniques described in the following sections.

3.4.2.1 Pycnometry

In the pycnometry technique, the granule envelope and true density were measured separately and then the porosity was calculated. Envelope density is defined as mass of the particle over its total volume including all pores (Figure 3.10 (a)) (Litster, 2016b).

A Geopyc 1360 Envelope & T.A.P Density Analyzer (Micromeritics, Norcross, USA) (Figure 3.11) was used to determine the envelope density and volume of particle samples through measuring the displacement of Dryflo powder. This type of powder has ability to achieve close packing around the sample due to its high degree of flowability, spherical shape and small size (200 μm). The dry powder is unable to enter the pores of the sample but captures the irregularity of the particle shape, thereby giving a volume of displaced powder equal to the particle, including the pores (Wade *et al*., 2015).

For the measurements, granules with a size classification of 2000-2360 μm were weighed (0.20 g) and placed in the sample chamber (an amount less than 25 % of the chamber volume). The powder was compressed by a plunger at a force of 28 N. The measurements were performed in triplicate for each sample.

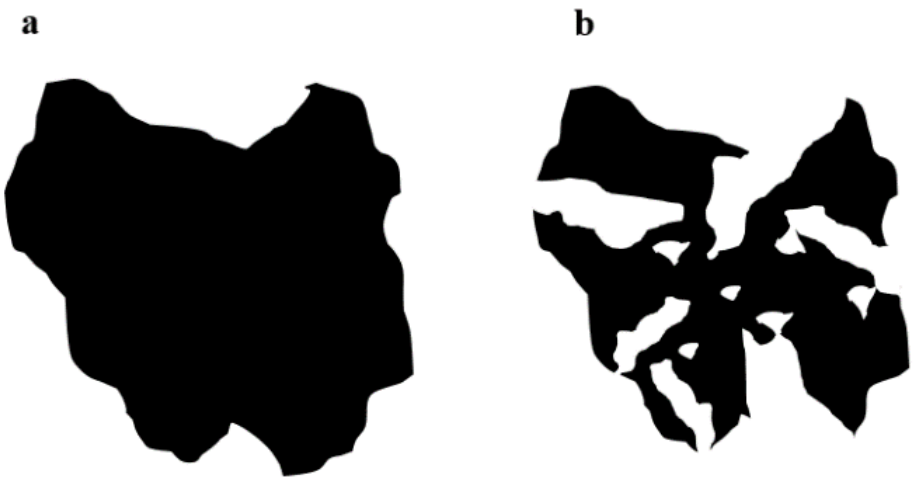

Figure 3.10: (a) Envelope density and (B) and true density (Litster, 2016b)

Figure 3.11: Geopyc 1360 Envelope & T.A.P Density Analyzer (Micromeritics, Norcross, USA).

Figure 3.12: AccuPyc 1340; Micromeritics (Norcross, Georgia, USA)

True density is comparable to envelope density, with the exclusion of the volume of closed pores (Figure 3.10 (b)). True density is calculated by dividing the mass of a solid material by its volume, minus any internal porosity. Helium pycnometry is a non-destructive technology since it measures volume using the gas displacement method. Helium gas is employed as a medium of displacement. It is regarded as the most accurate technique for measuring true volume and density (Micromeritics 2015; Nordström *et al*., 2015; Wade *et al*., 2015).

The true density of the 2000-2360 μm granules was measured by helium pycnometry; AccuPyc 1340, Micromeritics (Norcross, Georgia, USA) (Figure 3.12). 0.20 g of granules were weighed and deposited in the 10 cm^3 instrument chamber. Helium gas flows into the sample chamber (purging stage) to purge the chambers and pipes of all other gases, particularly oxygen and

nitrogen. Subsequently, the measuring phase began, which consisted of five cycles. During this phase, helium was introduced into the sample chamber until the desired pressure of 19 N/m^2 was achieved. The helium molecules filled the pores. Then, helium was introduced into a second chamber with a known capacity. Observing the pressures upon filling the sample chamber and then emptying it into a second chamber allowed for the computation of the sample solid phase volume. The acquired volume was divided by the weight of the sample to determine the gas displacement density. Afterwards, the pressure was released into the atmosphere. The mean of three measurements was calculated for each sample of granules. The granule porosity was then calculated from the granule envelope and true density using Equation (3.1):

$$\varepsilon = 1 - \left(\frac{\rho_e}{\rho_t}\right) \times 100 \tag{3.1}$$

where ε is the granule porosity, ρ_e is the envelope density and ρ_t is the true density.

3.4.2.2 Mercury porosimetry

For many years, porosity and pore size distribution have been measured using mercury intrusion porosimetry (MIP) (Liu *et al.*, 2014). Equation (3.2) explains how the Washburn equation was used to determine the diameter of pores: where *P* is the pressure difference across the mercury interface to the equivalent pore size (r), and γ is the mercury's surface tension (mN/m), θ is the contact angle between the mercury and the material (Giesche, 2006).

$$\Delta P = \frac{2\gamma\cos\theta}{\mathrm{r}} \tag{3.2}$$

By using the Washburn equation, the values of the intrusion pressure are immediately converted into the equivalent pore size (Giesche, 2006). The volume of pores in the relevant size class can be calculated by measuring the volume of mercury that enters the sample material with each change in pressure. A mercury penetrometer measures the amount of mercury that enters pores (an electrical capacitance dilatometer). These instruments are extremely sensitive and can pick up changes in mercury volume under 0.1 µL (Liu *et al.*, 2014). However, it is important to recognise that mercury porosimetry has limits. One of the most significant limitations is that it only measures the largest entrance to a pore (Figure 3.13), not the true inner size of the hole. It also cannot be used to evaluate closed pores for obvious reasons, as the mercury has no method of entering those pores. (Giesche, 2006).

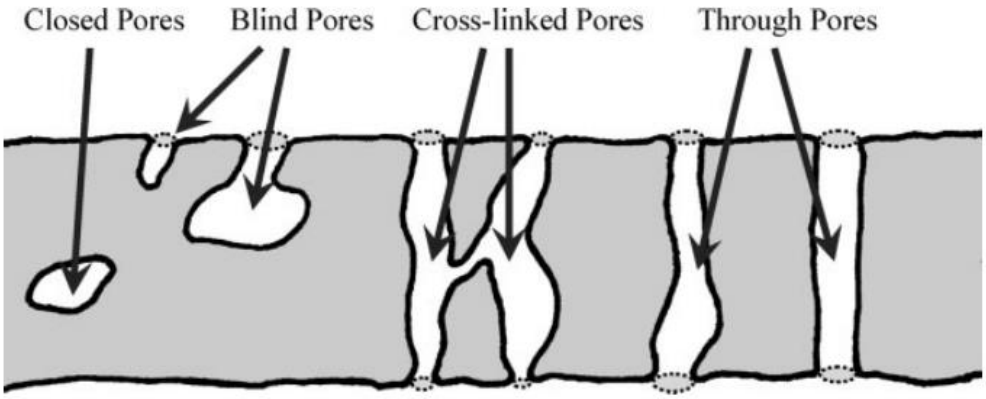

Figure 3.13: Schematic representation of pores (Giesche, 2006)

Mercury porosimetry drives mercury into the pores of a porous solid using external pressure based on the physical fact that mercury is a non-wetting fluid for the majority of materials. Mercury can be squeezed into pores that are getting smaller while being subjected to greater pressure. Consequently, the fundamental mercury porosimetry experiment entails gradually increasing the applied pressure while measuring the amount of mercury that enters the sample during each pressure increase (Moura *et al.*, 2005). Both the applied pressure, *p*, and the mercury volume, *V*, are recorded during the measurement. From the collected data, the sample's pore structure can be determined. Pores of approximately 3.5 nm can be investigated. Complete analysis may require considerable time. Mercury porosimetry gives an extensive range of data, such as the pore size distribution, the total pore volume or porosity, the skeletal and apparent density, and the specific surface area of a sample (Giesche, 2006).

For the measurements, 0.3 g of sample was weighed and carefully transferred to the penetrometer chamber. The top of the chamber around the outermost edge was greased with Apiezon H grease and sealed with the metal lid. The lid was secured and the assembled penetrometer was weighed and recorded. The bulk density of the sample was calculated by win9500 software and the low and high pressure analysis can be performed through loading the sample in the specific port (Figure 3.14).

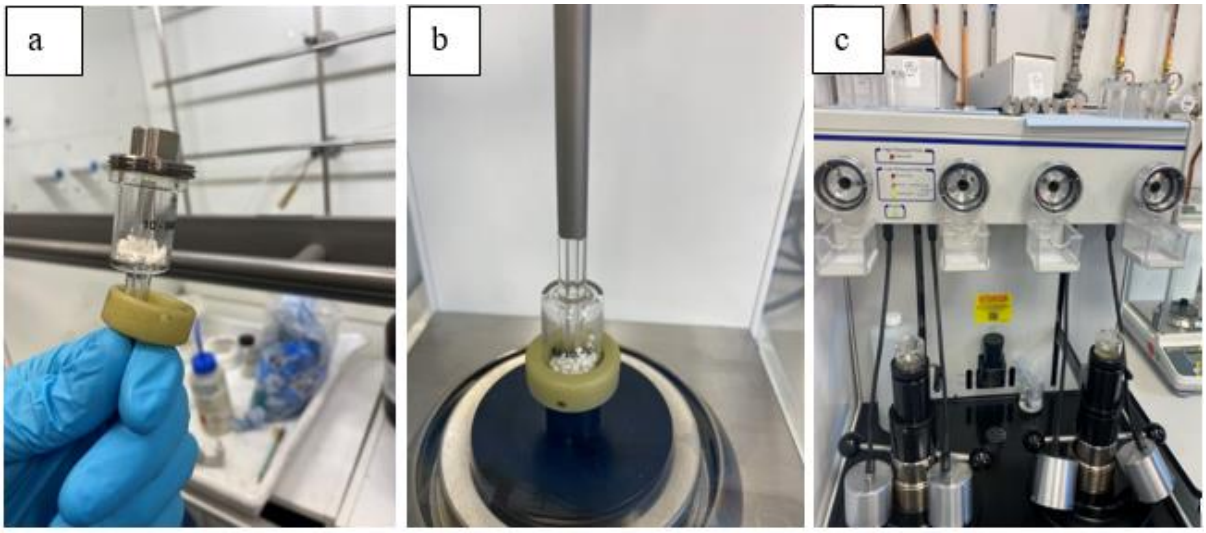

Figure 3.14: Mercury porosimetry measurement (a) sealing the camper with metal lid, (b) weighing the assembled penetrometer and (c) low and high pressure ports

3.4.2.3 X-ray computed tomography for internal structural analysis

Mercury porosimetry, as mentioned in the previous section, is a common method for measuring porosity. However, it is a destructive method with handling concerns, is time consuming and is a rather costly apparatus. Additionally, mercury is a dangerous substance. X-ray computed tomography is an alternate approach for measuring granule porosity (XRCT) (Farber *et al.*, 2003).

The late 1970s saw the development of XRCT, a relatively new technique that analyses differences in material density and is non-destructive technique. To characterise the porosity and morphology of granules with a size of 4 µm or larger, XRCT is a very promising tool. The pore shape and its spatial distribution can be determined qualitatively by XRCT. Additionally, it can provide a numerical measurement of granule total and local porosity (Farber *et al.*, 2003).

The instrument rotates the sample while the X-ray source and detector remain stationary (Zeitler *et al.*, 2009). An object that is placed in a specific sample holder is exposed to X-rays from a high power source and collected on the detector on the other side. With an angular increment, the sample holder is rotated around its z-axis (Perfetti *et al.*, 2010). In addition to the energy of the X-rays employed, the atomic number and density of the material being examined will also affect how much the X-rays attenuate after each rotation increment. The detector measures the X-rays' reduced intensity by using mathematical techniques, and two-dimensional sectional images are produced after the sample has been completely rotated and

from various angles. Using XRCT reconstruction techniques, high-resolution 3D visualisation images can be created from a series of successive two-dimensional intensity slices (Sondej *et al.*, 2015; Perfetti *et al.*, 2010; Farber *et al.*, 2003).

In this work, the granule microstructure was studied using XRCT (Skyscan 1172 Bruker, Belgium) with 4.17 µm pixel size resolution. A single granule was mounted on the sample stage of the XRCT (Figure 3.15). Then granule was scanned from 0-180° at intervals using a 0.7° rotation increment. A medium camera binning mode with 2000 x 1024 pixels was used. From each sample, three representative granules were measured. NRecon v.1.6.3 software (Bruker-micro CT) was used to reconstruct the images and then the cross sectional images of the granule were visualized. By selecting the region of interest of the reconstructed images, the total granule porosity was automatically measured using CTAn v1.14.4, Bruker-micro CT software. A total of 250 images were selected in each measurement and then the region of interest was selected for each image before starting the granule porosity measurements. The average of three porosity measurements was taken. Subsequently, the reconstructed images were inserted into CTvox64 software to create the 3D images of each granule.

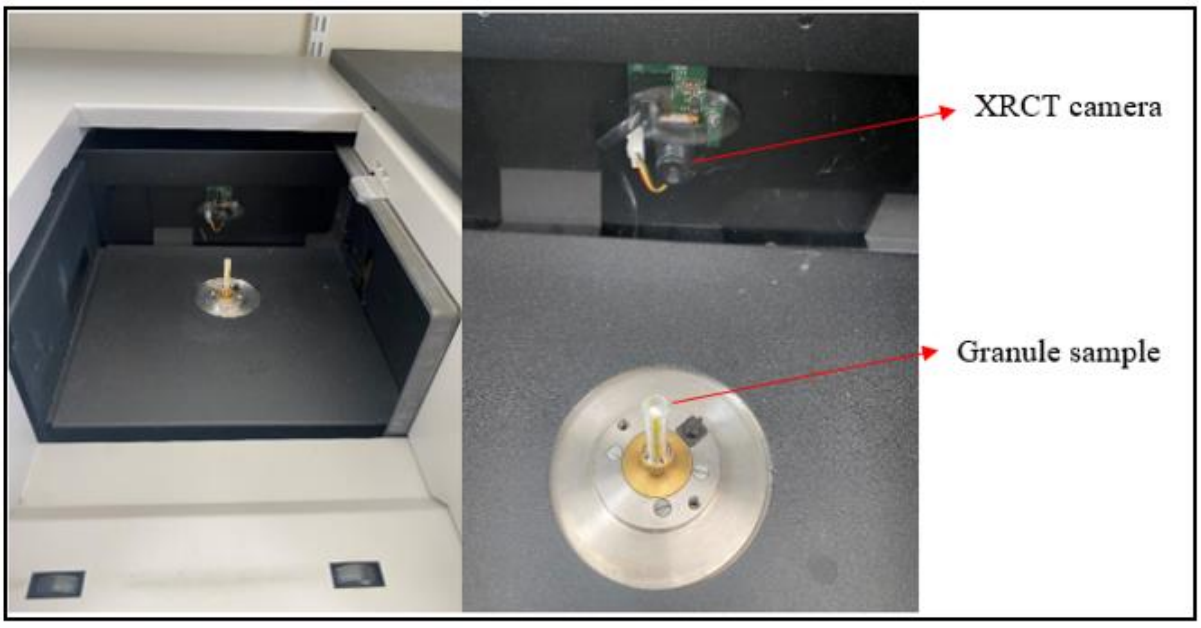

Figure 3.15: Individual granule stabilized on a plastic straw

3.5 Drug release performance

The dynamic drug release performance of the dried granules was performed in two stages: dissolution of granules followed by UV spectrophotometry (Thermo Scientific Genesis 10S) for measuring the aspirin concentration.

In general, the term “optical radiation” refers to electromagnetic radiation in the wavelength range between 100 nm and 1 mm. The terms “light” and “visible radiation” (VIS) refer to the wavelength range between 360 nm and 830 nm, which can be perceived by the human eye. Optical radiation with wavelengths shorter than 400 nm is called ultraviolet (UV). Optical radiation with wavelengths longer than 830 nm is called infrared radiation (IR).

A molecule of any substance has an internal energy which can be considered as the sum of the energy of its electrons, the energy of vibration between its constituent atoms and the energy associated with rotation of the molecule. The electronic energy levels of simple molecules are widely separated and usually only the absorption of a high energy photon, that is one of very short wavelength, can excite a molecule from one level to another. The sample composition has an impact on this feature, potentially revealing what is in the sample and at what concentration. A specific amount of energy is needed for the promotion of electrons in a substance to a higher energy state, which is observed as absorption. It takes varied amounts of energy to transfer electrons in different bonding situations in a substance to higher energy states. This clarifies why different substances absorb light at varied wavelengths. UV light has wavelengths that are about 100 nm shorter than visible light. UV-Vis spectroscopy, which locates the specific wavelengths that correlate to peak absorption, can be used to assess or identify distinct compounds since the wavelength of light can be utilised to define it. (Kothekar, 2012). UV-Vis spectroscopy is an analytical technique that used to measure the amount of discrete of visible light or UV wavelengths that are transmitted or absorbed by a sample in comparison to a blank or reference sample. According to beers lambert law (Equation 3.3), the unknown sample concentration can be calculated. In this equation, A is the sample absorbance, ε is the molar absorptivity which measure of how well a compound absorbs a given wavelength of light, L is the path length and c is the sample concentration.

$$A = \varepsilon L c \qquad \text{Equation (3.3)}$$

In this work, and for the calibration curve plotting, three distinct stock solutions of aspirin were prepared. Each stock solution was prepared by dissolving 50 mg of aspirin powder in 100 ml of distilled water. Seven serial dilutions from each stock solution were prepared. The absorbance of these dilutions was measured using a Thermo Scientific Genesis 10S UV spectrophotometer at 270 nm (Figure 3.16). The average of their absorbance was used to plot an aspirin calibration curve against the concentration (see Chapter 5, Section 5.2.1).

The dissolution of granules was carried out using a USP2 (paddle) apparatus in a Caleva 9ET dissolution tester (Figure 3.17). For each experiment, 0.3 g of granules was used. 900 ml of distilled water was used as dissolution media (pH = 6.8) at 37 °C (± 0.5), and the paddle rotation was set at 100 rpm. The dissolution media was sampled frequently. For the first 5 min of the test, 2.5 ml samples were withdrawn every 10 sec. Between 5 min and 60 min, samples were taken every 5 min, and every 30 min for the following four hours. A final sample was taken at the 5 hour mark. It must be noted that the sample volumes were replaced with distilled water as the same rate as they were drawn from the vessel. Solution samples were analysed using a Thermo Scientific Genesis 10S UV spectrophotometer at 270 nm to monitor drug release as a function of time.

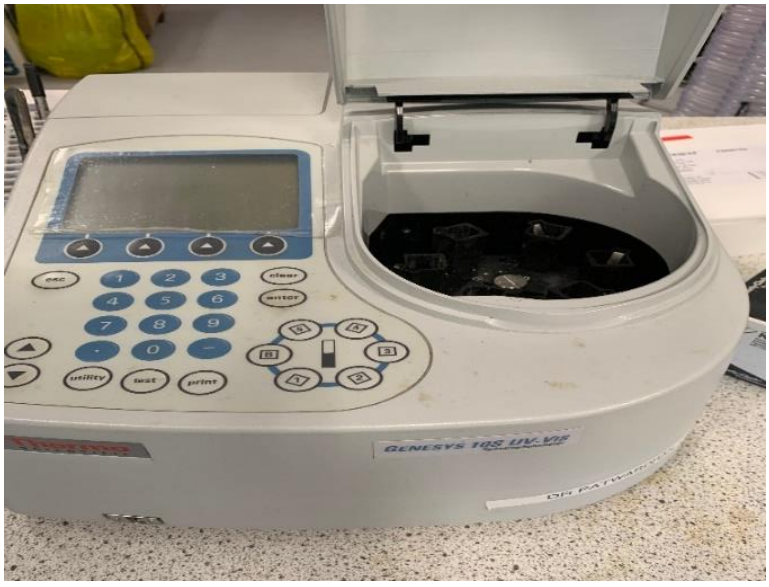

Figure 3.16: Thermo Scientific Genesis 10S UV spectrophotometer

Figure 3.17: Solution samples were analysed using a Thermo Scientific Genesis 10S UV spectrophotometer at 270 nm to monitor drug release as a function of time

3.6 Individual granule swelling study

Individual granule swelling behaviour during disintegration was studied by using a purpose-built flow cell method adapted from Soundaranathan *et al.*, (2020) and was equipped with an digital imaging technique and an optical coherence tomography technique (OCT), separately. In the digital imaging technique, a Navitar 12X zoom lens, coupled with a Pixelink PL-D753 colour camera (with uScope standard software) was used to visualize single granule behaviour under a continuous stream of water and measuring the changing in granule size as a function of time. In addition, the flow cell was equipped with optical coherence tomography (OCT) to perform 2D granule cross section imaging. Figure 6.18 shows schematic diagram of the experimental setup of the flow cell equipped with the chosen optical technique. The main objectives were to assess the feasibility of the flow cell for a single granule to quantitatively monitor and measure the granule diameter and granule swelling area with time. The purpose-built flow cell was 3D-printed, with OCT experiments performed in collaboration with the University of Strathclyde. The OCT experiments were specifically performed within the CMAC Advanced Future Manufacturing Research Hub laboratory facilities.

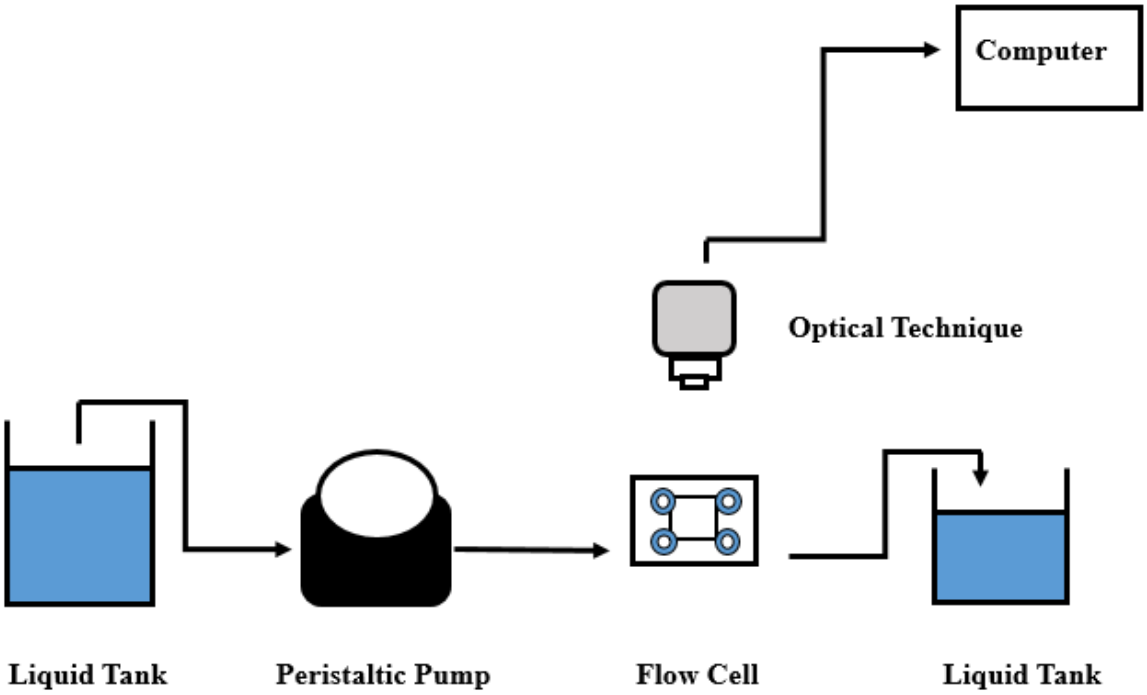

Figure 3.18: Schematic diagram of the experimental setup of the flow cell equipped with an optical technique (digital imaging or OCT)

The key features and considerations of the flow cell are:

1. As the granules are larger than 2 mm in radius, it is assumed that there is no granule movement during disintegration.
2. The granule is assumed to be wetted in all directions given the design of the sample holder.
3. A filter mesh or other materials such as a sponge can be added to assist with uniform flow (i.e., no bubbles), avoid back-flow and removal of particles within the process stream.
4. A lid was manufactured from transparent acrylic material which was suitable for digital imaging and OCT imaging (Figure 3.19).
5. The depth of the lid was 2 mm and the thickness was 1 mm to give a best visibility through the flow cell window.

In the experiments, granules (2000-2360 μm) with different porosities were investigated using the flow cell as shown in Table 3.3. The following steps followed are outlined:

1- A single dry granule was placed in the sample holder of the flow cell.
2- Deionised water (pH = 6.8) at room temperature was continuously fed from a glass bottle into the flow cell by using a calibrated peristaltic pump with a fixed flow rate of 5.6 ml/min. The inlet and outlet tubing dimensions consisted of an O.D. of 6 mm and I.D. of 2 mm (Figure 3.19a and b).
3- The disintegration process was continuously monitored with a digital camera with a zoom lens and optical coherence tomography. For the digital imaging, the images were captured every 5 sec for the first 4 min, then every 1 min for 10 min, and from 10 min to 2 hrs images were captured every 5 min. For the OCT, in the first 5 min of the test the images were taken every 5 sec, and from 5 min to 2 hrs images were captured every 1 min.
4- The outlet receiving vessel was raised higher than the feed vessel to avoid bubble formation by creating a pressure difference.
5- Filter mesh or a small quantity of material sponge were used in the filter area to avoid air bubbles that may cause granule movement (Figure 3.20)
6- Each experiment was repeated three times.
7- Images were processed through an in-house image analysis algorithm for quantitative size analysis.
8- Images from the OCT technique were processed using the 2D software for calculation of the swelling area with time.

Table 3.3: Experimental conditions using generated granules of varying size and porosity. Key process conditions that were used to generate granules were the liquid to solid ratio (L/S) and granulation time.

Experiment No.	Mass of Aspirin (g)	Mass of MCC (g)	Mass of PEG (g)	L/S Mass Ratio	Binder injection time (sec)	Wet massing time (min)	Total granulation time (min)
1	10	90	80	0.8 L/S	60	4	5
2	10	90	100	1.0 L/S	75	3.75	5
3	10	90	120	1.2 L/S	90	3.5	5
4	10	90	120	1.2 L/S	90	1	2.5
5	10	90	120	1.2 L/S	90	8.5	10

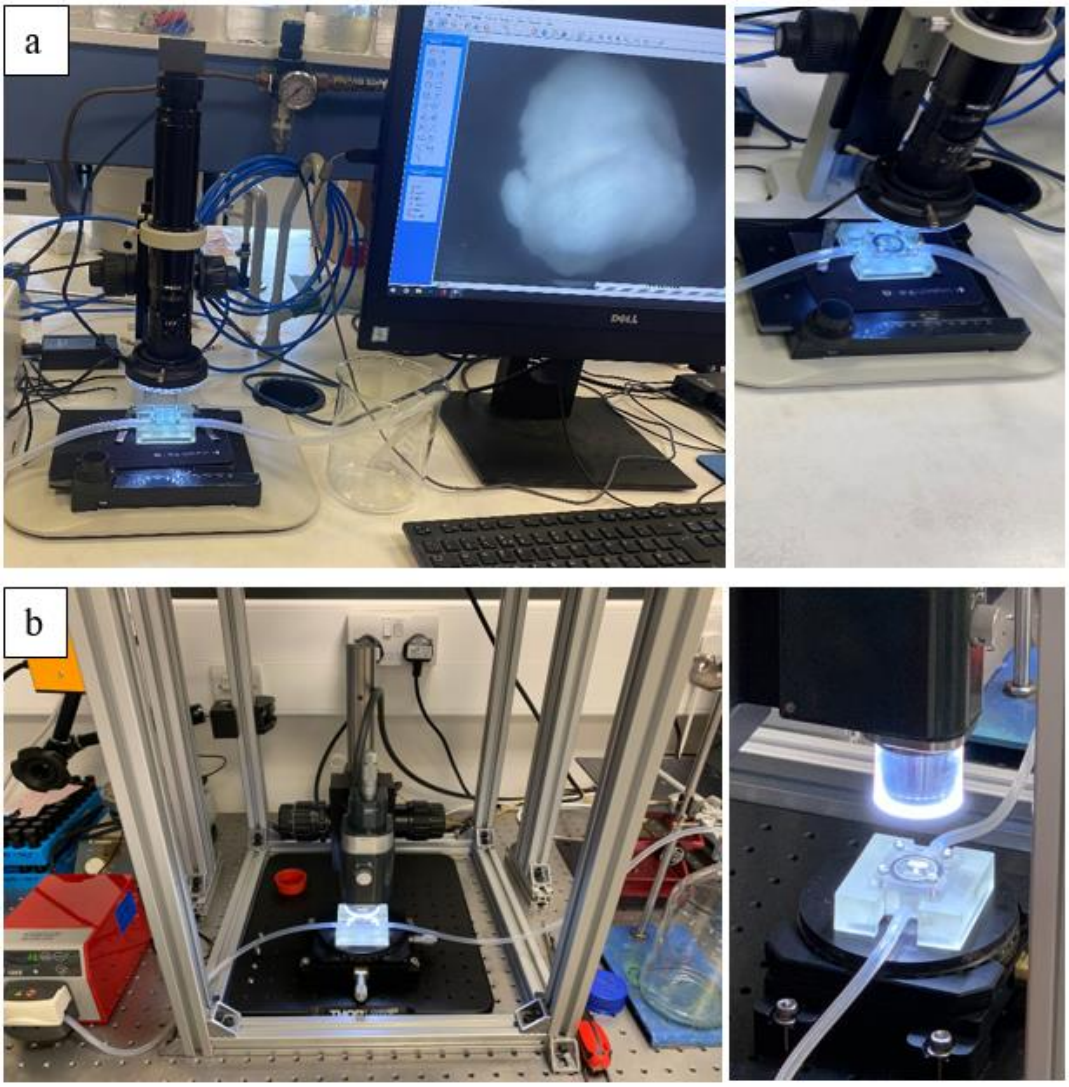

Figure 3.19: Flow-cell experimental set-up (a) digital imaging set up, and (b) OCT set up

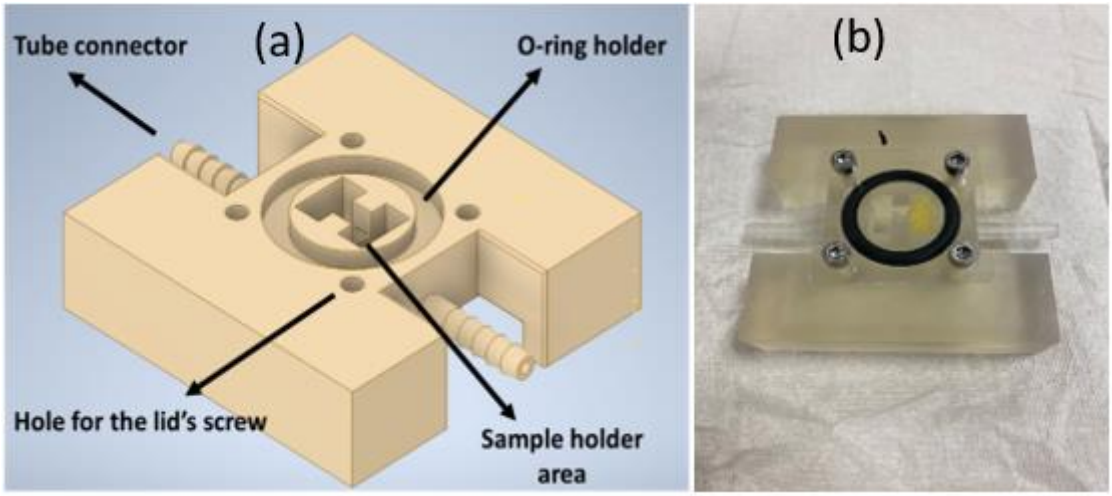

Figure 3.20: Schematic representation of (a) proposed flow cell and (b) printed flow cell

The captured images using the digital camera were processed using a specially developed in-house image analysis app in MALTAB (Figure 3.21). The app was developed to include features such as local noise reduction, batch calibration and export options. After importing the selected images, sharping and smoothing options were adjusted to get maximum noise reduction.

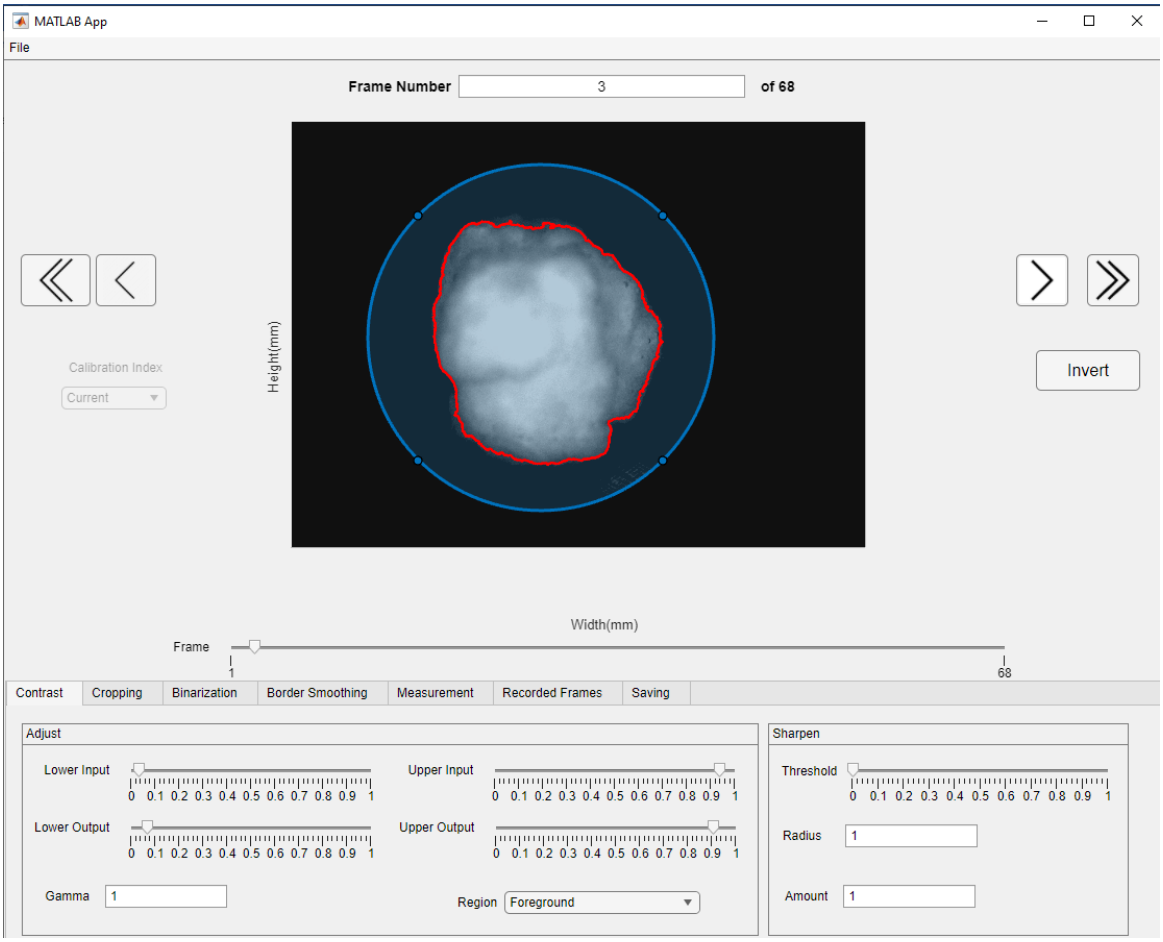

Figure 3.19: The app developed for the image analysis of granules

OCT is a non-invasive imaging technique that can be utilised to analyse such morphological changes due to its capacity to create images with sub-micron resolution through a line scan that carried out cross the granule (Rija and Kolios, 2020). Similar to X-ray computed microtomography (XRCT), magnetic resonance imaging (MRI), and terahertz pulse imaging (TPI), OCT generates cross-sectional depth-resolved two- and three-dimensional images of translucent materials. Physically, OCT is based on low-coherence interferometry (LCI), which employs light sources with high spatial and low temporal coherence (i.e., a broad spectrum

corresponding to coherence lengths of several microns (Markl *et al.* 2014). In practice, the final A-scan image is created by applying the Fast Fourier Transform (FFT) to the detected signal. The A-scan provides information regarding the spatial dimensions and locations of sample structures. A two-dimensional cross-sectional image is constructed by performing a series of axial scans at different points to perform transverse scanning (B-scan) (Rija and Kolios, 2020). OCT has several advantages over other spectroscopic and tomographic techniques. It is a non-destructive technology, it can be utilised for in line measurement, and it has a largest depth penetration, even when compared to TPI.

In this work, the swelling characteristics of different structure granules was investigated by measuring the swelling rate of the granule surface with a specific time. 2D (analyzer 2022.1) software was used to measure the height and width of the granule surface from the selected images (Figure 3.22). In total, 32 images were selected in each specific time; every 10 sec for first 1 min of the experiment, then every 1 min for 10 min, then every 10 min to 140 min. The increase of granule area of each image was calculated by subtracting the area from the previous image. The swelling rate was then calculated by dividing the swelling area of each image by the total swelling area (after 140 min).

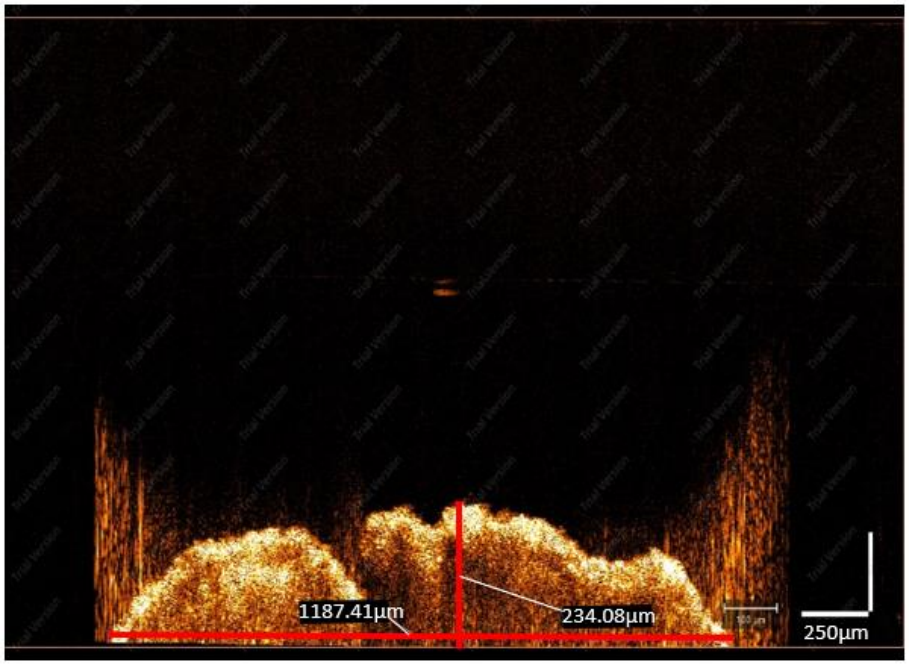

Figure 3.20: Image from 2D software measuring the granule surface height and width.

3.7 Summary

In this chapter, the methods of characterisation of the raw powders are described. The three different techniques for porosity measurements are discussed. Results are presented in Chapter 4. The experimental set-up for analysing granule dissolution and drug release is presented. Results of these experiments can be found in Chapter 5. Finally, the flow cell set-up for studying the swelling and break-up of individual granules has been summarised. Results of these experiments can be found in Chapter 6.

CHAPTER 4 - Influence of the granulation process on granule porosity and internal structure

4.1 Introduction

Granule porosity and internal structure are mainly dependent on the granulation process conditions. High binder volume causes a decrease in the granule porosity due to an increased fraction of the inter-particle void space which would be occupied by the binder (Ansari and Stepanek, 2008). The amount of liquid binder used during the granulation process is primarily determined by formulation properties, such as water absorption capability and solubility. From the literature, inadequate liquid binder results in porous and fragile granules with a high fines content, whereas excessive liquid binder results in large, dense granules, or over-wetted granules (Sakr *et al.*, 2012).

Increasing the liquid saturation of the granules enhances granule coalescence and the higher liquid saturation makes the granule more easily deformable which results in more liquid being available at the granule surface. Liquid bonds between primary particles are generated during the wet granulation process, resulting in the formation of semi-permanent aggregates. Inadequate massing time results in uneven distribution of liquid binder, leading to uncontrolled granule formation. On the other hand, a longer massing period results in granules with decreased porosity (Rahmanian *et al.,* 2011). The amount of energy carried to the powder mass by mixing intensity, which is mainly effected by the wet massing time, can affect the level of densification and intragranular porosity (van den Ban and Goodwin, 2017).

In this chapter, the effect of both L/S mass ratio and granulation time on the granule porosity and internal structure were studied. The main objectives of this work were:

- Investigate the effect of liquid/solid ratio and the granulation time on the granule porosity using three different techniques:
    1. Pycnometry technique
    2. Mercury porosimetry
    3. X-ray computed tomography
- Study of the 3D internal structure of the different porosity granules.

4.2 Granule morphology

The effect of binder content on granule microstructure and porosity was investigated. This investigation focused on defining the operating range for the liquid to solid mass ratio (L/S). An insufficient amount of liquid binder (less than 0.8 L/S) generated under-granulated, fragile granules with a high fractions of fines. Increasing the L/S to more than 1.2 produced lumps and an over-wetted mass. For this reason, L/S ranging from 0.8 to 1.2 was selected for this study. Furthermore, a liquid to solid mass ratio of 1.2 was chosen to investigate the effect of granulation time on granule structure because the L/S of 1.2 produced granules with lower porosity. Three different granulation times were selected: 2.5, 5 and 10 min. Figure 4.1 and 4.2 show representative digital images of the granule morphology and structure at different L/S ratios and granulation times using a Pixelink PL-D753 Camera with µScope x64 software.

Figure 4.1 shows digital images of granules at different L/S. From these images, the 0.8 L/S granule appears to have many void spaces between the particles. These voids appear to have disappeared in 1.0 L/S and 1.2 L/S granules. Figure 4.2 shows images of granules at different granulation times and surface cracks can be easily seen in granules produced after f 2.5 and 10 min granulation. However, these surface cracks disappear in the granule produced after 5 min granulation. The 5 min granule looked smoother at the surface with less cracks. The detailed internal structure will be discussed in Section 4.3.3.

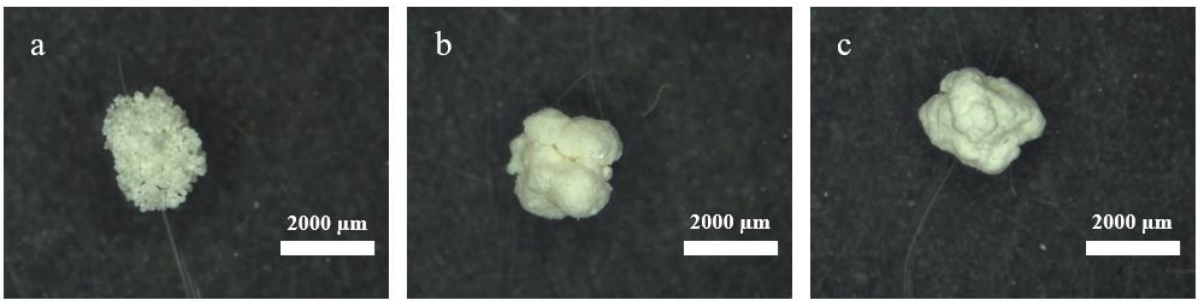

Figure 4.1: Effect of L/S on granule structure after 5 min granulation time: (a) 0.8 L/S (b) 1.0 L/S, (c) 1.2 L/S.

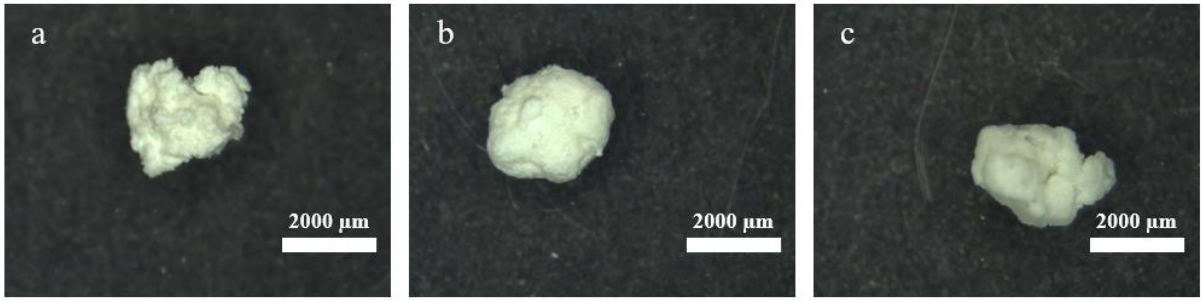

Figure 4.2: Effect of granulation time on granule structure at L/S of 1.2: (a) 2.5 min; (b) 5 min; (c) 10 min

4.3 Granule porosity

As discussed in Chapter 3 (Materials and Methods), assessing granule porosity can be very challenging. To address this, three techniques were used to assess granule porosity.

4.3.1 Dry powder and helium pycnometry

The granule porosity for the granule size range of 2000-2360 µm was studied using pycnometry techniques. In the pycnometry technique, the granule envelope and true density were measured separately using dry pycnometry and helium pycnometry respectively. The porosity was then calculated (Chapter 3, Section 3.4). Table 4.1 shows the granule porosity as determined using pycnometry.

Table 4.1: Granule porosity calculated from true density (using AccuPyc 1340 analyser) and envelope density (using Geopyc 1360 Envelope & T.A.P Density Analyzer)

Liquid/Solid mass ratio (L/S)	Granulation time (min)	Porosity
0.8	5 min	53 %
1.0	5 min	22 %
1.2	5 min	18 %
1.2	2.5 min	26 %
1.2	10 min	19 %

Figure 4.3 gives the porosity data for varying L/S. Note that each of these experiments was granulated for 5 min. This figure shows that the L/S had a clear effect on the granule porosity, with a low L/S (0.8) producing granules with a high porosity (53 %). These highly porous granules were extremely fragile and difficult to handle without breaking, likely due to a large volume of voids between binding particles. By raising the L/S to 1.0, the porosity was significantly reduced due to the influence of the liquid binder that filled the voids between binding particles and strengthened their bonding. As L/S was increased, the empty spaces were nearly filled with binder and fine particles, as demonstrated when the L/S was increased to 1.2 and the granule porosity decreased from 22 % to 18 %. At 1.2 L/S, the granules were less porous and the liquid binder was abundant around the complete granule particles, reducing the empty spaces to a minimum (these void spaces are seen in 3D images in Section 4.3.3).

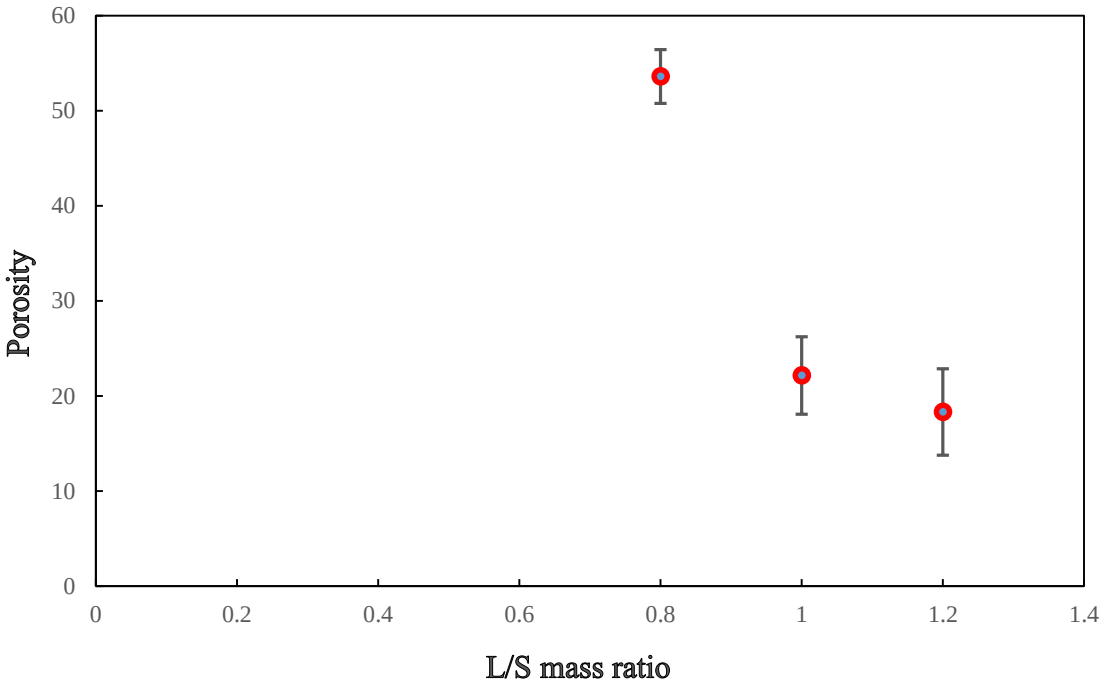

Figure 4.3: Granule porosity calculated from true and envelope density. Varying L/S mass ratio with a fixed 5 min granulation time. Error bars represent standard deviation

In addition to the L/S, the effect of granulation time on granule porosity was investigated and is shown in Figure 4.4. Three granulation times were chosen: 2.5, 5 and 10 min. The 2.5 min granules showed a high porosity in comparison to other granulation times. The particles were not tightly attached at this time, and the void area was significantly large. This is likely because there is insufficient time for the binder to circulate around all particles, and the particles required a greater number of impacts and longer shear times to assure contact and binding (Liu *et al.*, 2000). By increasing the granulation time from 2.5 to 5 min while maintaining the same L/S, lower porosity granules were formed. In this instance, it appears this granulation time was sufficient for the liquid binder to spread throughout the dry powder and bind the particles together. The granular porosity was reduced from 26 % to 1 %. Increasing the granulation time to 10 min, on the other hand, caused an increase in granule porosity to 19 % compared to 5 min generated granules. It was suspected that this was caused by the extended influence of the impeller on the granule, and the longer time period causes granule particles to undergo a higher number of collisions, generating larger cracks within the granule microstructure. As this level of detail could not be captured by simple pycnometry methods, further investigation to improve

understanding of the internal structure was carried out, using both MIP and micro CT (see Sections 4.2.2 and 4.2.3).

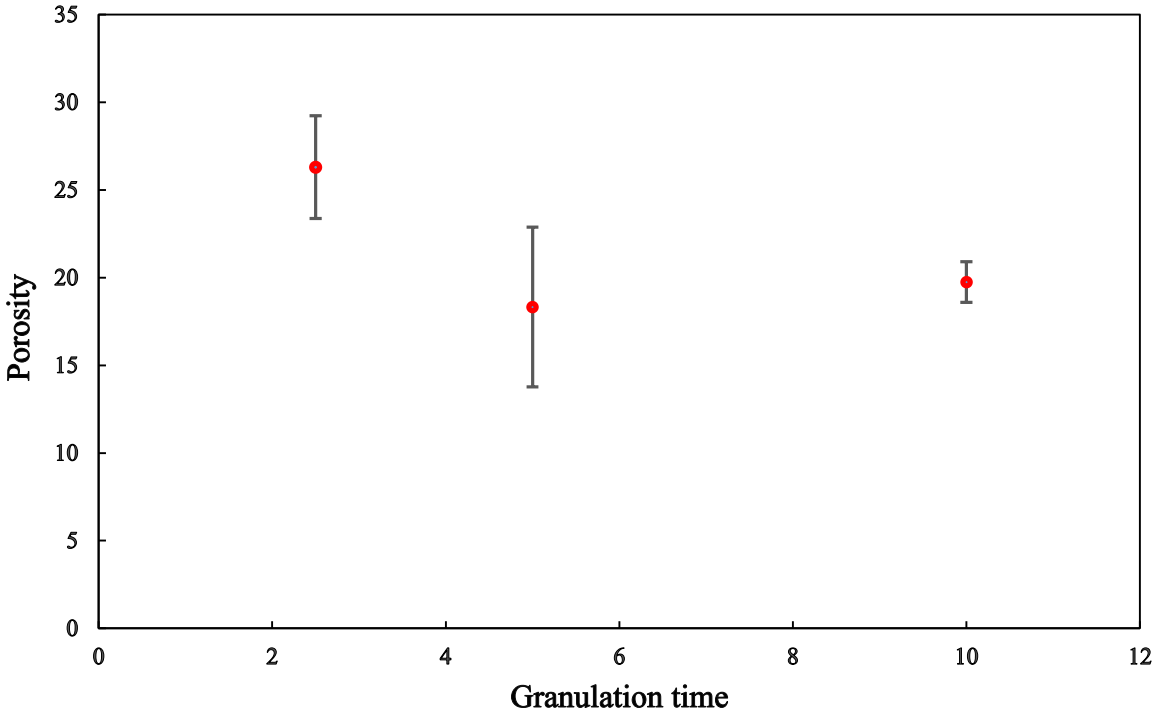

Figure 4.4: Granule porosity calculated from true and envelope density. Varying granulation time with a fixed 1.2 L/S ratio. Error bars represent standard deviation

4.2.2 Granule porosity: MIP

In this work, the granule total porosity was measured using MIP. Increasing the L/S reduced the granule porosity (see Table 4.2 and Figure 4.5). The average pore diameter was strongly affected by the L/S (Figure 4.6). Granules formed at a L/S of 0.8 have the highest pore diameter (631 nm) as the liquid binder was inadequate to fill the pores and make the particles stick together. When particles are subjected to densifying pressures in a high shear granulator, the binder acts as a lubricant, lowering inter-particle friction and allowing particles to flow more freely within the granules. (Iveson, et al., 1996). When the L/S is raised to 1.0, the average pore size abruptly decreases (148 nm). In this configuration, there is enough liquid to bind the particles together. Further increasing the binder volume to 1.2 L/S further reduces the pore diameter to 58 nm. This results in extremely dense granules.

Table 4.2: Granule total porosity using MIP

Liquid/Solid mass ratio (L/S)	Granulation time (min)	Porosity
0.8	5 min	63 %
1.0	5 min	40 %
1.2	5 min	26 %
1.2	2.5 min	40 %
1.2	10 min	31 %

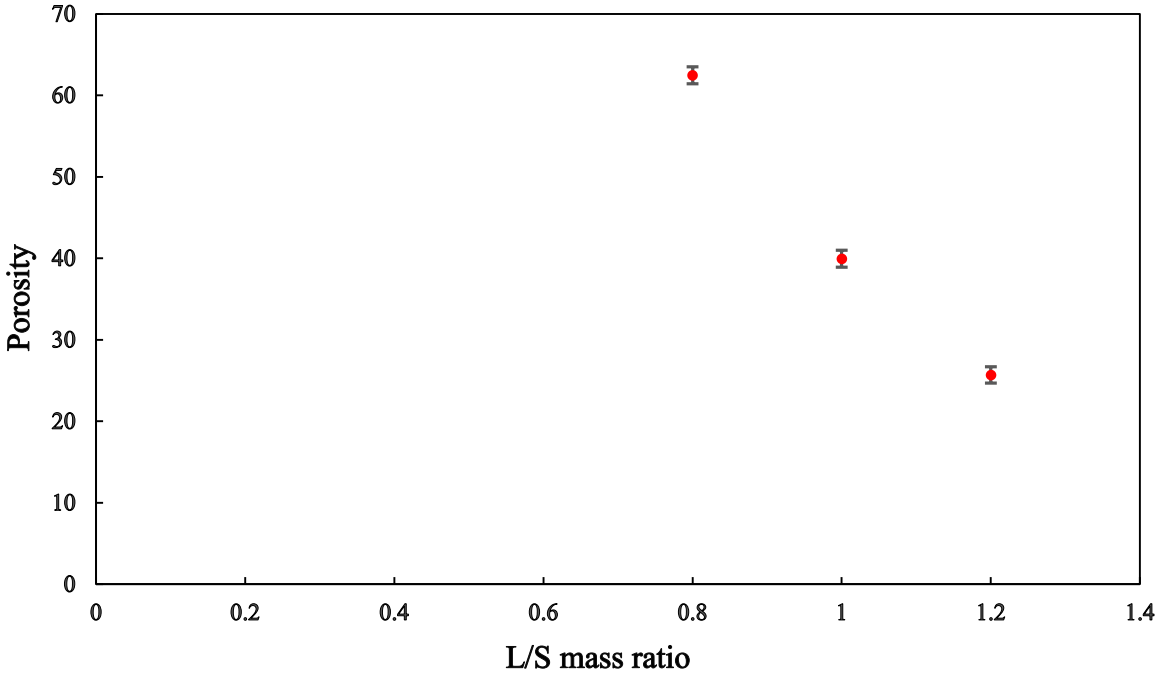

Figure 4.5: Granule porosity from using MIP technique. Varying L/S mass ratio. Fixed granulation time of 5 min. Error bars represent standard deviation

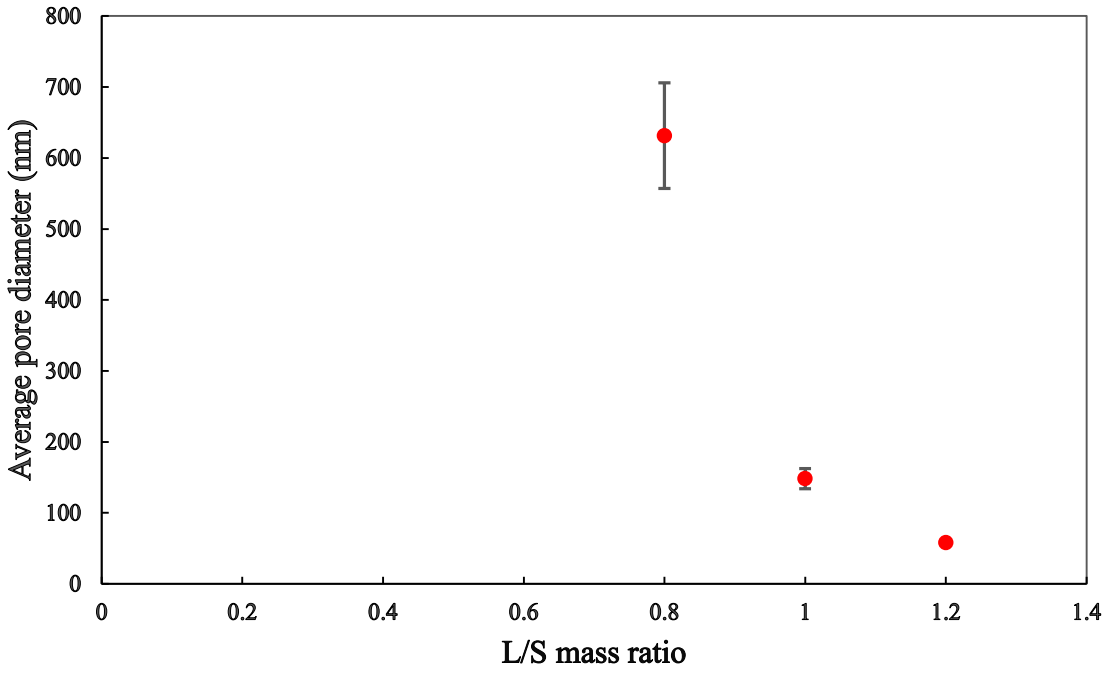

Figure 4. 6: The average pore diameter of varying L/S ratio using MIP technique. Fixed granulation time of 5 min. Error bars represent standard deviation

Figure 4.7 shows the pore size distribution of different L/S granules. All granules show a bi-modal pore size distribution. The first mode, between 100 to 1000 nm, indicates the MCC particle pore sizes, and the second mode, larger than 10000 nm, indicates the granule pore sizes. In both modes, 0.8 L/S granules show the largest volume of pores. 1.0 L/S granules show a high pore size above the 10000 nm, which is likely due to the cracks within the granule surface. The lowest porosity granules (1.2 L/S) shows a low volume of small pores, with an increasing volume of pores above 10000 nm, however the volume of these large pores is still small compared to granules formed at L/S of 0.8 and 1.0.

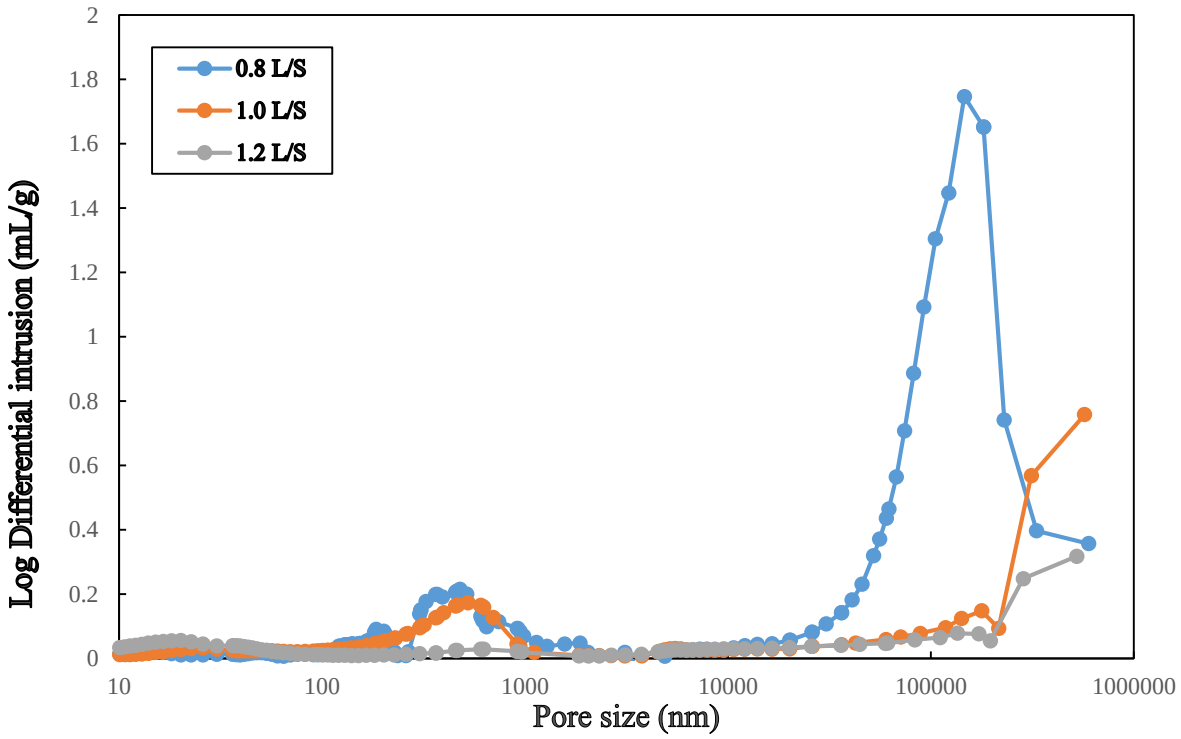

Figure 4.7: Pore size distribution of different L/S mass ratio granules with a fixed 5 min granulation time vs the log differential intrusion

MIP was used to examine the effect of granulation time on granule porosity and the average pore size diameter. In general, the effect of granulation time on the average pore diameter of the granules was lower than the effect of the different L/S. The granulation times of 2.5, 5, and 10 min were tested on granules formed at a L/S of 1.2. Short granulation times generated granules with the highest porosity (38 %). When the granulation time was increased to 5 min, the granule porosity sharply decreased (26 %) (Figure 4.8). The average pore diameter also decreased from 189.13 nm to 58.18 nm (Figure 4.9). However, increasing the granulation time to 10 min, increased granule porosity to 31 % and also resulted in an increase of the average pore diameter to 114.39 nm. These trends are consistent with the measurements that were performed using the pycnometry technique, however the MIP porosity values were higher. It is likely this discrepancy is due with to: 1) Errors in the pycnometry technique which leads to an underestimation of porosity. For instance; the dryflo powder is not completely surrounding the whole granule during the measurement; this can be avoided by spending time in rolling the plunge to insure positioning the dryflo powder around the granule. 2) Limits in the ability of the mercury to enter enclosed pores and accounting for them. The difference in values between these two techniques gave motivation to study the granule porosity and internal micro-structure using the XRCT technique.

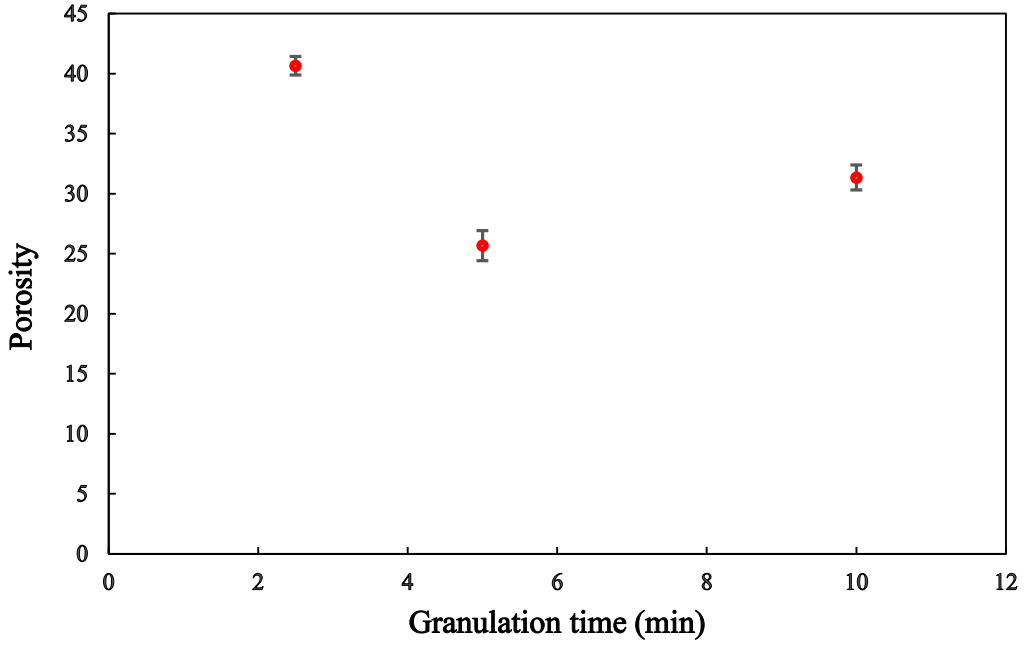

Figure 4.8: Granule porosity from using MIP technique. Varying granulation time with a L/S of 1.2. Error bars represent standard deviation

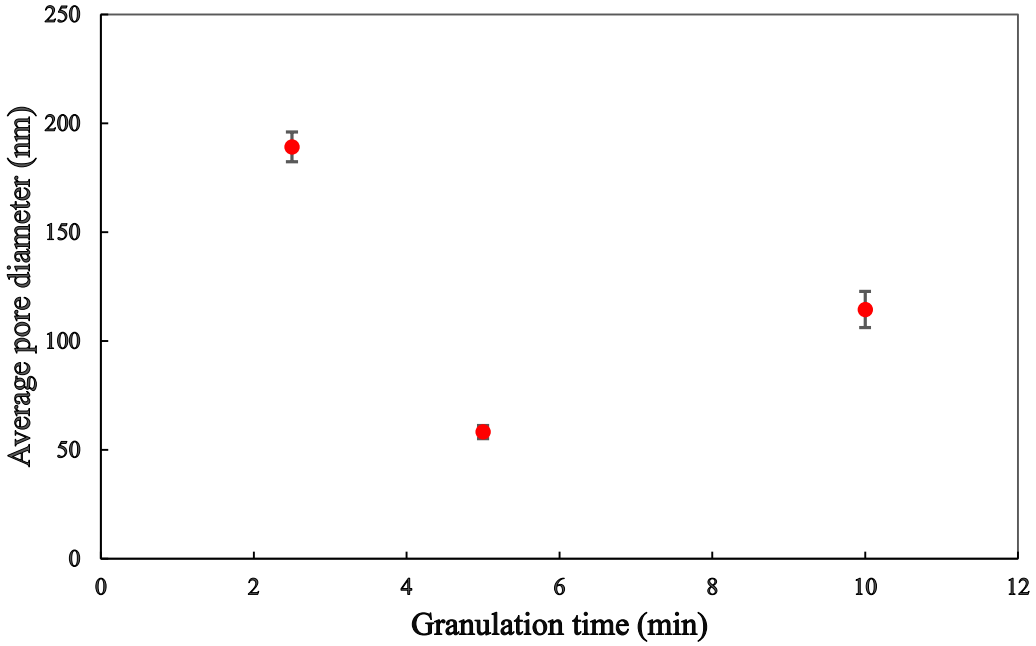

Figure 4.9: The average pore diameter when varying granulation time with a L/S of 1.2 using the MIP technique. Error bars represent standard deviation

The pore size distribution of granules produced at different granulation times are shown in Figure 4.10. The granules produced after 2.5 min show the highest volume of small pores. The pore size around 1000 nm reflects the MCC pore size. On the other hand, granules produced after 5 min show the lowest volume of small pores. The pore size above the 100000 nm may reflect the cracks within these granules.

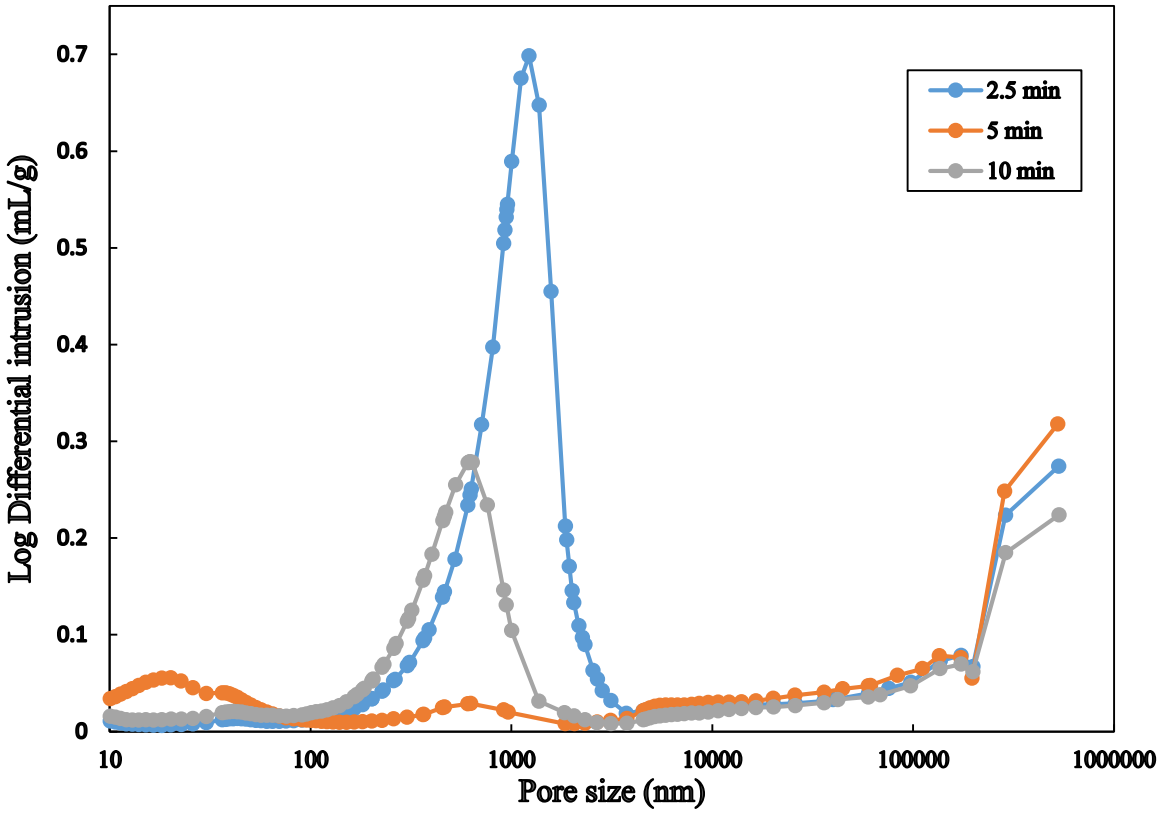

Figure 4.10: Pore size distribution of granules after different granulation time granules plotted against the log differential intrusion.

4.3.3 Granule microstructure and porosity: XRCT

The granule microstructure of single granules was studied using X-ray computed tomography (XRCT) (Skyscan 1172 Bruker, Belgium). The total granule porosity was calculated automatically after the image reconstruction step (The steps of measuring granule porosity were explained in Chapter 3, Section 3.4.2.3). The cross-sectional reconstructed images of the granule were visualized (Figure 4.11 and 4.12). Table 4.3 shows the total granule porosity results.

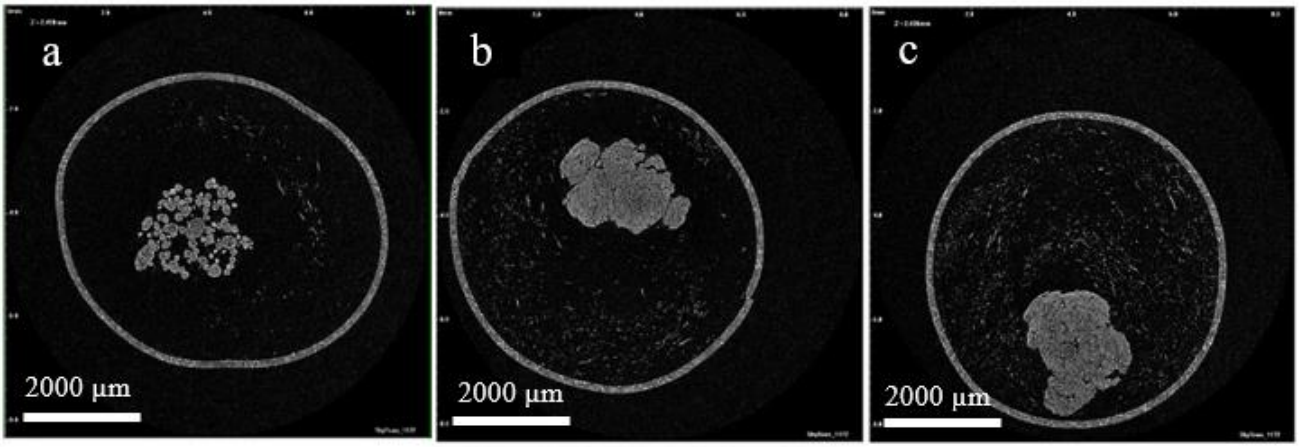

Figure 4.11: Reconstructed images of different L/S mass ratio granules: (a) 0.8 L/S, (b) 1.0 L/S and (c) 1.2 L/S after 5 min granulation time

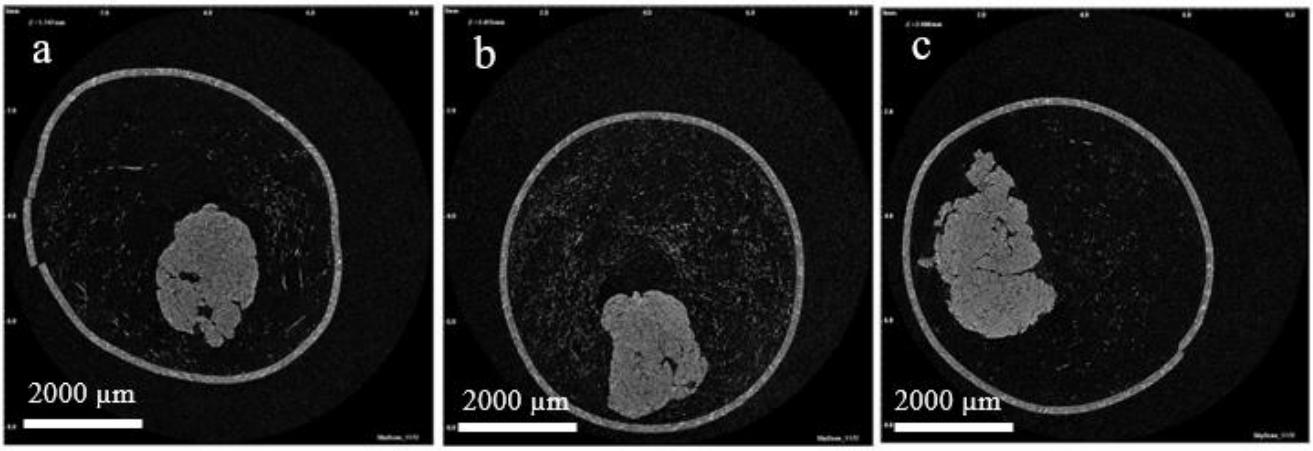

Figure 4.12: Reconstructed images of granules at different granulation times at a L/S of 1.2:. (a) 2.5 min, (b) 5 min and (c) 10 min

Table 4.3: Granule total porosity using X-ray CT scan

Liquid/Solid mass ratio	Granulation time (min)	Porosity
0.8	5 min	62 %
1.0	5 min	39 %
1.2	5 min	25 %
1.2	2.5 min	38 %
1.2	10 min	32 %

Figure 4.13 shows the granule porosity decreased as the L/S increased. As with the previous measurements (pycnometer and MIP technique), high binder volume causes a decrease in the granule porosity. This is most likely due to increased granule deformability, which increases the consolidation rate in response to forces within the granulator. This increases the fraction of the inter-particle void space which would be occupied by the binder (Ansari & Stepanek, 2008). Increasing the liquid saturation of the granules enhances granule coalescence and the higher liquid saturation makes the granules more easily deformable and results in more liquid being available at the granule surface. This increases the probability of successful coalescence with low void space between coalescing particles (Liu *et al*., 2000). By adding the liquid binder, the granule size and porosity are decreased, trapped air is released, and possibly even liquid binder is squeezed to their surface. Granules can exist in a variety of liquid saturation conditions. Newitt and Conway-Jones provided the initial descriptions of these states. The pendular state when the liquid bridges at the contact points between particles hold them together in the pendular bonds. The funicular state, when the spaces are not completely saturated with liquid, is a transitional stage between the pendular and capillary states. In the capillary state, the liquid fills all the voids, and the liquid on the surface is drawn back into the pores by capillary action and this state the granule is saturated (Figure 4.14) (Liu *et al.*, 2000).

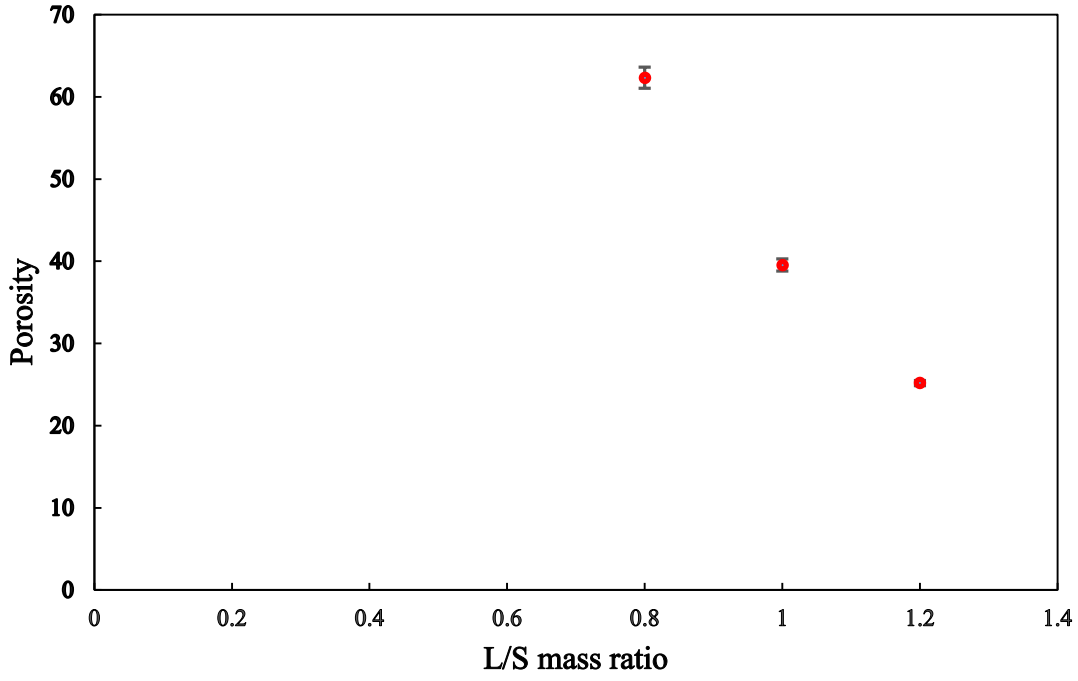

Figure 4.13: Effects of L/S mass ratio on the granule porosity using X-ray CT scan. The granulation time was fixed at 5 min. Error bars represent standard deviation.

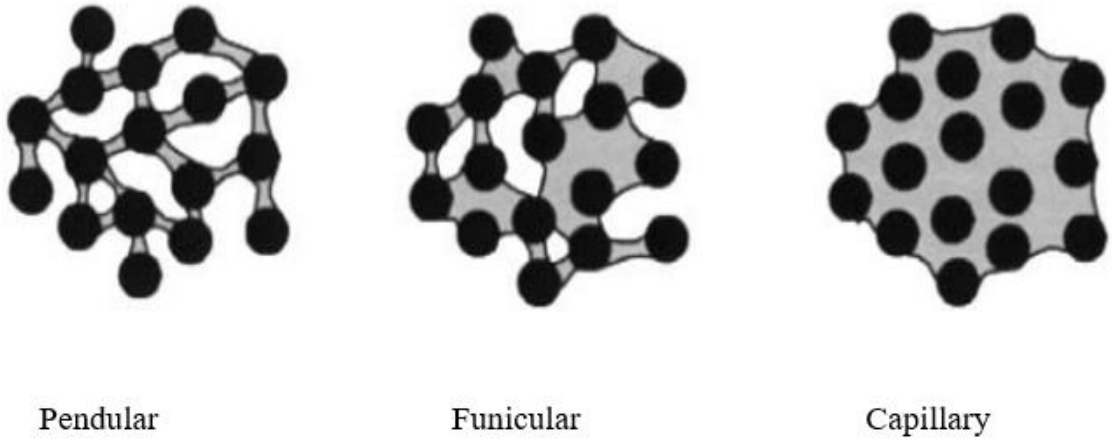

Figure 4.14: The different states of saturation of liquid-bound granules (Liu *et al.*, 2000)

Figure 4.15 shows the 3D cross-sections of a granule produced at lower L/S (0.8). Through this granule it is easy to see the void spaces between particles, which contribute to the high fragility of these granules. These high porosity granules (62 %) are friable and broke easily when handled.

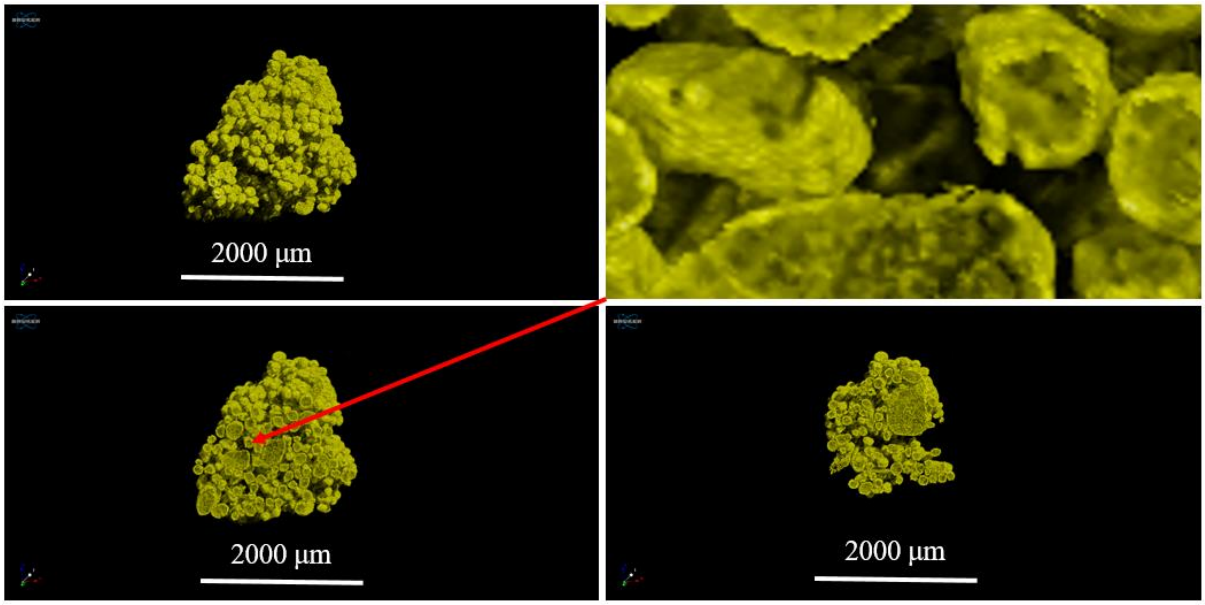

Figure 4.15: XRCT 3D images of a granule: 0.8 L/S, 5 min granulation time

Figure 4.16 shows the 3D cross-sections of a granule produced at 1.0 L/S. These granules demonstrated higher strength on handling than the 0.8 L/S granules. The granule porosity was decreased from 62 % to 39 %. It is likely the liquid saturation of these granules was in the funicular regime, where the void spaces are not completely saturated with liquid binder. Interestingly, these granules appear to be tertiary agglomerates, consisting of bound agglomerates with reasonably large pores between the individual agglomerates. Granules produced at a L/S of 1.2 were very robust, and on removal from the granulator appeared to be highly saturated with liquid binder. As it can be seen in Figure 4.17, the cracks and void spaces within the granule are difficult to visualise.

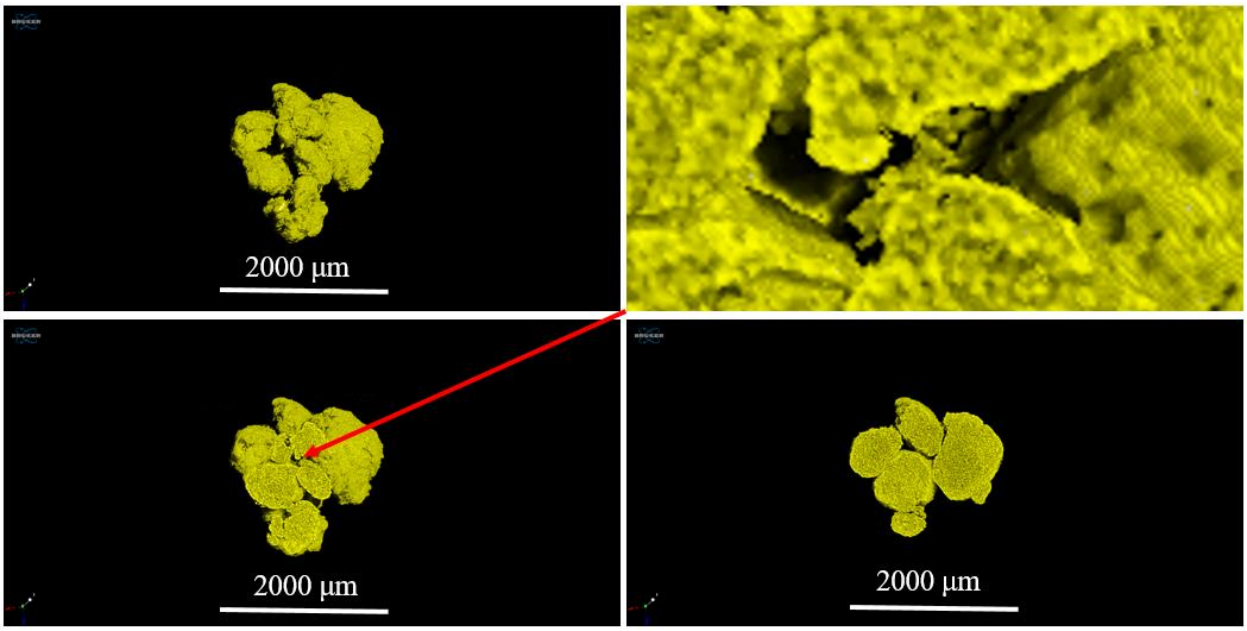

Figure 4.16: XRCT 3D images of a granule: 1.0 L/S, 5 min granulation time

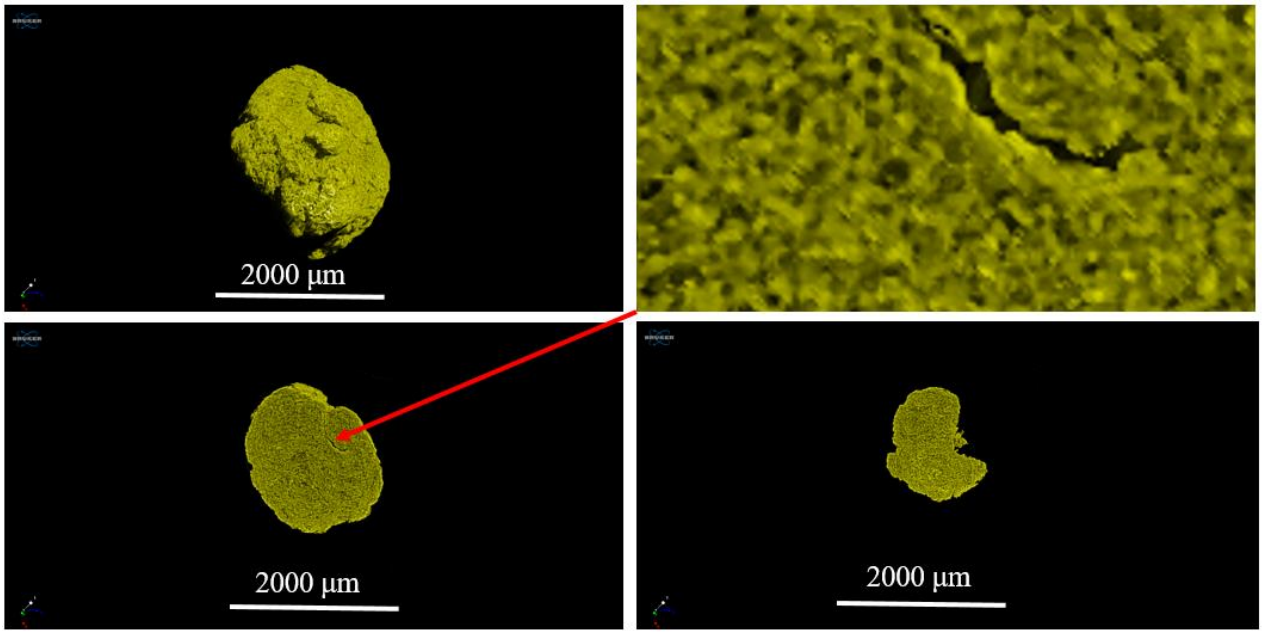

Figure 4.17: XRCT 3D images of a granule: 1.2 L/S, 5 min granulation time

Figure 4.18 shows the effect of granulation time on granule porosity using XRCT. Increasing the granulation time from 2.5 to 5 min leads to a marked decrease in granule porosity. This in agreement with other literature (Pathare *et al.*, 2011; Badawy *et al.*, 2012; van den Ban and Goodwin, 2017), who have demonstrated an increase in granule density with increasing granulation time.

This decrease in granule porosity is due to the granulated material sticking together during the continuing coalescence process. In this case, the material is sufficiently wet for granules to stick together and form even larger granules. Fine material adheres to the surface of granules during the layering step (Liu *et al.*, 2000). It is thought that after 5 min of granulation and as the granule porosity decreases, the granule yield stress increases. This reduces the amount of deformation caused by the collision of two granules, hence decreasing the probability of coalescence. However, consolidation also increases pore saturation, which in turn enhances granule flexibility and liquid accessibility at the granule surface. These two effects will promote coalescence. If granules become completely saturated, their repeated collisions may lead them to liquefy, which would aid coalescence further. Interestingly, the granules show an increase in granule porosity from 25 % after 5 min to 33 % after 10 min granulation time. The granule formed after 10 min appears to have large cracks within it, as seen in Figure 4.19, indicating that granule deformation may be generating large pores inside the granules at this longer granulation time.

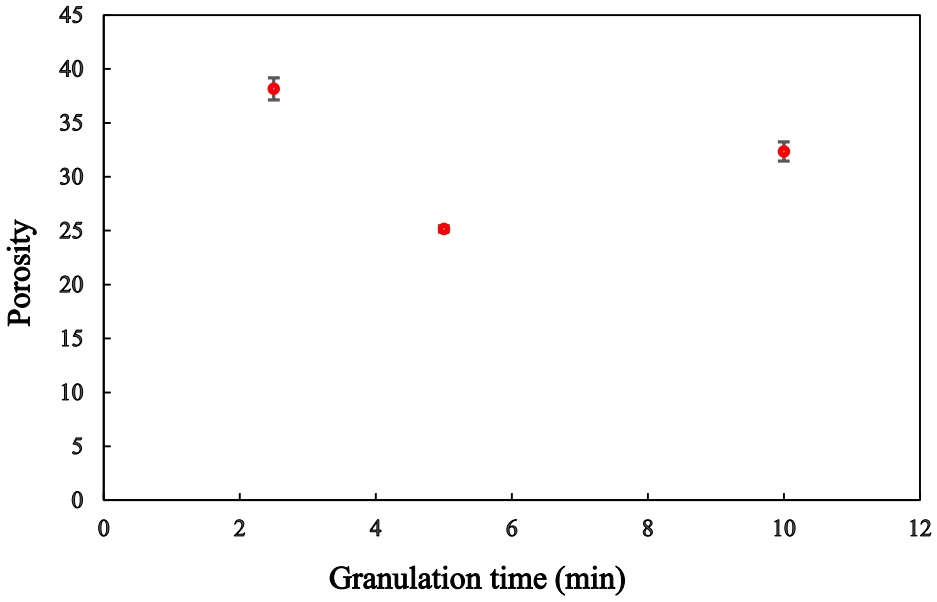

Figure 4.18: Effect of granulation time on the 1.2 L/S granule porosity using X-ray CT technique. Error bars represent standard deviation.

The short granulation time (2.5 min) was insufficient for all particles to bind together. As shown in Figure 4.19, the granule produced after 2.5 min appears to have a significant crack across the granule, indicating that the granule particles are not adequately bonded. Here, longer granulation time is important to ensure the interaction between the MCC and the binder and the degree of interaction between MCC and water would increase with increased granulation time, due to both the increased number of impacts at longer granulation times, and the change of the physical structure of MCC during hydration.

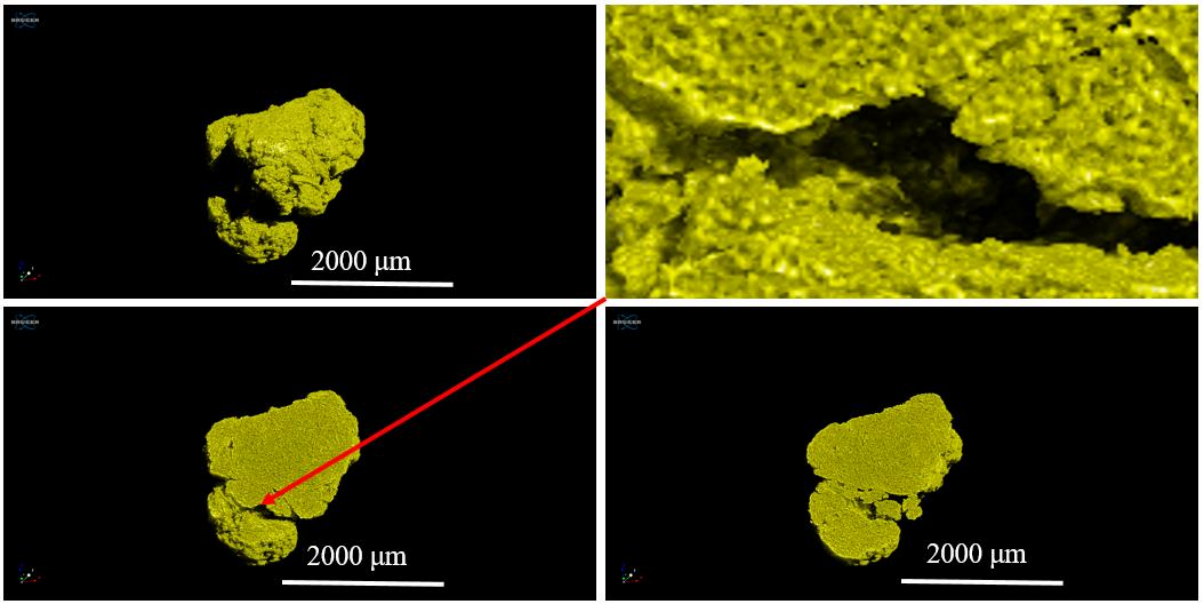

Figure 4.19: XRCT 3D images of a granule: 1.2 L/S, 2.5 min granulation time

Figure 4.20 shows a tiny fracture with a 1.2 L/S granule produced after 5 min, suggesting significant granule densification has occurred after this time. Liquid binder fills the vacuum spaces between particles. As seen in Figure 4.20, the cracks within the granule are difficult to visualise. On the other hand, and interestingly, increasing the granulation time further to 10 min causes an increase in porosity. This is consistent with the porosity results measured using pycnometry and MIP. The granule after 10 min appears to have large cracks within it (Figure 4.21), indicating that granule deformation may be generating large pores inside the granules. This is probably due to prolonged impeller impacts. Furthermore, this longer granulation time (10 min) may causes the MCC to start dehydrating, causing some particle breakage.

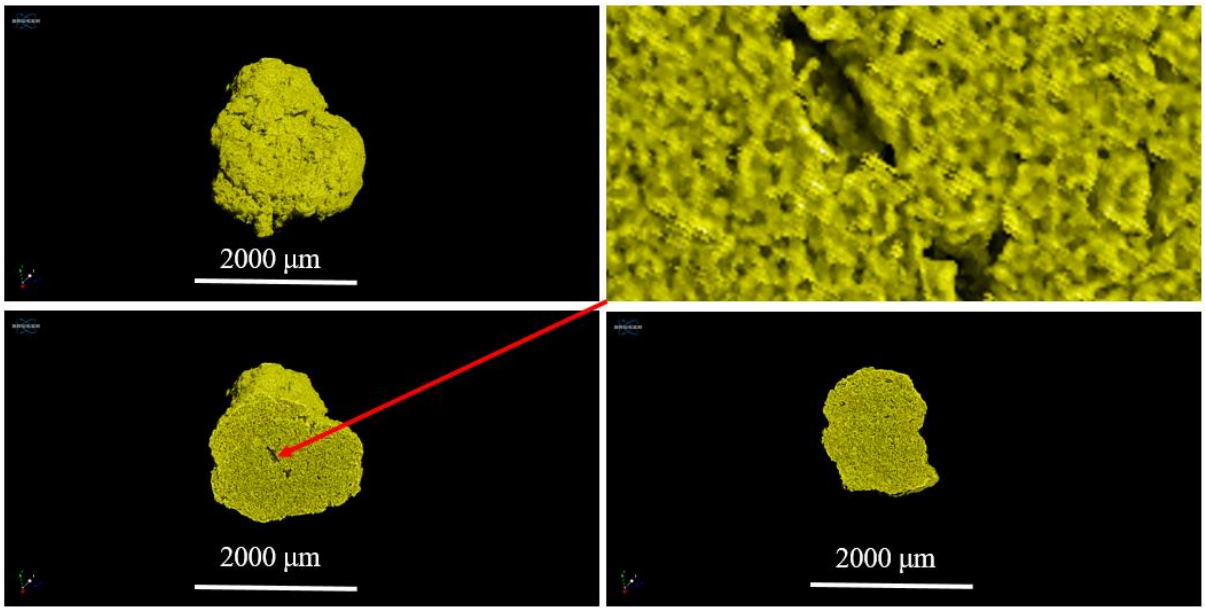

Figure 4.20: XRCT 3D images of a granule: 1.2 L/S, 5 min granulation time

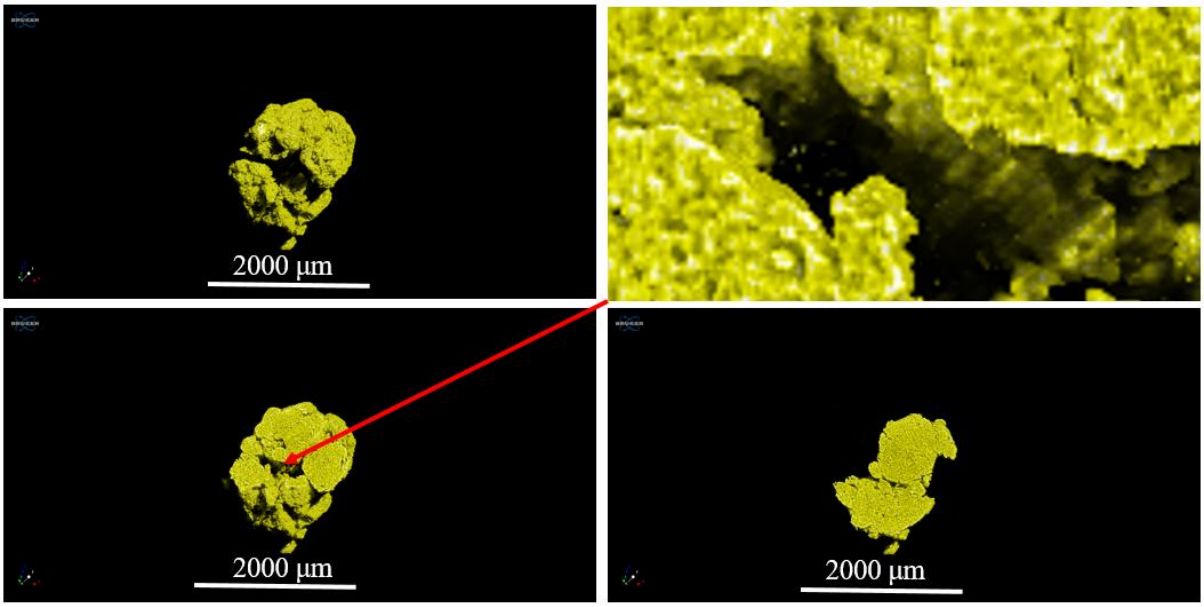

Figure 4.21: XRCT 3D images of a granule: 1.2 L/S, 10 min granulation time

4.3.4 Comparing the three methods of porosity measurement

Figures 4.22 and 4.23 show the comparison of porosity results obtained from the three different methods for varying L/S and granulation time respectively. The pycnometry porosity values were relatively low compared to the other methods. This may be attributed to the press effect of the quasi-fluid displacement media (DryFlo) on the granules. Some of void spaces in the granules may be broken and filled with dryflo material. Furthermore, the mercury's ability to interpenetrate granule pores increases the number of pores that are counted, resulting in MIP producing higher porosity results than pycnometry. The MIP and the XRCT porosity results were quite similar. It is very difficult to determine which is the best method to use, however for this research the XRCT method was chosen as the most reliable, due to ability of imaging and visualising the internal structure, especially fragile granules which are most likely to be influenced by mercury intrusion pressure in the case of MIP and the press effect of the DryFlo powder for dry powder pycnometry. From the XRCT images, it is possible to visualise the 3D internal structure, and this is especially required in this research to link to the granule performance.

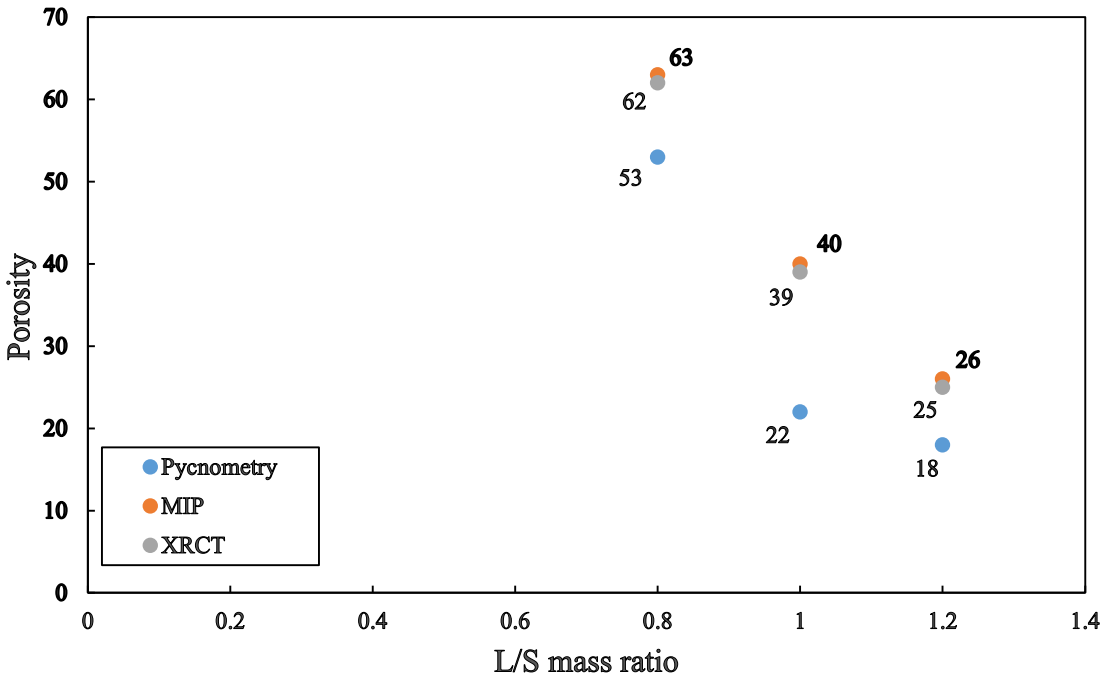

Figure 4.22: Porosity of varying L/S ratio granules after 5 min granulation time using different techniques

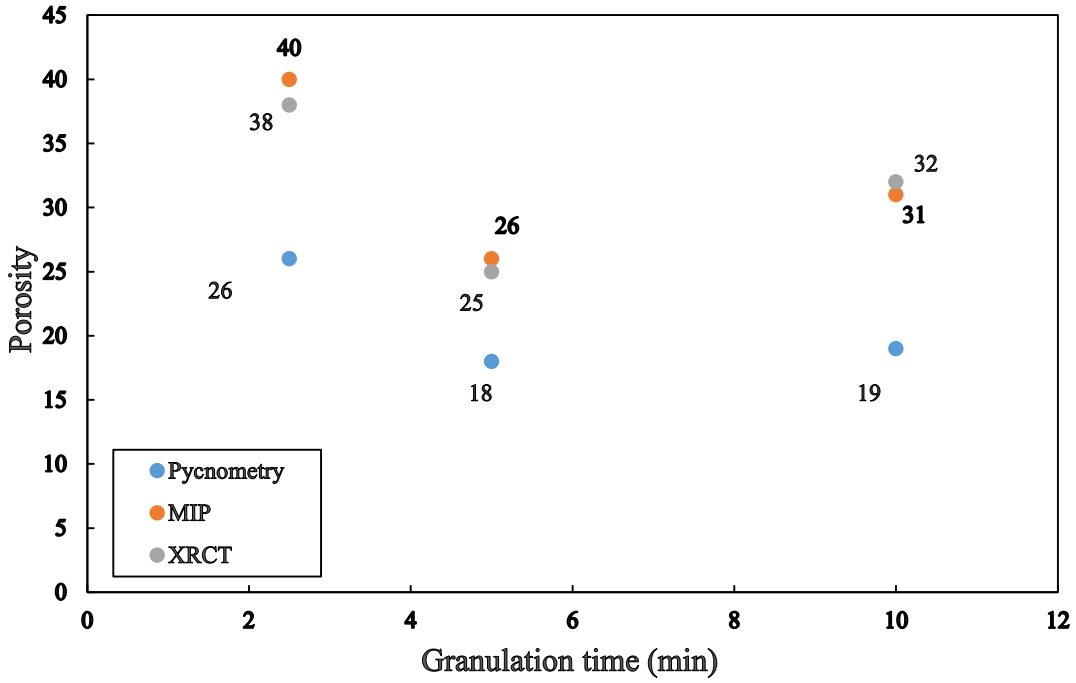

Figure 4.23: Porosity of different granulation time granules at 1.2 L/S using different techniques

4.4 Conclusions

In this chapter, an experimental methodology has been developed to investigate the links between granulation conditions and granule structure. Granulation at low liquid to solid mass ratio and short granulation times produced porous and fragile granules. Extending the granulation time to 10 min led the granules to grow in porosity and develop cracks. Three different techniques were used in this chapter to study the granule porosity (pycnometry, MIP and X-ray CT scan technique). In general, the pycnometry results for granule porosity were rather low. In contrast, the MIP and XRCT scan results were higher and quite similar. It was determined that for the purposes of this research, XRCT was the most suitable method for estimating porosity and visualising internal microstructure.

Following the production of these different structure granules and measuring the total porosity using various techniques, the performance of these granules, including dissolution and drug release performance, will be discussed in the following chapter.

CHAPTER 5 - Drug release performance: Effect of granule structure

5.1 Introduction

One of the most important characteristics which controls the kinetics of granule disintegration and dissolution is porosity, which is highly influenced by the granulation process (Ansari and Stepanek, 2008). It is the pore structure, in conjunction with the wetting characteristics, which controls the rate of liquid penetration into the granule and the subsequent break-up of the granule compact to release the drug particles from the structure within the surrounding fluid.

The previous chapter investigated the effect of the granulation process parameters on the porosity and internal structure of granules. Following this work, this chapter investigates the relationship between granule structure properties to product performance where drug release profiles from various granule structures are carefully examined.

5.2 Result and discussion

5.2.1 Aspirin calibration curve

UV spectroscopy was used to characterise the concentration of aspirin in the dissolution medium (water). An aspirin calibration curve was generated (Figure 5.1) which was detailed in Chapter 3 (Section 3.5). Seven dilutions were analysed using a Thermo Scientific Genesis 10S UV spectrophotometer at 270 nm (Table 5.1). The absorbance average was used to generate the aspirin calibration profile (Figure 5.1). This would then allow the capability to plot the aspirin concentration profile over time from the sampling method described in Chapter 3 (Section 3.5).

Table 5.1: The absorbance of different aspirin concentrations

	Concentration (mg/ml)	Experiment (1)	Experiment (2)	Experiment (3)	Average (absorbance)
1	0.25	1.1	1.099	1.095	1.098
2	0.125	0.511	0.509	0.504	0.508
3	0.0625	0.243	0.238	0.23	0.237
4	0.0312	0.12	0.109	0.107	0.112
5	0.0156	0.056	0.068	0.053	0.059
6	0.0078	0.037	0.034	0.037	0.036
7	0.0039	0.019	0.023	0.018	0.02

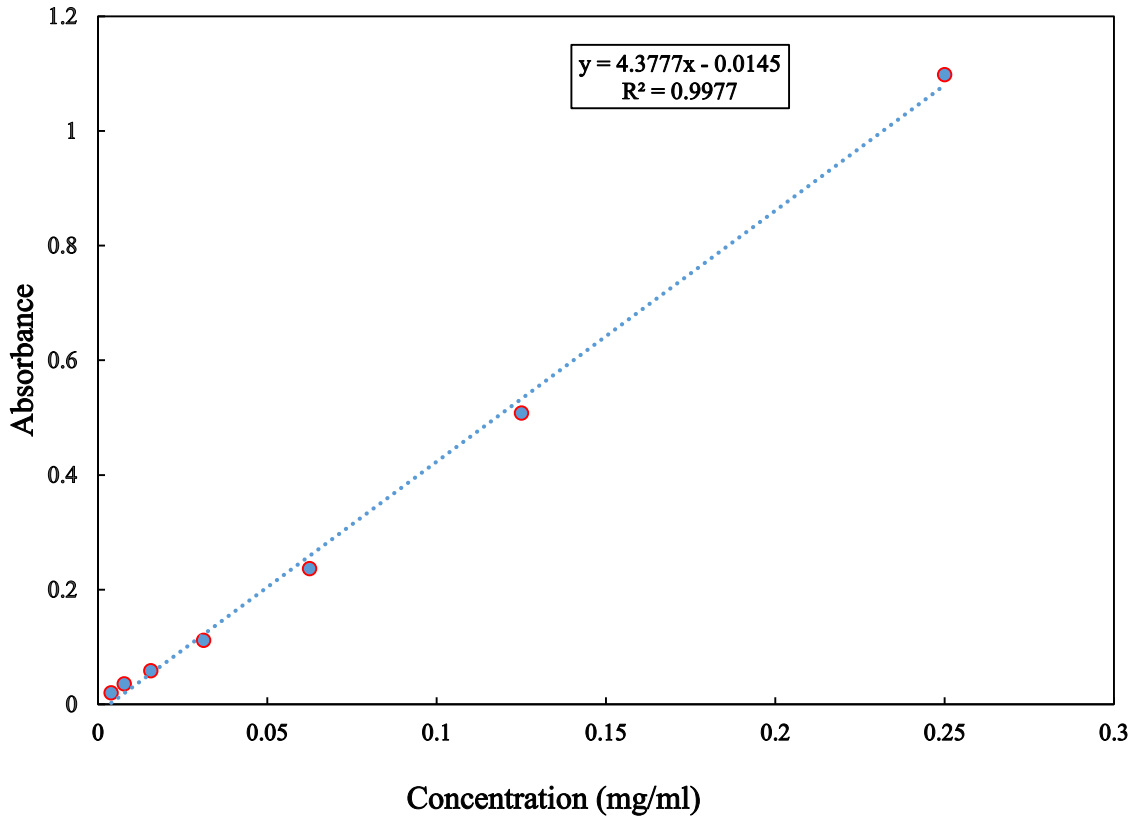

Figure 5.1: Aspirin calibration curve

5.2.2 Effect of liquid to solid ratio (L/S) on granule dissolution and aspirin release

In Chapter 4, it was demonstrated that increasing the L/S mass ratio parameter reduced granule porosity, because of less void space within the structure due to a higher concentration of binder and finer particles. Also, it was proposed that a higher content of the liquid binder was abundant around the complete granule particles. This reduces the void space within the granule particles, affecting the final granule porosity. In this work, all granule samples tested in Chapter 4 were investigated for their drug concentration profiles during 300 min of dissolution, with the entire drug release procedure completed within 300 min. For clarity, three different granule compositions were tested (Table 5.2):

Table 5.2: The compositions and conditions of L/S mass ratio granules

Experiment No.	Mass of aspirin (g)	Mass of MCC (g)	Mass of PEG (g)	L/S mass ratio	Binder injection time (sec)	Wet massing time (min)	Total granulation time (min)
1	10	90	80	0.8 L/S	60	4	5
2	10	90	100	1.0 L/S	75	3.75	5
3	10	90	120	1.2 L/S	90	3.5	5

Figures 5.2 and 5.3 demonstrate that at 100 min all of the aspirin was released from the granules produced at a L/S of 0.8. These 0.8 L/S granules have a porosity of 62 % (Porosity result of the XRCT technique) which is the highest compared to granules produced at L/S of 1.0 and 1.2. For the case of 1.0 L/S (porosity 39 %), the aspirin continued to be released for 150 min, at which point the final aspirin concentration was achieved. On the other hand, the dissolution was much slower for 1.2 L/S granules (porosity 25 %), with the final concentration reached at 250 min. This is expected this is a direct result of the change in the pore structure, with the 1.2 L/S granules possessing a much smaller pore size.

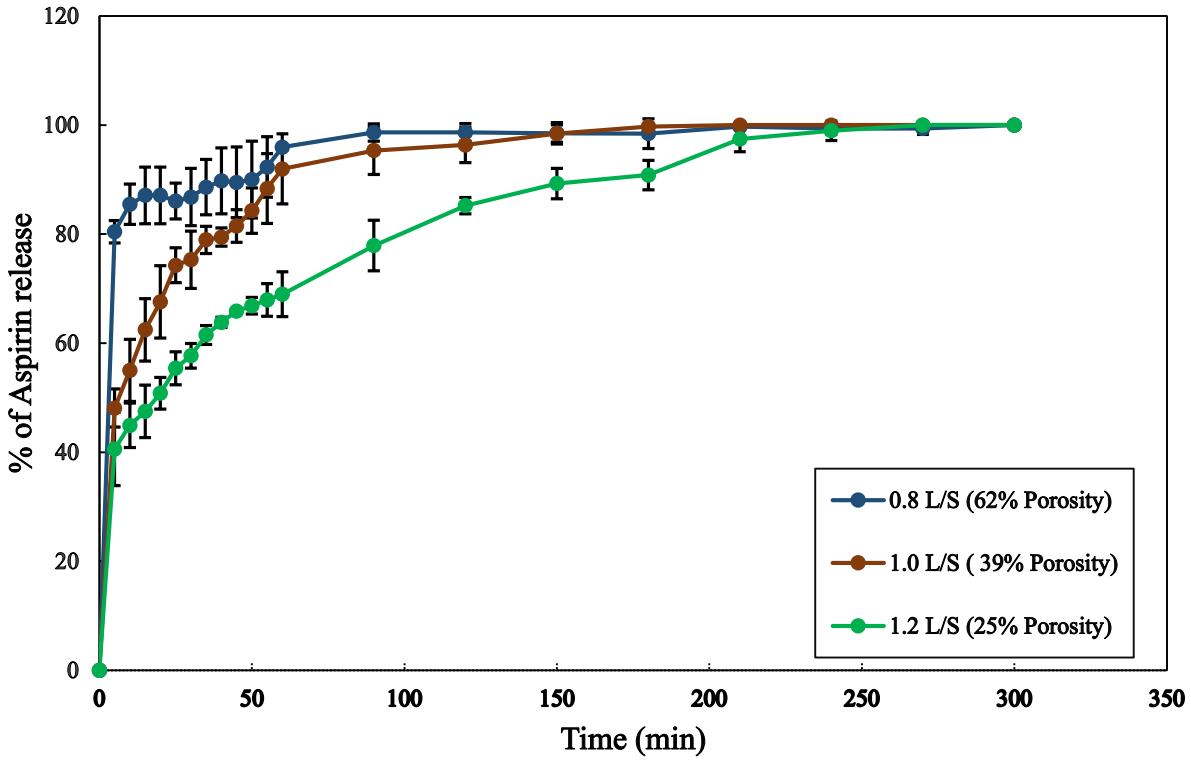

Figure 5.2: Normalised aspirin dissolutions profiles for granules with varying L/S ratios; 0 – 300 min. Error bars represent standard deviation for three repeats

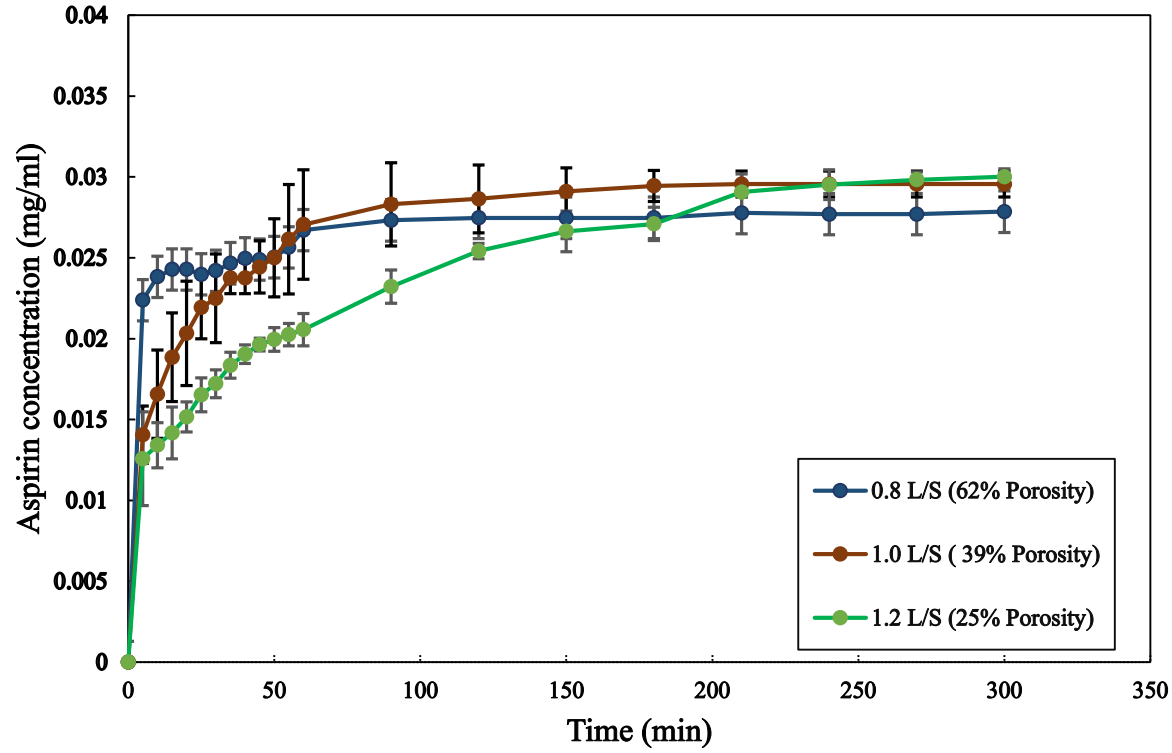

Figure 5.3: Un-normalised aspirin dissolutions profiles for granules with varying L/S ratios; 0 – 300 min. Error bars represent standard deviation for three repeats

The results displayed interesting behaviour exhibited by the 0.8 L/S granules (Figure 5.2 & 5.6). Initial dissolution was rapid, reaching over 80 % release within 5 min. This was followed by a plateau in the concentration profile until 40 min, and then a second period of increasing concentration (Figure 5.2). It is hypothesised that a transition in granule structure during this time may be responsible for this rapid change in the dissolution rate. This observation is supported by single granule swelling studies which are later discussed in Chapter 6. The transition occurred due to some loss of some granule particles facilitating the dissolution liquid to move around these granule particles and therefore increasing the granule effective surface area (the contact area between the granule particle surface and the dissolution liquid). These fragile granules appear noticeably disintegrated compared to the denser granules. Here, the rate of mass transfer of solute particles (drug particles) into the bulk solution is directly proportional to the surface area of the exposed solid (Seager *et al.*, 2018).

To discuss granule dissolution, it is important to address the liquid penetration mechanism which is believed to be the first step of granule dissolution (Markl and Zeitler, 2017). Several works have been published examining liquid penetration and, in general, larger void spaces between granule particles can accelerate the penetration of liquid into granule particles. Penetration of dissolution liquid into porous granules can be calculated using the well-known Washburn's Equation (2.1) (Hayata, 2002).

According to Equation (2.3), larger pores lead to a decrease in the time required for liquid penetration into the porous medium (Desai, *et al.* 2016). In this study, 0.8 L/S granules with an average pore diameter of 631 nm allowed for the fastest liquid penetration. In contrast, the average pore diameter of 1.0 L/S granules was 148 nm, which increases the period of liquid penetration in comparison to 0.8 L/S granules. The granules with the smallest pore diameter are the 1.2 L/S granules (58 nm). These tiny pores hinder liquid from penetrating granule particles, prolonging the aspirin release process.

After the liquid penetration step is completed and the dissolution liquid comes into contact with the solid phase, the drug particles dissolve in three consecutive steps as depicted in Figure 5.4. The first process involves the solute being wetted by the solvent (Smith, 2016) and the second step is freeing solute molecules from the solid phase due to the interfacial interaction between the solid and liquid phases. The final step is for molecules to diffuse from the interface into the

main solution (Figure 5.4). The diffusion process is analogous to a solute surface immersed in solvent. When a solid dissolves, its components travel along a diffusion gradient (diffusion layer) until the particle is totally dissolved and reaches the main solution (Chu *et al.*, 2012).

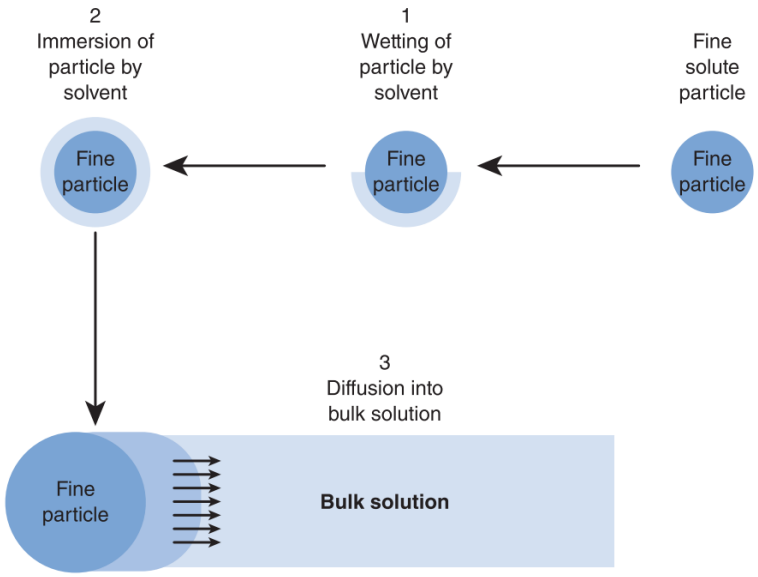

Figure 5.4: Three steps of particle solute dissolution (Smith, 2016)

During granule dissolution, these three steps, particularly wetting, are influenced by granule porosity, which accelerates the granule particle's ability to contact the solvent. In the case of dissolving high porosity granules (0.8 L/S), the large pores increase the surface area of the solid particle exposed to the dissolution liquid, resulting in a faster aspirin diffusion step. The step of wetting is important for dissolution. Typically, wetting properties are assessed using the contact angle. The contact angle is defined in accordance with the Young's equation as the angle between the tangent to the liquid–solid interface (Equation 5.1) (Forny *et al.*, 2011):

$$\gamma_S = \gamma_{LS} + \gamma_L . cos\theta \tag{5.1}$$

where γ_S is interfacial tension between the gaseous and solid phase, γ_{LS} is the interfacial tension between the liquid and the solid phase, γ_L is the surface tension of the liquid and θ is the wetting or contact angle. At a high contact angle, the attraction between solid and liquid molecules is strong, which accelerates the process of wetting.

As a result of intermolecular interactions between the solvent and large granule particles, these particles are reduced to fine particles. Dissolution has been ongoing since the solute particles separated from the bigger granule (Figure 5.5). However, after the solute particles are reduced to smaller particles, the increase in total available surface area allows for increased solvent interaction. The total solute surface area grows dramatically as the system/total particle size decreases. Wetting takes place once the solute has been reduced to finer particles. Wetting involves removing air from the particle surface as well as establishing good interfacial contact between the solute and solvent.

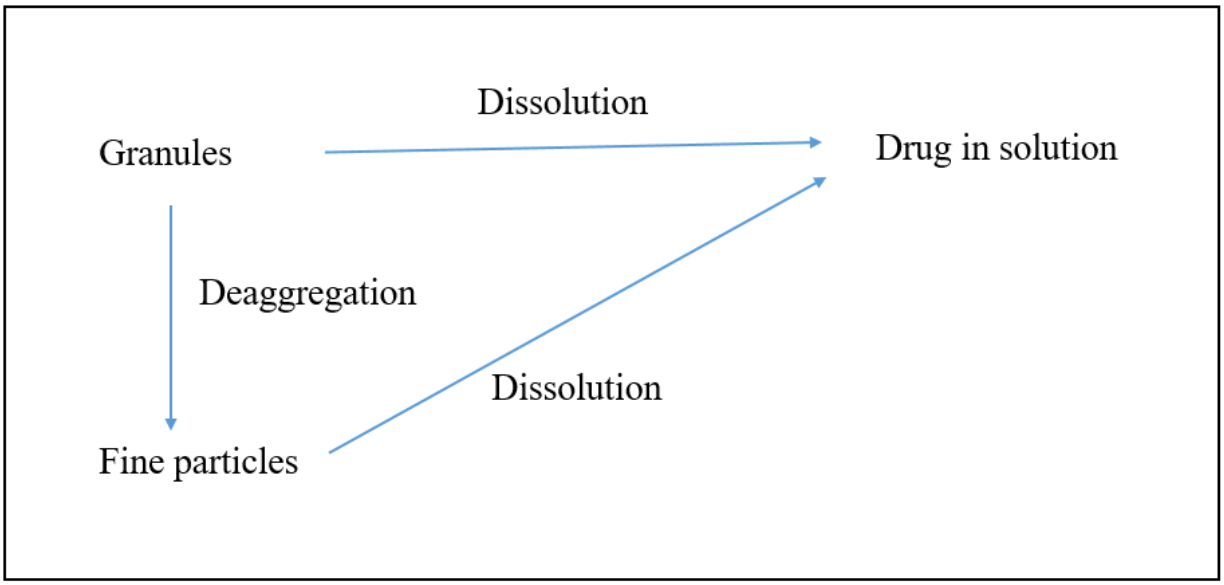

Figure 5.5: Process of granule dissolution. Adapted from (Smith, 2016)

The last step of the dissolution is particle diffusion into the bulk solution **(**mass transport). In this step, the drug particles are transported from the saturated layer into the bulk solution by the diffusion mechanism. Noyes and Whitney first defined the rate of mass transfer of solute particles (drug particles) into the bulk solution as a diffusive process (Equation 2.3) (Seager *et al.*, 2018): The rate of dissolution is directly proportional to the surface area of the exposed solid, diffusion coefficient and the concentration of solute particles present at the diffusion layer.

To understand the effect of granule structure, particularly porosity, it is necessary to investigate the first stage of dissolution, when the granules first come into contact with the dissolution liquid. Figure 5.6 shows the initial stage of dissolution during initial 5 min dissolution profiles

for granules produced at different L/S. According to the biopharmaceutical classification system, aspirin is a class 1 drug. It is slightly soluble in water, however, during the first 10 sec of the test, the dissolution of the 0.8 L/S granules was significantly more rapid than at other L/S ratios; during this time, nearly 50 % of the aspirin was released before the rate plateaued at 1.5 min. It is likely this rapid dissolution occurs as there was practically unhindered ingress of the dissolution liquid into the large void spaces within these granules, with rapid dissolution of the exposed drug particles. This was likely then followed by much slower ingress into finer pores in the granule, resulting in a plateau in concentration. These fragile granules have the highest pore size distribution compared to other L/S granules (Chapter 4, Section 4.2.2, Figure 4.7). Interestingly, Figure 5.7 (a) shows the 3D cross-section within the granule, demonstrating the large pore spaces in the 0.8 L/S granule, and the much finer pores. The 3D cross-sections were taken by applying various cuttings of the entire granule using CTvox 64 software (see Chapter 4 Section 4.3.3). Because these granules were produced with a relatively small amount of liquid binder, the binding forces between particles are weak and easily influenced by dissolution liquid. It is expected this weak particle-to-particle adhesion allows the dissolving liquid to rapidly distribute around each particle, resulting in rapid aspirin leaching. Granule porosity decreased significantly as the increasing L/S mass ratio increased and large cracks were reduced, indicating that significant granule densification had occurred (Figure 5.7 (b)). 1.2 L/S granules had the lowest granule porosity and the large cracks were not evident (Figure 5.7 (c)).

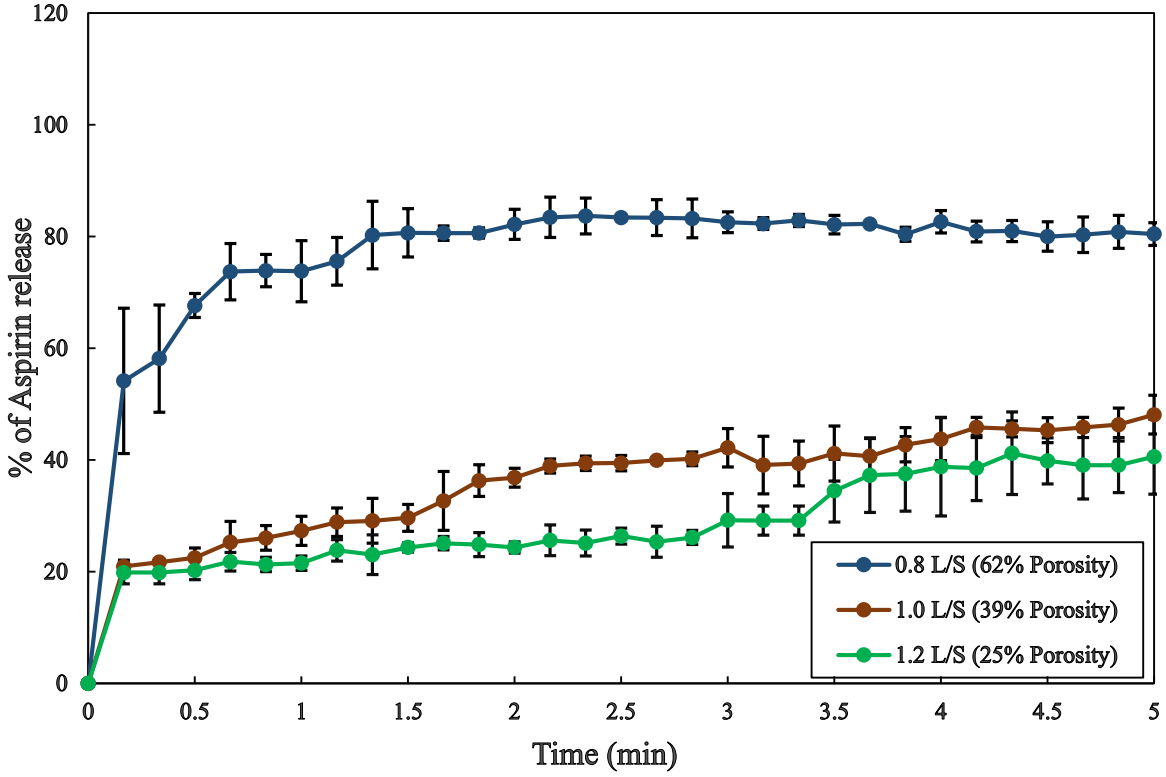

Figure 5.6: Aspirin dissolutions profiles for granules with varying L/S ratios; 0 – 5 min. Error bars represent standard deviation for three repeats

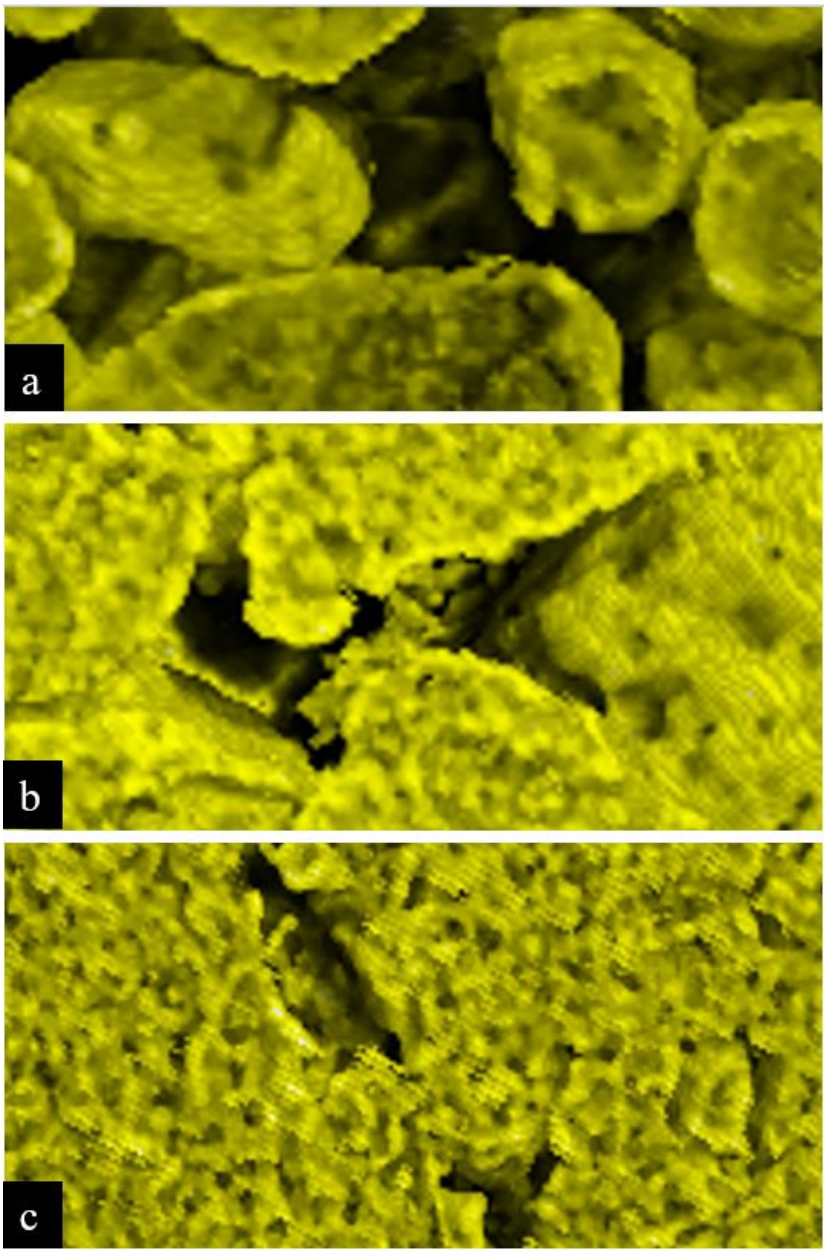

Figure 5.7: 3D cross-sections of granules with different L/S ratio (a) 0.8 L/S, (b) 1.0 L/S and (c) 1.2 L/S: 5 min granulation

The dissolution profiles for granules at both 1.0 and 1.2 L/S were lower compared to granules at 0.8 L/S for the first 5 min of dissolution. A rapid initial dissolution occurred within the first 5 sec which was most likely due to the dissolution of the aspirin on the granule surface, followed by a much slower increase in concentration (Figure 5.6). It is also clear that aspirin release from 1.2 L/S granules was slower compared to the 1.0 and 0.8 L/S granules. Overall, reduced granule porosity resulted in slower dissolution. In general, narrow pores decrease the ability of the fluid to enter the granule pores. Here, in 1.0 L/S and 1.2 L/S granules, the average pore diameter markedly decreased compared to 0.8 L/S granules. In this case and according to

Washburn's Equation (2.3), the dissolution liquid penetration will extend as the pore diameter decreased. Wider pores, enhanced surface tension of the liquid and an increase in the contact angle between liquid and granule matrix led to a decrease in the time required for liquid penetration into the pores.

A study conducted by Meng et al., (2019) studied the effect of L/S of a continuous high shear mixer granulation process on tablet dissolution kinetics. Consistent with these results, the authors found that increasing L/S ratio (0.35, 0.45 and 0.55 L/S were used) reduced porosity and increased granule size. A L/S of 0.55 generated the most densified granules with a small porosity of 33.7 % while a 0.35 L/S produced the most porous granules with a large porosity of 61.9 %. In contrast to this current focus on granule dissolution, they investigated tablet dissolution. Nevertheless, the authors found that denser, lower porosity granules produced slower drug release (Meng *et al.*, 2019).

5.2.3 Effect of granulation time on granule dissolution and aspirin release

In this work, granules were produced under different granulation (time conditions (Table 5.3). A liquid to solid ratio of 1.2 was chosen to investigate the effect of granulation time on granule structure because 1.2 L/S ratio produced lower porosity granules. Figures 5.8 and 5.9 show that for granules produced after 2.5 min, full aspirin release was achieved after approximately 100 min of dissolution. These 2.5 min granules have a total porosity 38 % which is the highest compared to the other granules in this series;5 min (25 %) and 10 min (32 %).

Table 5.3: The compositions and conditions of L/S ratio granules

Experiment No.	Mass of Aspirin (g)	Mass of MCC (g)	Mass of PEG (g)	Binder injection time (sec)	Wet massing time (min)	Total Granulation time (min)
1	10	90	120	90	1	2.5
2	10	90	120	90	3.5	5
3	10	90	120	90	8.5	10

As shown in Figure 4.12 (Chapter 4), the granules produced after 2.5 min have large pores or voids, which allows rapid ingress of water into the granule. On the other hand, granules produced after 5 min spent twice the time (200 min) releasing the whole aspirin content. This is because of the difficulty of the dissolution liquid to enter small pores within the granules. The dissolution liquid spent approximately 150 min to leach out the whole aspirin from 10 min granules. This result may at first glance be counter-intuitive, as the 10 min granules release faster than the 5 min, however as is explored below, this can be explained by the interesting microstructure of the 10 min granules. As shown in Figure 5.9, the aspirin concentration in 2.5 min granules was higher,.This is possible because the time of granulation was insufficient to equally distribute all aspirin powder between granules.

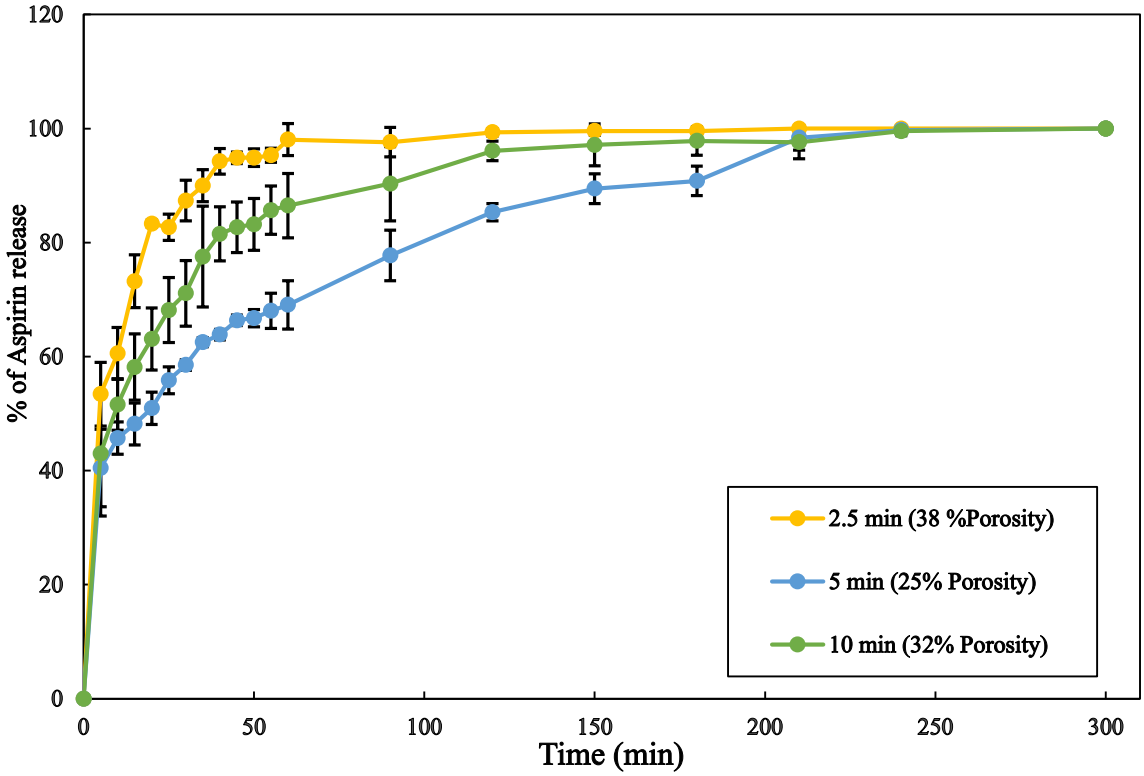

Figure 5.8: Normalised aspirin dissolutions profiles for granules with varying granulation time for a L/S of 1.2: 0 – 300 min. Error bars represent standard deviation for three repeats

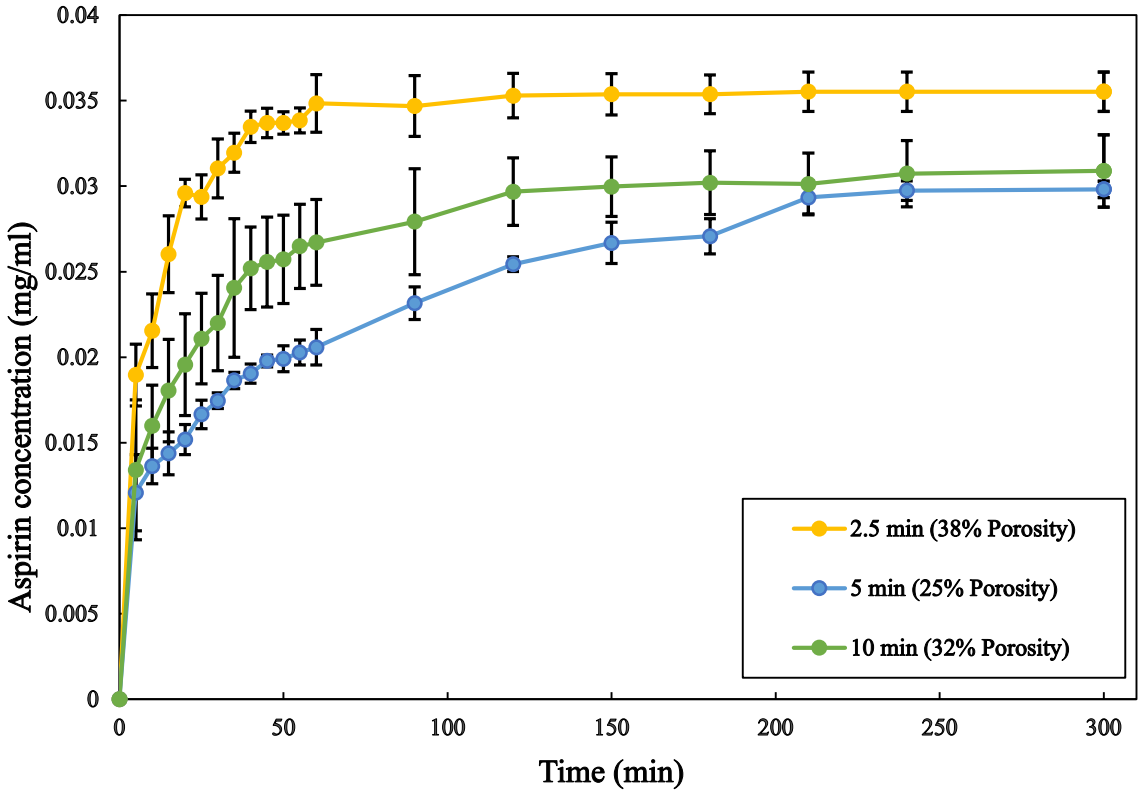

Figure 5.9: Un-normalised aspirin dissolutions profiles for granules with varying granulation time for a L/S of 1.2: 0 – 300 min. Error bars represent standard deviation for three repeats

The effect of granulation time on the initial stage of aspirin dissolution is studied during the first 5 min. Figure 5.10 shows the first 5 min of aspirin release, and in a similar fashion to that seen for the effect of changing L/S, granule dissolution rate was fastest for the highest porosities, and slowest for the lowest porosity. The granules produced with the shortest granulation time of 2.5 min had the highest measured porosity (38 %) and dissolved the quickest (50 % the total aspirin concentration was released within 5 min). This high porosity improves the contact between the dissolution liquid and granule particles, which enhances the likelihood that more aspirin particles will come into contact with and dissolve in the dissolution liquid.

The 3D cross-section images of granules produced after 2.5 min (Figure 5.11 (a)) shows a wide crack within the granules that also increases contact with the liquid. As previously discussed, the granulation period of 2.5 min was insufficient to achieve substantial granulation consolidation, resulting in significant cracks within the granule, and hence a more porous granule structure. During granule dissolution, the dissolution liquid can quickly enter these

wide cracks, allowing for a rapid liquid-solid interaction in a short amount of time. In the first 5 min, the 2.5 min granules exhibit the fastest aspirin release.

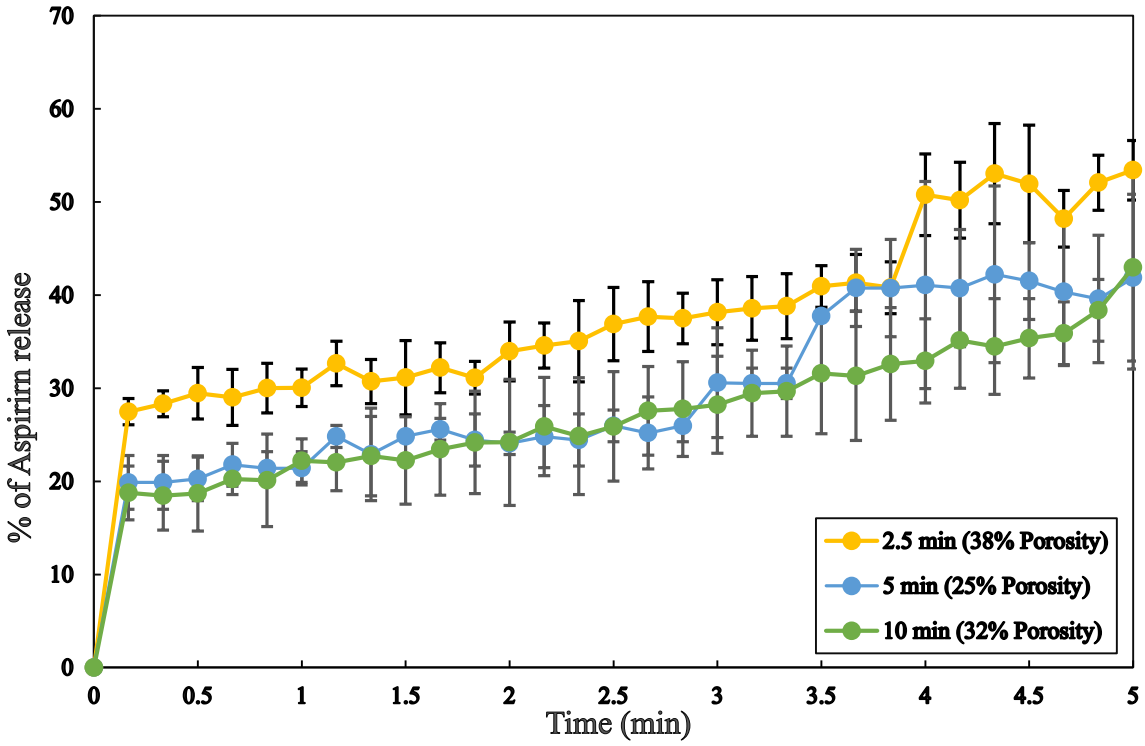

Figure 5.10: Aspirin dissolutions profiles for granules with varying granulation time for a L/S of 1.2: 0 – 5 min. Error bars represent standard deviation for three repeats

Increasing the granulation time to 5 min reduced the porosity from 38 % to 25 %. This is consistent with the 2012 study conducted by Badawy, who found that as granulation time was increased from 10 sec to 50 sec, the mean pore diameter of granules decreased. Despite the short granulation period employed in this study compared to the time used in this current investigation, granule coalescence and growth may occur, resulting in a decrease in granule porosity.

In this thesis, increasing the granulation time to 5 min reduces the size of the large cracks with the granule (Figure 5.11 (b)). Granule porosity has decreased significantly, and large cracks have reduced, indicating that significant granule densification has occurred. 5 min granules had the lowest granule porosity. The 10 min sample showed higher porosity (32 %) than the 5 min sample (25 %), and as expected, demonstrated faster dissolution than the 5 min sample and some cracks reappear (Figure 5.11 (c). This is possibly due to the granule's prolonged exposure

to impeller impacts and shear forces. Furthermore, the shear forces generated during the 10 min blending process in a granulator can indeed contribute to drying of the granules.

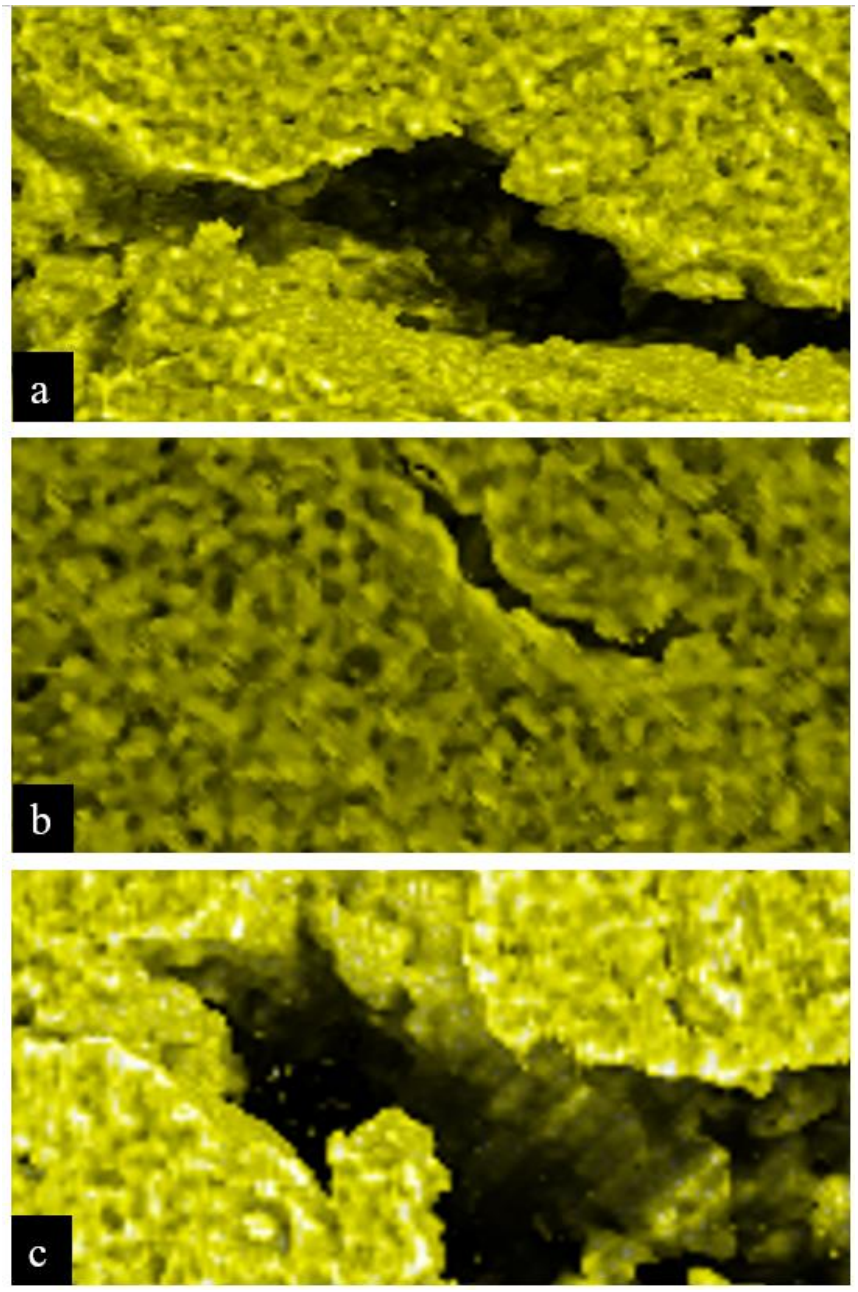

Figure 5.11: 3D cross-sections of 1.2 L/S granules with different granulation time: (a) 2.5 min, (b) 5 min and (c) 10 min

Shi et al. (2011) investigated the influence of extended granulation time on the porosity of MCC granules, and found the porosity dramatically decreased when granulation time increased from 1 to 10 min. After 10 min of granulation, there was no further granule consolidation, and the granular porosity remains constant after 40 min. It is known that the breakage/deformation and consolidation behaviour of granular materials is strongly related to material properties as

well as granulation conditions (Iveson *et al.*, 2001) and it is unsurprising that different granulation systems demonstrate different consolidation and deformation kinetics.

5.2.4 Granule porosity and aspirin release

The release of aspirin was strongly influenced by the granule porosity as shown in Figure 5.12. The time required for 95 % of aspirin release was decreased by increasing the granule porosity and approximately 200 min was required for the denser granules (25 %) to release 95 % of the aspirin. On the other hand, 53 min was sufficient to release 95 % of the aspirin from the highest porosity granules (62 %). Figure 5.13 shows the relationship between the granule porosity and the entire aspirin release for 5 hrs. The denser granules (25 %) release aspirin very slowly, as the dissolution liquid is assumed to slowly enter the narrow pores and contact the aspirin molecules. Aspirin was quickly released from the 62 % porosity granules where 80 % of aspirin particles were released in within approximately the first 2 min of the dissolution test due to rapid liquid penetration and absorbance into the granules.

This demonstrates two extremes of porosity induced release differences. An interesting result is that 38 % porosity granules give faster aspirin release compared to 39 % porosity granules. This is because 38 % porosity granules were prepared by 2.5 min granulation and these granules generally contained large surface cracks and a higher pore size distribution compared to 39 % porosity granules (1.0 L/S) which were prepared by 5 min granulation time (Figures 4.7 and 4.10, Chapter 4). These voids allow for more liquid penetration and thus, accelerating the rate of aspirin release. The effect of these large voids is also seen in the 32 % porosity granules (10 min granules) which show aspirin release much faster compared to 25 % porosity granules (5 min).

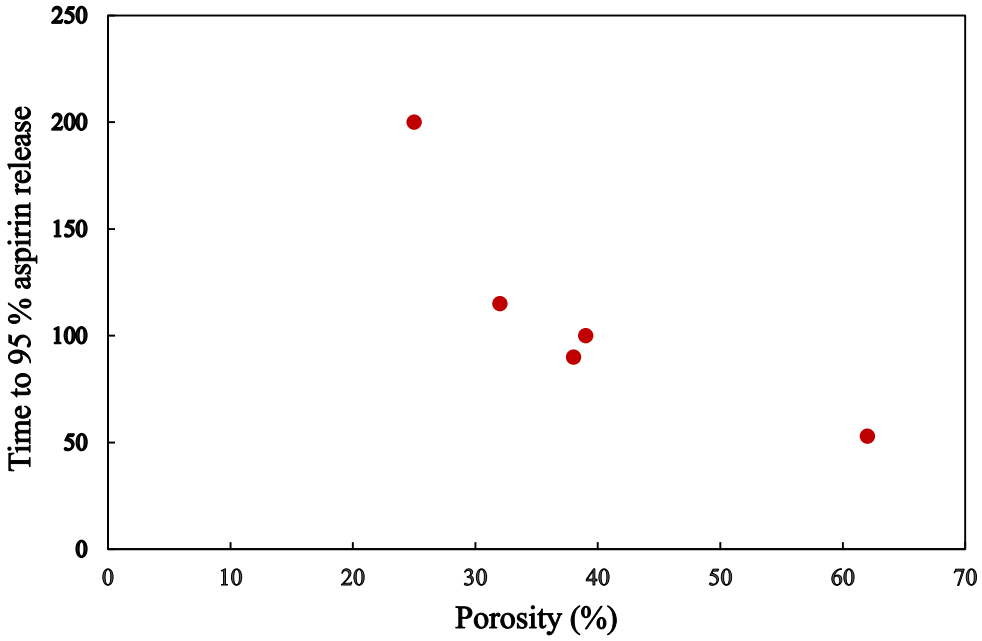

Figure 5.12: Time for 95 % aspirin release of different pores granules.

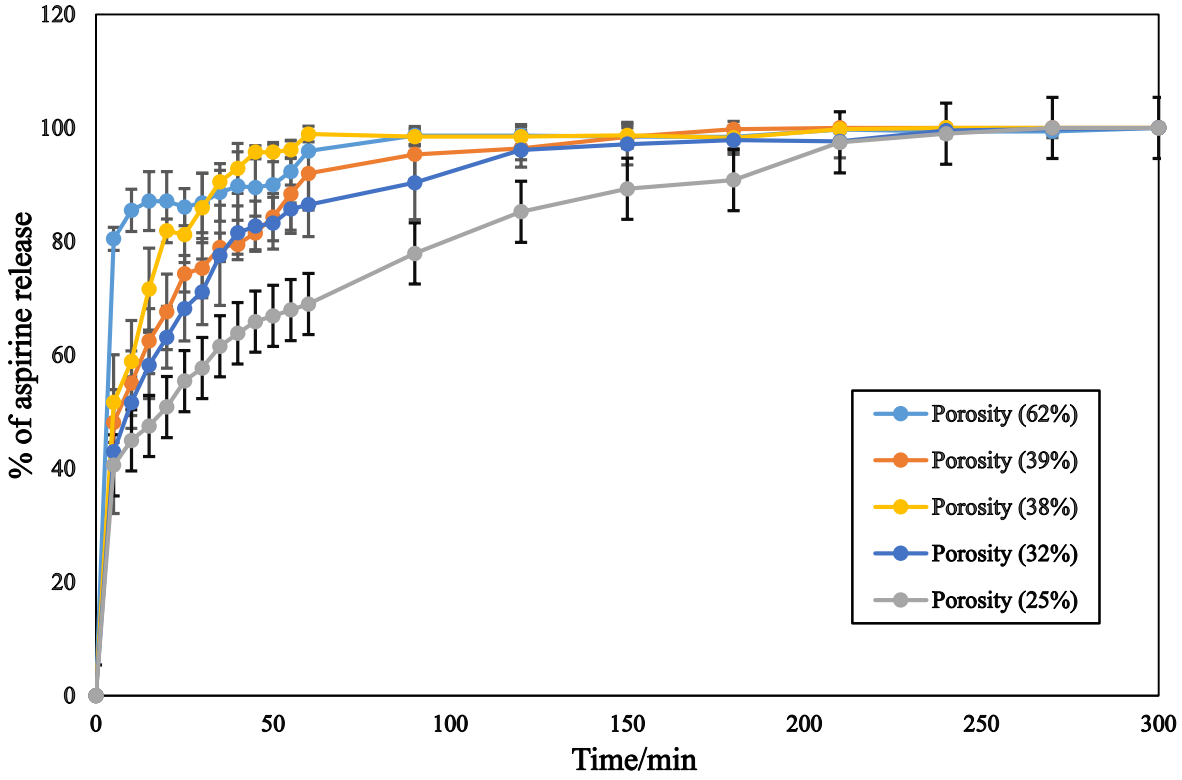

Figure 5.13: Aspirin dissolutions profiles for granules with different porosities: 0 – 300 min. Error bars represent standard deviation for three repeats

5.3 Conclusions

In this chapter, a mechanistic relationship between the granule product performance to process parameters was studied. This work specifically established the significant influence of liquid to solid mass ratio and granulation times on granule microstructure and, subsequently, the dissolution rate. A low liquid to solid ratio and short granulation time promoted higher porosity granules which displayed faster dissolution rates when compared to selecting a longer granulation time and high liquid to solid ratio. The results revealed important insights where a longer granulation time caused the granules to increase in porosity due breakage taking place within the granulator. It is likely that the higher porosity granules experienced accelerated liquid uptake regarding penetration and absorbance into the granule pores which, evidently, led to faster dissolution of the drug into the dissolution media. This was further supported by advanced characterisation of the granule structure where differences in crack observations were noticed.

Whilst these results support the link between granule structure, process and performance, further deep understanding into the granule and liquid interaction is essential for robust linking. The following chapter investigates this interdependence by characterising and examining the interaction between liquid and a single granule to understand the early stage mechanisms of drug dissolution such as disintegration.

CHAPTER 6 - Analysis of individual granule swelling performance

6.1 Introduction

The results shown in Chapter 5 displayed strong links between the granule structure and the drug release performance. This was examined through varying formulation (L/S ratio) and process parameters (granulation time) and measuring the aspirin release concentration profiles. A key outcome from Chapter 5 highlighted the need and importance for carefully studying and establishing further links between the product structure (i.e., granule composition) to product performance (i.e., other than the release concentration profile).

Granules are often formulated to produce some desired function and performance. For example, in the manufacture of oral solid dosage forms, the performance of a drug upon patient administration is typically determined by the granule disintegration and dissolution mechanisms (Smrčka *et al.*, 2016). Whilst a key performance indicator for any drug product is the release profile of the active ingredient and the resulting shape of the profile (Azarmi *et al.*, 2007), disintegration is also an important performance measure (Markl *et al.*, 2017). Current disintegration tests as defined by the pharmacopeia, do not provide information on the contributing mechanisms driving various stages of API release, and do not provide insight into the relationships between internal microstructure and release profile. Measuring the wetting and disintegration rate would provide further information on the final product performance and its variability. To enable break-up of the inter-particulate bonds within the compact, a disintegrant is usually added to the formulation which is a pharmaceutically inert, hydrophilic excipient that is insoluble in water and gastrointestinal juices. Depending on the type of chosen disintegrant (e.g., crosslinked polymers, starch- & cellulose-based excipients), disintegration mechanisms can vary considerably (Markl and Zeitler, 2017).

Disintegration mechanisms consist of swelling, wicking (capillary action), strain recovery, interruption of the particle-particle bonds and heat of interaction (Desai, *et al.*, 2016). The relative rates of these competing mechanisms can have a profound impact on the active ingredient particle size distribution and surface area (Figure 6.1) as well as the overall release profile (Desai, *et al*., 2016). Disintegrants are a critical part of the dosage form as they ensure

the break-up of the dosage form into smaller fragments upon ingestion, to allow the onset of drug dissolution and eventual absorption.

In this chapter, the behavior and underlying disintegration mechanisms for pharmaceutical granules is examined by varying the microstructures produced from different formulation and process parameters. A systematic experimental study was designed to provide insight into the several competing mechanisms within the early stages of disintegration, which are shown to be highly dependent on the product structure. Individual granules were subjected to a well-controlled, continuous streams of fluid (water) within a purpose-built, 3D-printed flow cell. The platform was coupled to microscope digital camera system and image analysis algorithm for quantitative monitoring of the evolving granule diameter. Optical coherence tomography (OCT) was also implemented to examine and reveal cross-sectional 2-dimensional surface imaging changing over time. This provided a powerful and deep insight into the swelling kinetics which was evidently impacted by the granule microstructure.

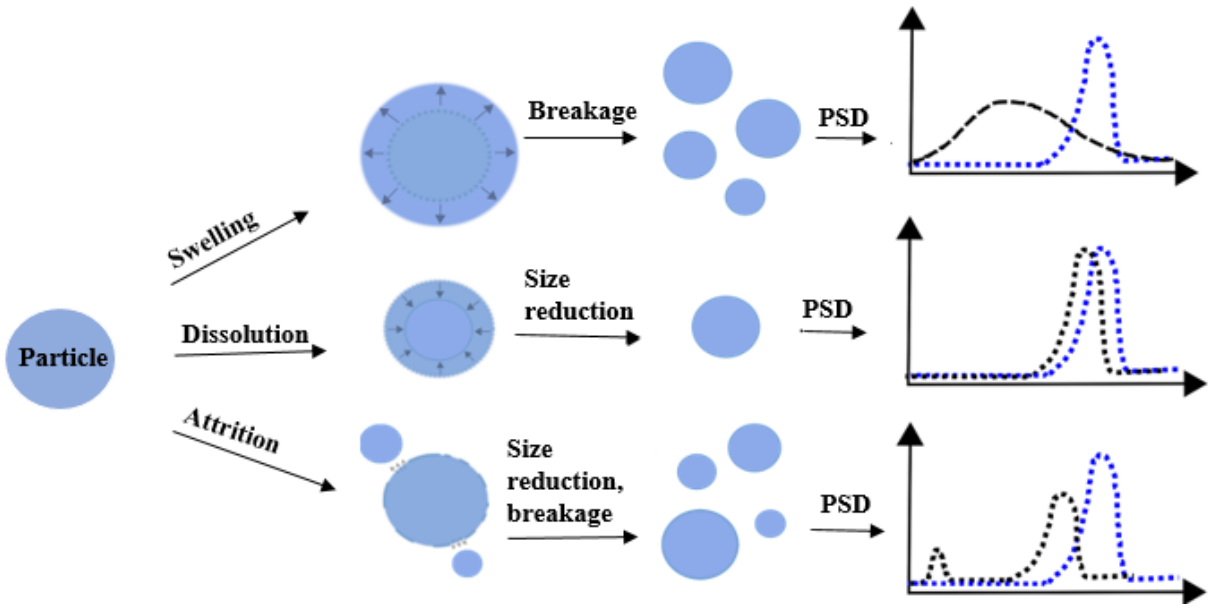

Figure 6.1: Particle dissolution and disintegration process. Adapted from D. Smrčka, J. Dohnal, F. Štěpánek, *European Journal of Pharmaceutics and Biopharmaceutics*, 106 (2016)

6.2 Results and discussion

In this work, all granule samples tested for drug release and dissolution in Chapter 5 were tested for swelling and disintegration through an individual granule study as shown in Table 6.1. These granules were produced using a high shear wet granulator with different L/S ratio and granulation times (Chapter 3, Section 3.3). Table 6.1 shows the conditions and compositions of these granules.

The experiments were designed to study the swelling behaviour of individual granules during disintegration comprising of different microstructures by using a customized flow-cell. Each flow cell experiment was repeated three times. The flow cell was designed to hold the granule while allowing for continuous water flow to wet and pass through the granule. Full details of the experimental procedure are reported in Section 3.6, Chapter 3.

Table 6.1: Conditions and compositions of selected granules

Experiment No.	Mass of Aspirin (g)	Mass of MCC (g)	Mass of PEG (g)	L/S Mass Ratio	Total Granulation time (min)	Granule sieve size fraction (μm)
1	10	90	80	0.8 L/S	5	2000-2360
2	10	90	100	1.0 L/S	5	2000-2360
3	10	90	120	1.2 L/S	5	2000-2360
4	10	90	120	1.2 L/S	2.5	2000-2360
5	10	90	120	1.2 L/S	10	2000-2360

6.2.1 Effect of liquid to solid ratio (L/S) on single granule performance

6.2.1.1 Monitoring granule mechanisms and size

Granule structures generated from varying the L/S mass ratio parameter were visualised at different time points for a period of 2 hours (Figure 6.2). Captured images were then analysed to provide the evolving size profile over time (Figure 6.3 & Figure 6.4).

Figure 6.2 (a) shows 0.8 L/S granules and their swelling over time. These granules exhibited the highest porosity, measured in Chapter 5 (62 %), and the images display noticeable voids within the microstructure. Liquid penetration into the granule is assumed to be instantaneous and results in a gradual loosening of the granule microstructure, accompanied by an initial size increase during the first 30 min (Figure 6.3 & Figure 6.4). No significant changes occurred from 60 min to 120 min which is further supported by the full size profile (Figure 6.3).

For the 1.0 L/S ratio granule (Figure 6.2 (b)), which has a lower porosity (39 %), a different behaviour was observed. Cracking was formed within the microstructure after 30 min which widened over time (60 & 120 min). This produced a slower increase in the granule size and after 60 min, no further changes occurred (Figure 6.3). The results for the 1.2 L/S granule which consisted of the lowest porosity (25 %), also show differences compared to 0.8 & 1.0 L/S granules. Here, crack formation was observed along with a larger increase in the granule size over the entire duration of the experiment (Figure 6.3).

Increasing the L/S ratio produces granules with lower porosity which, in turn, are denser. This influences the disintegration behaviour and the relative contributions of each mechanism. However, in all cases, it is believed that wetting and swelling kinetics were significantly affected by varying the granule porosity as was noted from the evolving full granule size profiles (Figure 6.3) and the zoomed in profiles during the first 5 min (Figure 6.4). Figure 6.5 shows a typical swelling profiles for 1.0 L/S mass ratio granules for three time experiments as example of experiment repeats.

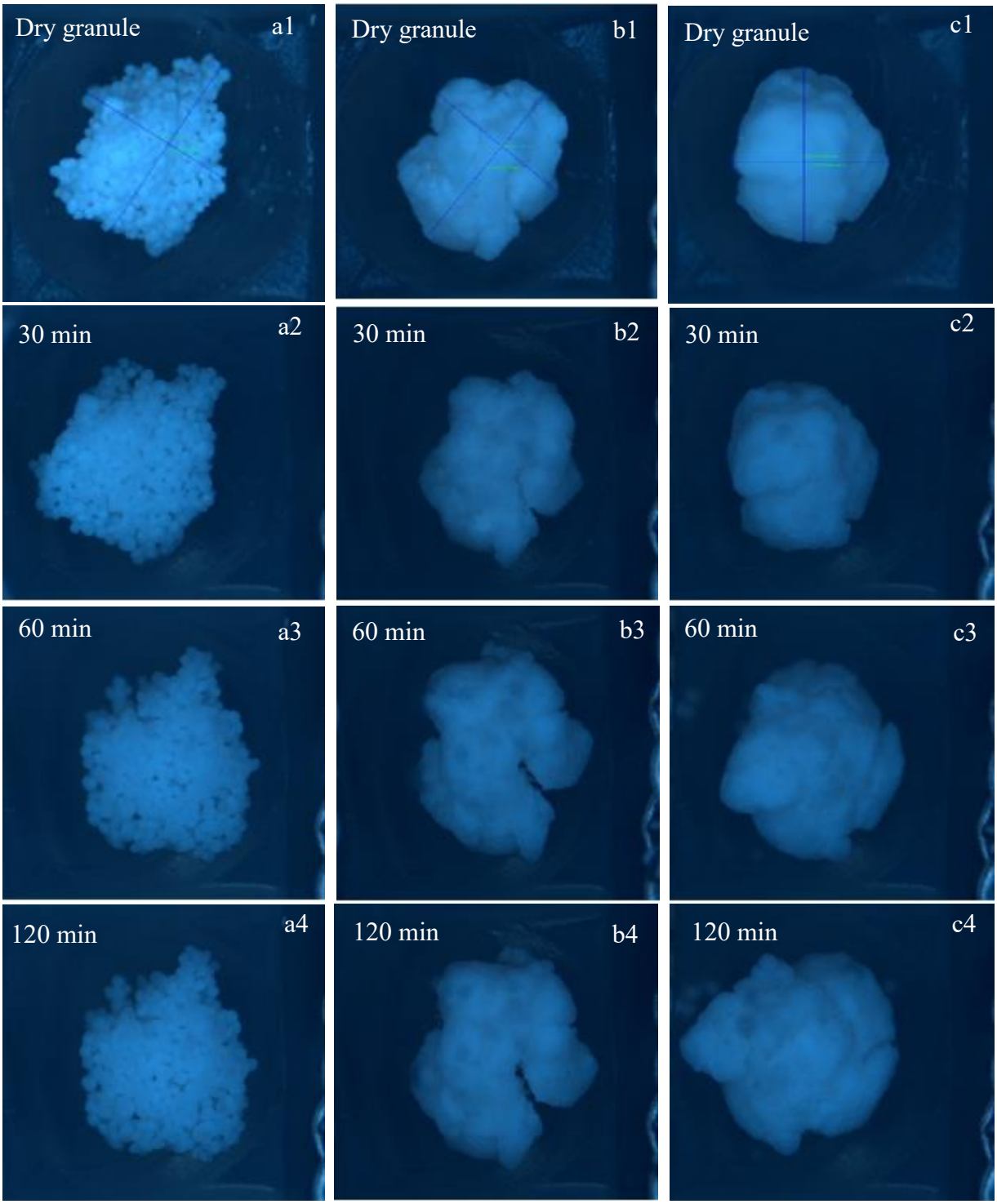

Figure 6.2: Images of granules with varying L/S ratio (a) 0.8 L/S, (b) 1.0 L/S and (c) 1.2 L/S at different times

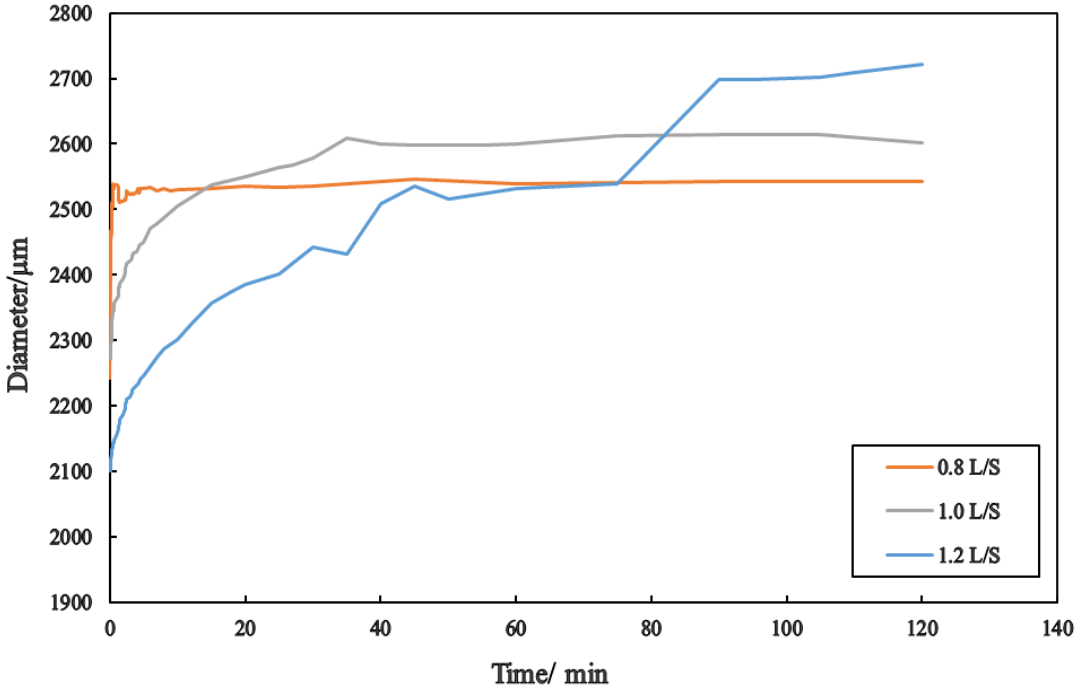

Figure 6.3: Granule diameter profiles of varying L/S ratio granules within 120 min

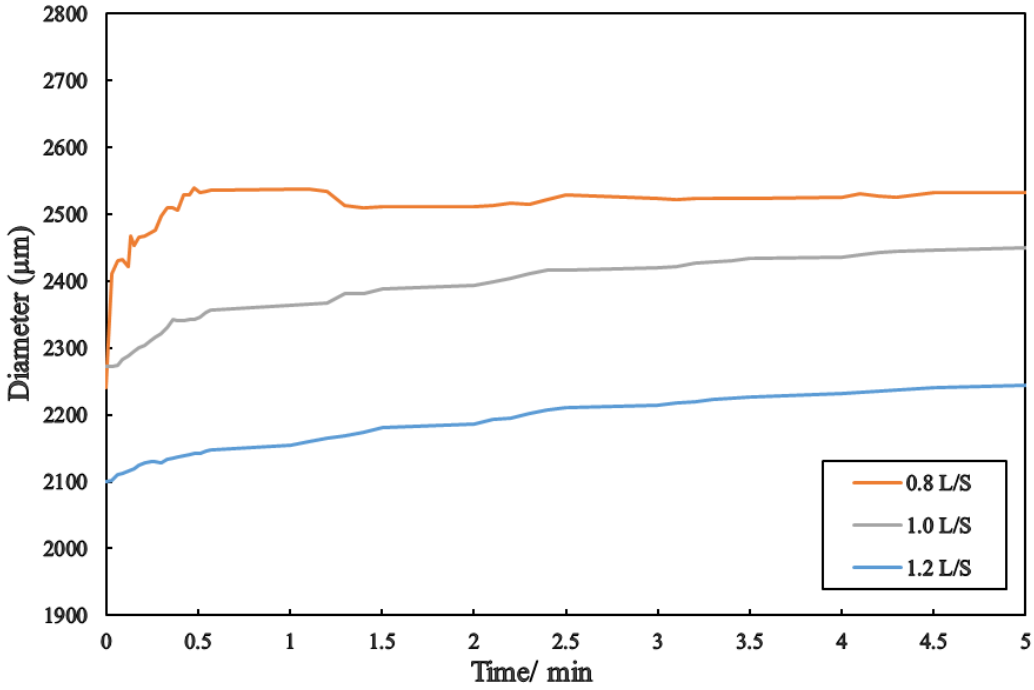

Figure 6.4: Granule diameter profiles of varying L/S ratio granules within the initial 5 min.

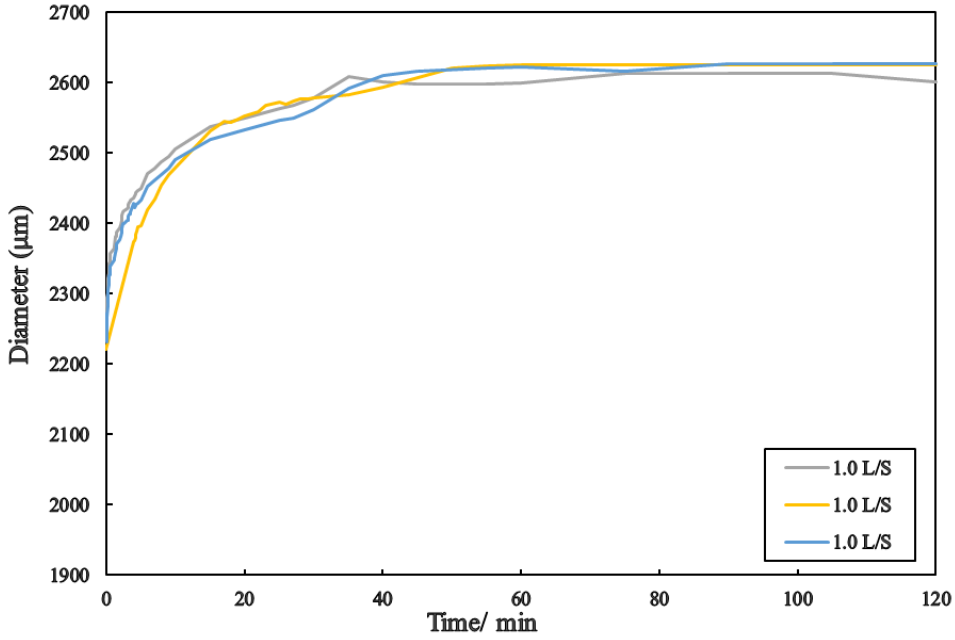

Figure 6.5: Typical swelling profiles for 1.0 L/S granules for three repeats

6.2.1.2 Further analysis of surface features and swelling

To enable a deeper analysis of the microstructure, particularly at the surface level, granules from varying the L/S mass ratio parameter were also visualised separately using the OCT technique (described in Section 3.6 Chapter 3) which produces 2-dimensional cross-sectional surface imaging over time. This technique provides non-invasive, high-resolution, and real-time visualization of granule structures (Figure 6.6). The depth that can be visualized using OCT depends on several factors, including the specific OCT system used and the type of tissue being imaged. However, in general, OCT can provide imaging depths ranging from a few millimetres to a few centimetres.

Figure 6.6 shows captured OCT images for a 0.8 L/S mass ratio granule at different time points during the experiment. As shown earlier from Figure 6.2, loosening of the microstructure was believed to be a key contributor to the overall swelling mechanism. Upon careful examination, it becomes apparent that the granule featured in Figure 6.6 possesses a certain level of fragility. The images reveal that following an initial period of 10 minutes, the granule experiences a notable transformation within a specific region. This transformation is characterized by the movement and loosening of particles within the granule. The observed particle mobility and microstructural rearrangement contribute to the overall swelling process.

However, it is noteworthy that after the initial 10 minutes, the images do not exhibit any significant changes. This implies that the granule reaches a relatively stable state, where further alterations in its microstructure or particle distribution become less pronounced. The stability observed beyond the 10 min mark suggests that the majority of the swelling process has taken place during this early stage, and the granule has achieved a state of equilibrium.

In the context of liquid penetration into the compact granules, the strength of inter-particle bonds plays a crucial role. The force generated by the liquid within the granule pores is only effective if the bonds between solid particles are weak (Peppas and Colombo, 1989; Markl and Zeitler, 2017). Figure 6.6 illustrates the dissolution liquid's ability to break down inter-particle bonds within 10 minutes. The rate of liquid penetration depends on the balance between capillary and opposing viscous forces. Capillary flow can be described by Washburn's equation (Desai et al., 2016). It can be anticipated that larger pore sizes would allow for more liquid uptake, potentially enabling faster dissolution.

In this scenario, it is assumed that within 10 sec, the liquid rapidly penetrates into the porous structure, initiating the disruption of particle-particle bonds. As the granule compact loosens over time, the liquid gains improved access to the granule's void space, facilitating swelling. Consequently, the granule particles rapidly expand, enabling them to freely migrate within the dissolution liquid.

In summary, the strength of inter-particle bonds determines the effectiveness of liquid penetration in compact granules. Figure 6.6 demonstrates the dissolution liquid's capability to break these bonds within 10 min. The balance between capillary and viscous forces governs the rate of liquid penetration. Larger pore sizes accommodate greater liquid uptake, leading to faster dissolution. As the granule compact loosens, the liquid can enter the granule's void space, promoting swelling and allowing the granule particles to move freely within the liquid medium.

The comparison between the OCT images of granules with a 0.8 L/S mass ratio and a 1.0 L/S mass ratio revealed significant differences. The OCT technique proved to be effective in capturing the gradual expansion of the granule's surface, providing evidence of its sensitivity in tracking swelling phenomena. This capability was observed to manifest after 0.5 min, indicating that OCT can detect changes in the granule's structure and size over time.

On the other hand, the presence of cracking in the granules was clearly visible in the digital images (Figure 6.2). However, this observation was challenging to confirm solely based on the OCT images. While the OCT technique did not provide a direct visualization of the cracks, it did show gaps at the granule's surface. These gaps were specifically marked at three time points: 10 min, 60 min, and 120 min (Figure 6.7).

The gaps detected in the OCT images suggest the possibility of cracks within the granules, although they might not be as clearly discernible as in the digital images. It is important to note that the OCT technique primarily relies on the detection of changes in the internal and external structures of the granules using light waves, whereas digital images provide a higher level of detail at the microscale

Figure 6.7 displays the swelling behaviour of a 1.2 L/S ratio granule, which exhibited the lowest porosity value at 25 %. In contrast to the 0.8 L/S and 1.0 L/S granules, the expansion of the granule's surface commenced after 1 minute of the test. This disparity could be attributed to the presence of smaller pore sizes within the granule, which potentially hindered water penetration into the granule particles. The gradual expansion of the granule's surface continued for the duration of 120 min, exerting pressure on the granule particles, leading to some surface fragmentations that became visible after 60 min (as shown in Figure 6.6 and Figure 6.8).

Comparatively, both the 1.0 L/S and 1.2 L/S mass ratio granules demonstrated a greater capacity for swelling. This can be attributed to the presence of small pores within the granules, allowing for adequate space for pressure build-up, which in turn caused disintegration. Generally, a low porosity, coupled with a small void space, intensifies the forces generated by the swelling of excipients. Consequently, higher swelling forces lead to increased time required for the breakdown of inter-particle bonds. This phenomenon is supported by previous studies by Lowenthal (1972) and Markl and Zeitler (2017).

In summary, Figure 6.7 presents the swelling performance of a 1.2 L/S granule with the lowest porosity. The delayed onset of surface expansion, the subsequent pressure exerted on the granule particles leading to fragmentation, and the enhanced swelling capacity of the 1.0 L/S and 1.2 L/S granules collectively highlight the influence of porosity and pore size on the swelling behaviour of the granules.

Several studies have shown that MCC particles exhibit omnidirectional swelling (Desai et al., 2012; Quodbach and Kleinebudde, 2014; Berardi et al., 2018). Omnidirectional swelling is

usually driven by the chosen formulation and material. On the other hand, uni-directional swelling is commonly referred to as strain recovery. When the particle comes in contact with liquid, these particles recover to their original shape. Here, because no high force compaction process was applied to the granule, and no tableting process was used, the most likely swelling mechanism is omnidirectional swelling. The OCT images in Figure 6.8 shows the omnidirectional swelling of 1.2 L/S granule.

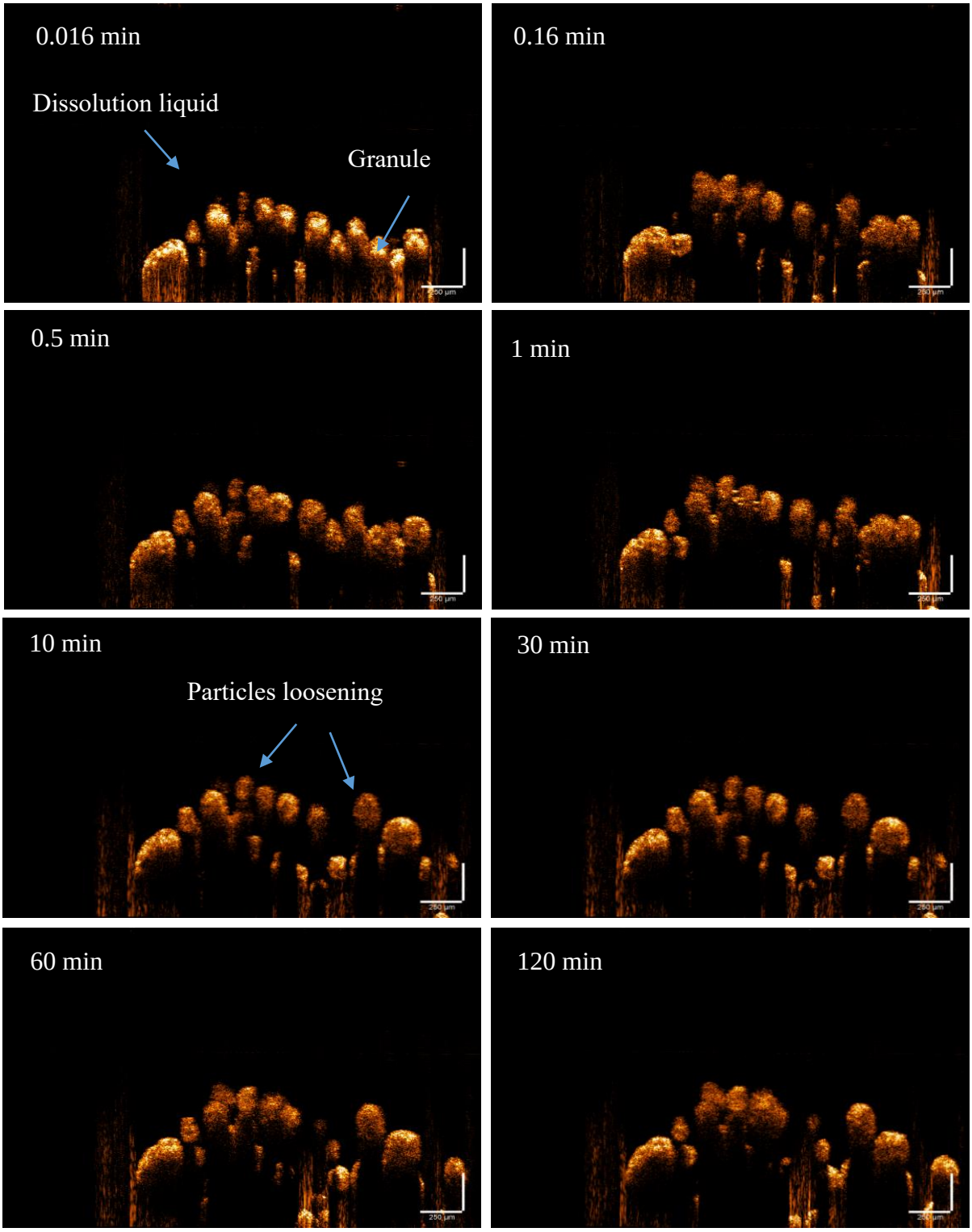

Figure 6.6: OCT images of the granule at 0.8 L/S ratio at different times. Scale bar = 250 µm

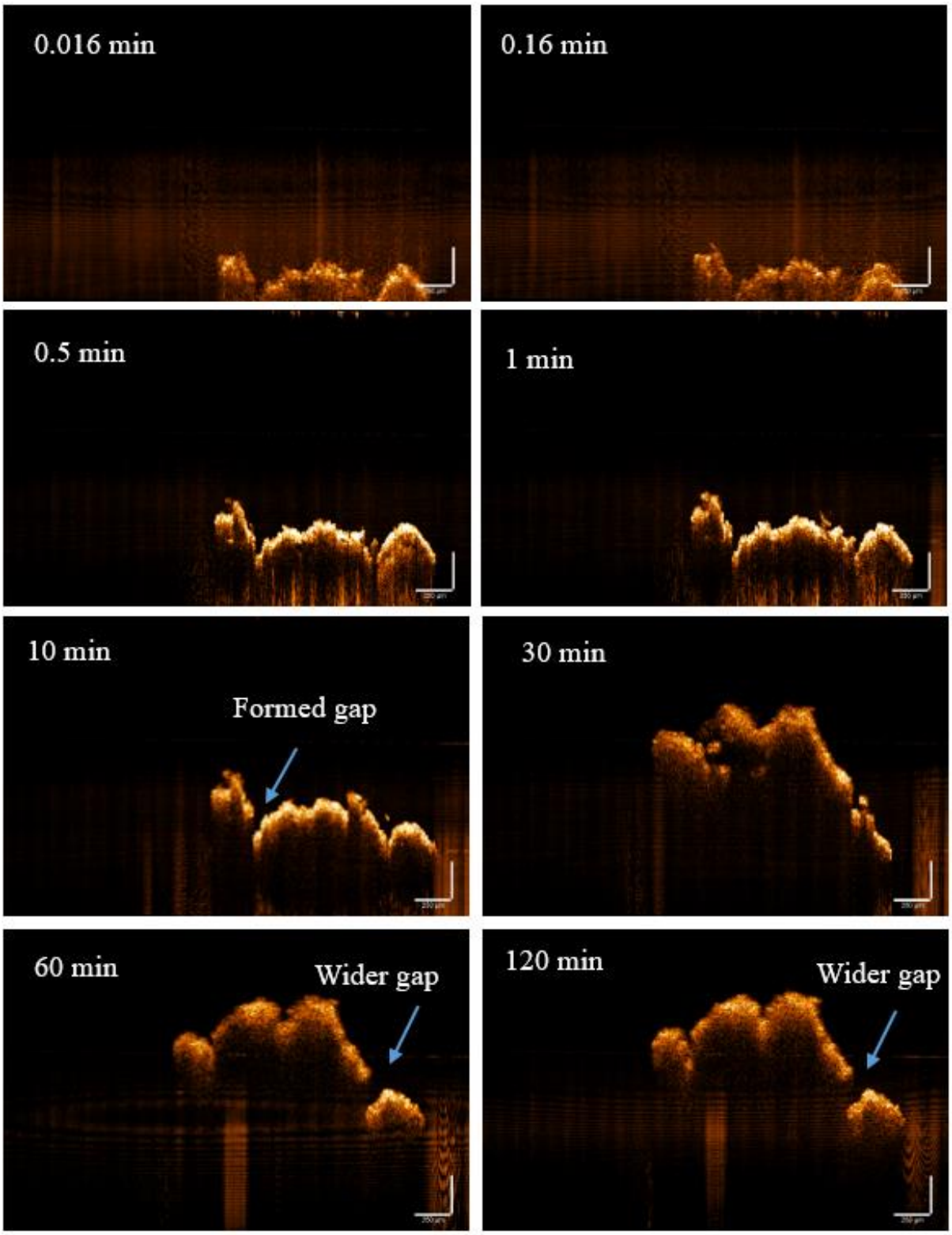

Figure 6.7: OCT images of the granule at 1.0 L/S ratio at different times. Scale bar = 250 μm

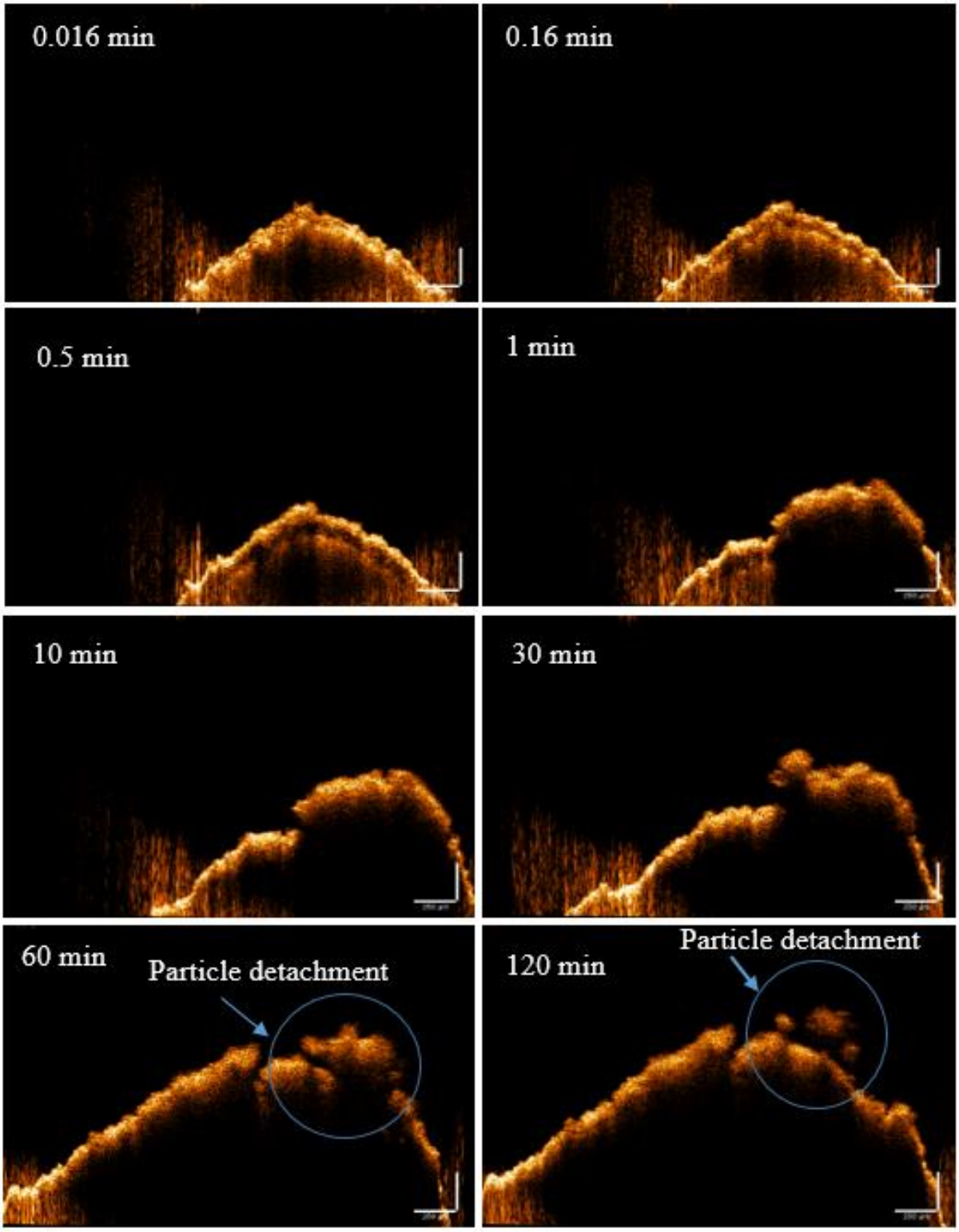

Figure 6.8: OCT images of the granule with 1.2 L/S mass ratio at different times. Scale bar = 250 µm

The swelling characteristics of L/S mass ratio granules were investigated by measuring the change in the surface swelling rate upon long duration of water contact. 2D (analyzer 2022.1) software was used to measure the height and width of the granule. The measurements were performed on selected images. In total, 32 images were chosen at specific time intervals: every 10 sec for the first minute of the experiment, then every 1 min for the next 10 min, and finally, every 10 min up to 140 min.

To determine the increase in granule area for each image, the area of the previous image was subtracted from the current image. The swelling rate was then calculated by dividing the swelling area of each image by the total swelling area observed after 140 min. The full swelling and the 5 min swelling profile are shown in Figure 6.9 & Figure 6.10 respectively. The 0.8 L/S granule which has a 62 % porosity swelled completely within 20 min. Due to the high granule porosity, water is assumed to quickly penetrate a large void space and flow around the granule particle, causing all particles to swell approximately at the same time and shows 80 % of it is swelling was within the first 5 min. After roughly 30 min, there is no more particle swelling observed, and this correlates with results from Chapter 5 which shows that 90 % of aspirin was released at first 30 min of 0.8 L/S granule water contact.

Compared to other porosity granules, the 1.2 L/S granule has a low porosity of 25 %. The observed swelling rate was slow, and only 6 % of the total swelling was achieved in this first 5 min. It is believed this is due to slow liquid penetration into granule particles, leading this granule to continue swelling for approximately 140 min (Figure 6.9 & Figure 6.10). On the other hand, the 1.0 L/S granule, which has a porosity of 39 %, shows a moderate swelling performance and shows 30 % of total swelling was within the first 5 min. The maximum and completed swelling of this granule occurred approximately within 100 min duration time (Figure 6.9).

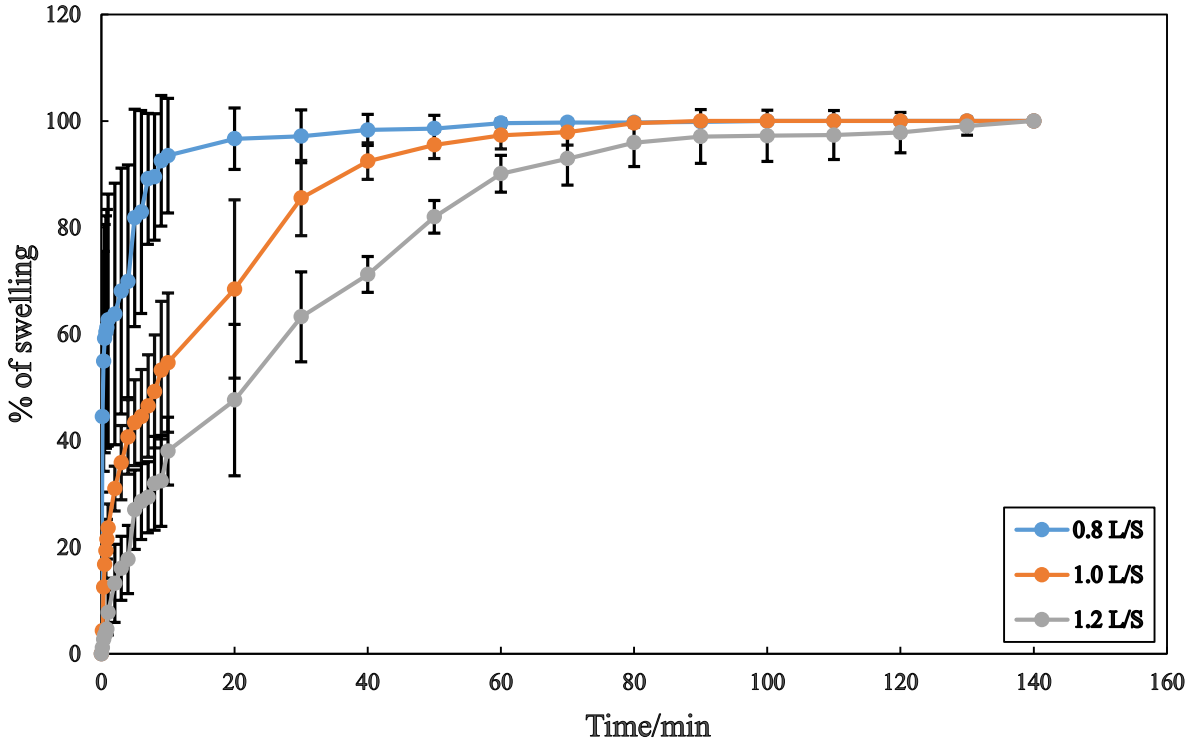

Figure 6.9: Swelling rate of varying L/S mass ratio granules. Error bars represent standard deviation for three for three repeats measurements.

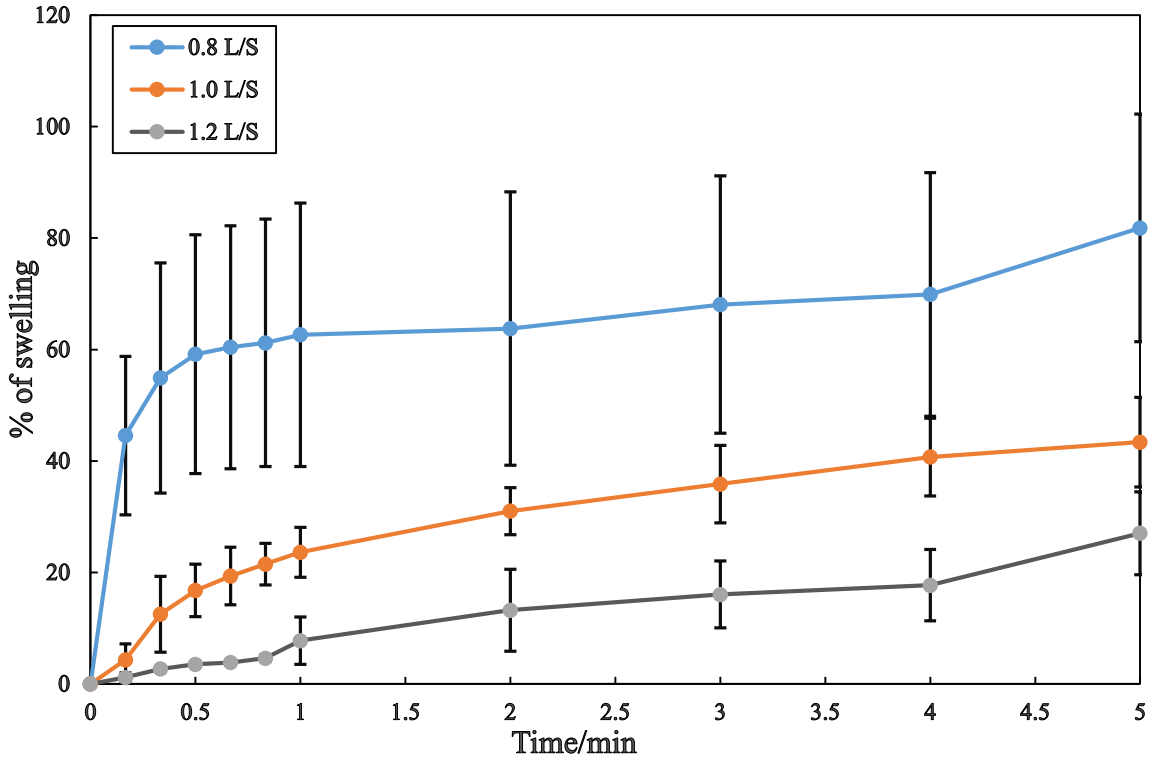

Figure 6.10: Swelling rate of the varying L/S ratio granules during the initial 5 min. Error bars represent standard deviation for three measurements

6.2.2 Effect of varying granulation time on single granule performance

6.2.2.1 Monitoring granule mechanisms and size

This study also investigated the effect of granulation time on the disintegration and swelling behaviour of the granules. Different porosity granules were generated by varying the granulation time parameter, and their size profiles were visualized at different time points (as shown in Figure 6.11, Figure 6.12, and Figure 6.13).

Figure 6.11(a) depicts a 2.5 min granule with the highest porosity at 38 %. The captured images reveal detached surface particles and a large crack along the granule, particularly noticeable at 120 min. Initially, the granule size increases during the first 60 min, followed by slow swelling (Figure 6.12 and Figure 6.13). This swelling process is accompanied by the development of a large crack within 120 min (Figure 6.11(a)).

On the other hand, Figure 6.11(b) represents a 5 min granule with the lowest porosity of 25 %. This granule exhibits a slower and more gradual change in size throughout the entire duration of the experiment (Figure 6.12 and Figure 6.13). The captured images demonstrate the influence of granulation time on the evolving size profiles of the granules.

Furthermore, Figure 6.11(c) illustrates a 10 min granule with a porosity of 32 %. Notably, large granule cracks can be observed detaching after 60 min of the test. The granule size fluctuates, particularly within the first 5 min, possibly due to surface cracking during disintegration. However, the granule size continues to increase until 90 min of the test (Figure 6.12 and Figure 6.13).

These findings indicate that the disintegration and swelling behaviour of the granules are primarily influenced by the granulation time. The evolving size profiles of the granules, as depicted in Figure 6.12 and Figure 6.13, clearly demonstrate the significant impact of varying granulation time on the granule microstructure, leading to distinct disintegration and swelling characteristics.

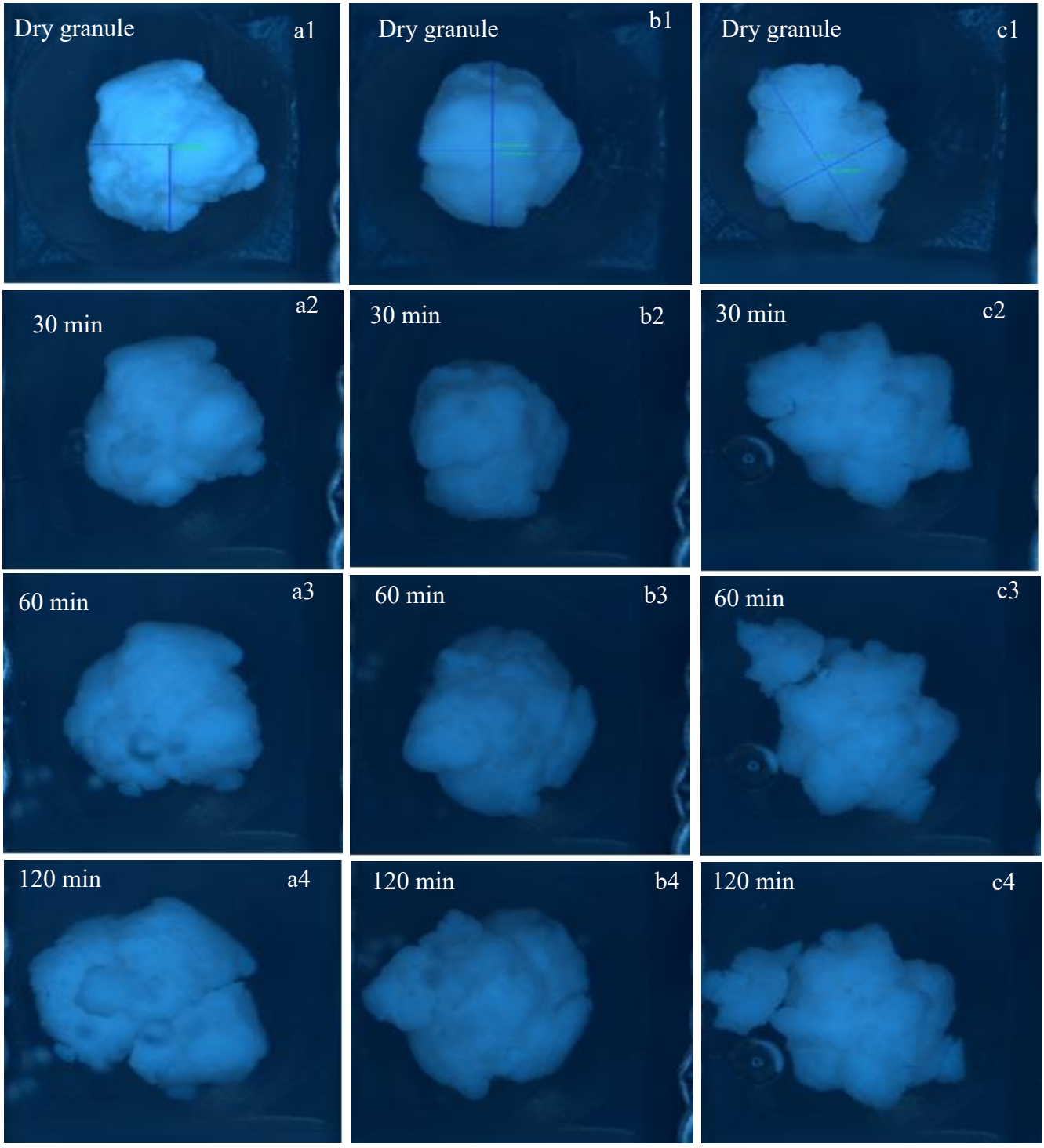

Figure 6.11: Images of granules with varying granulation time: (a) 2.5 min, (b) 5 min and (c) 10 min

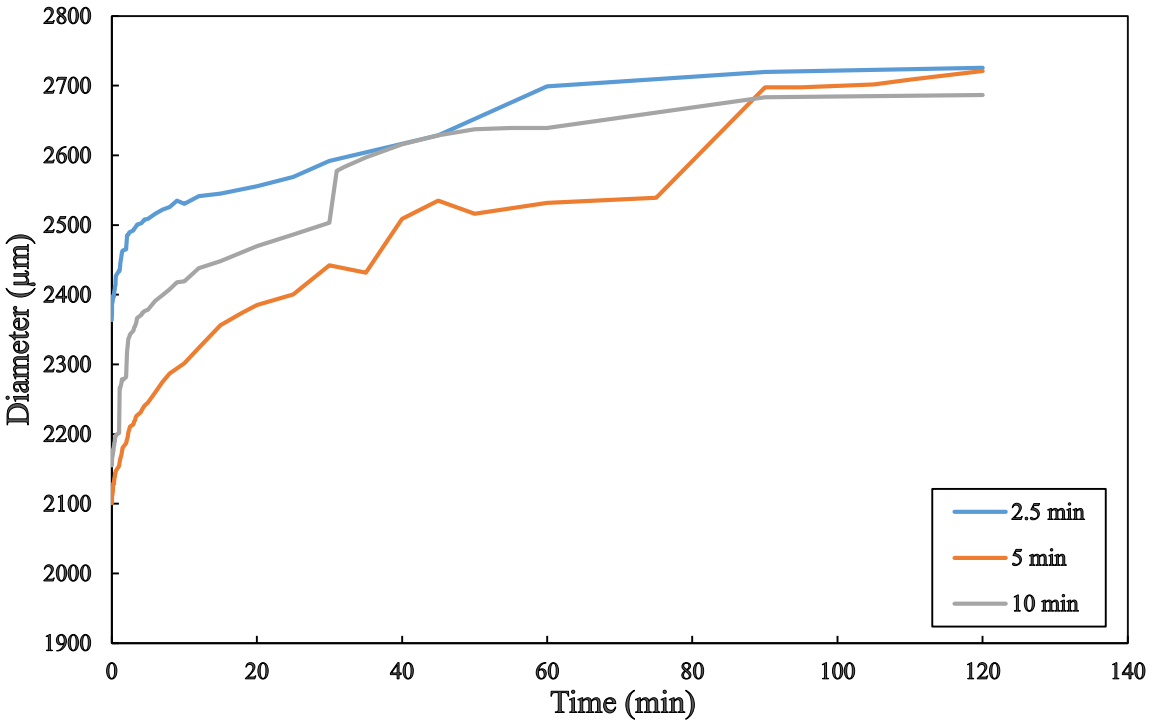

Figure 6.12: Granule diameter profile of different granulation time granules within 120 min

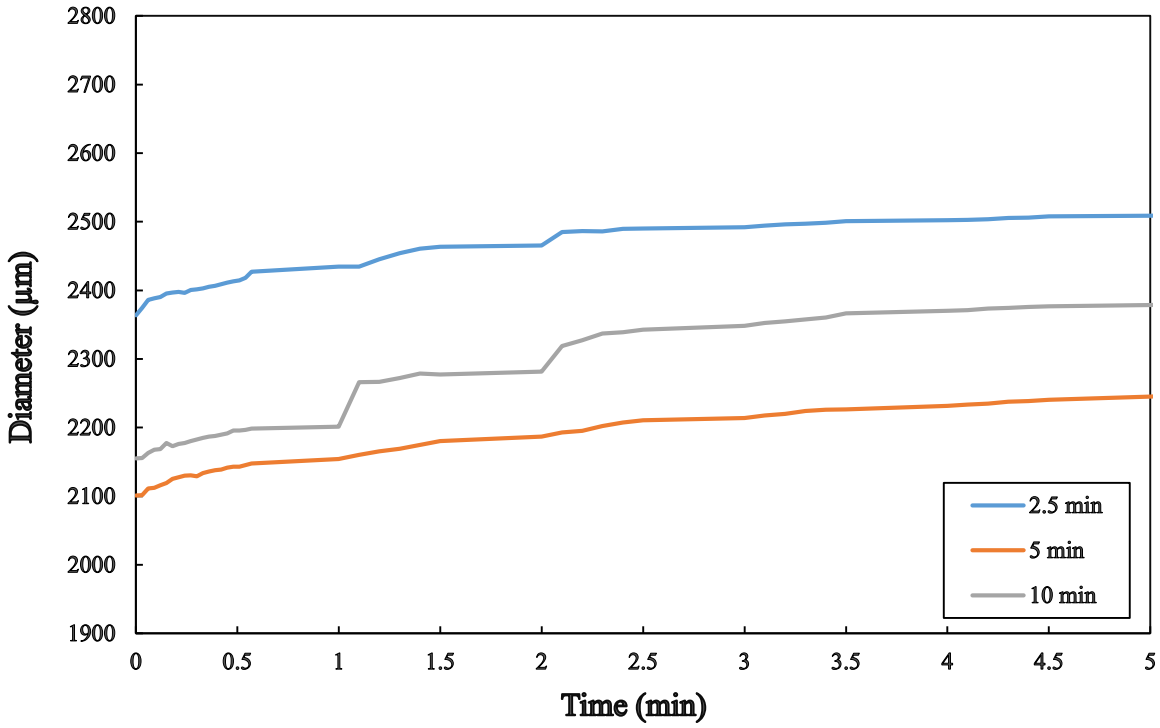

Figure 6.13: Granule diameter profile of different granulation time granules within 5 min

6.2.2.2 Further analysis of surface features and swelling

In addition to the visual analysis of the granules, the OCT technique was separately utilized to examine the microstructure of the granule surfaces in greater detail. Figure 6.14 presents the captured OCT images of a 2.5 min granule at various time points during the experiments. It should be noted that the 2.5 min granules exhibited the highest porosity among the different granulation time groups (5 min and 10 min). The liquid penetration into these granules was assumed to occur relatively quickly, resulting in rapid swelling of the granules with large particle detachment within the first 10 min of the experiment. However, the swelling process appeared to slow down after 60 min (as observed in Figure 6.14), a trend further supported by the measured swelling area profile (Figure 6.17).

Turning to the 5 min granules, which possessed the lowest porosity of 25 %, the captured OCT images showcased a slow swelling behaviour during the initial stage of water contact (up to 1 min). With prolonged exposure to the liquid, the granules gradually expanded, leading to the generation of internal pressure within the granule. This pressure ultimately caused fragmentation and particle detachment, occurring between 10 min and 120 min (as depicted in Figure 6.15).

The swelling behaviour of the granules produced with a 10 min granulation time was displayed in Figure 6.16. These granules had a porosity of 32 %. The captured OCT images revealed initial slow swelling behaviour during the first minute of the experiment. However, after 10 min, surface cracking became apparent and gradually expanded over time.

In summary, the OCT technique provided more detailed insights into the surface microstructure of the granules. The 2.5 min granules with the highest porosity exhibited rapid initial swelling followed by a slower progression. The 5 min granules displayed a gradual swelling process with pressure build up, resulting in fragmentation and particle detachment. The 10 min granules showcased slow swelling initially, with subsequent surface cracking and expansion.

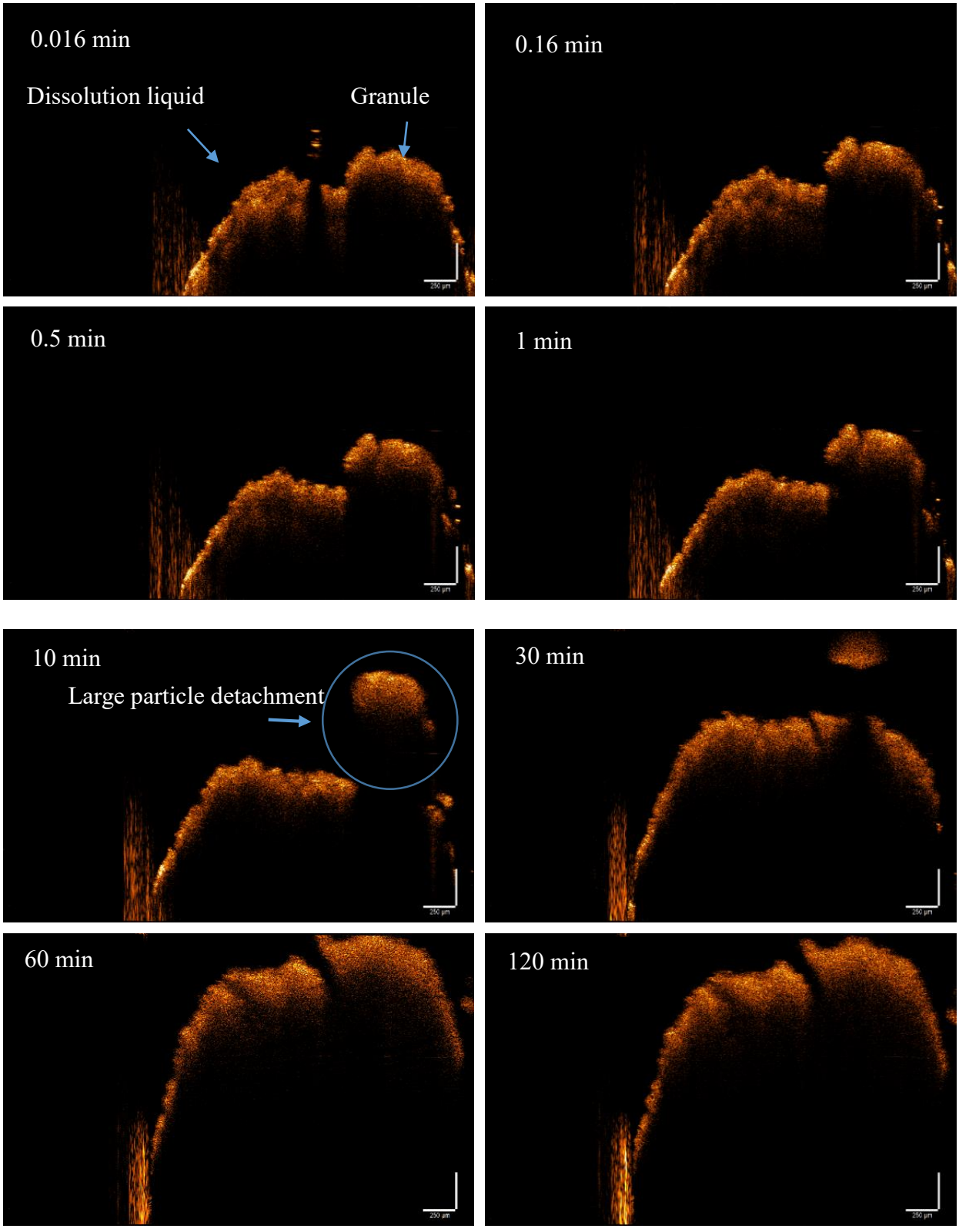

Figure 6.14: OCT images of the granule with 2.5 min granulation time at different times. Scale = bar 250 µm

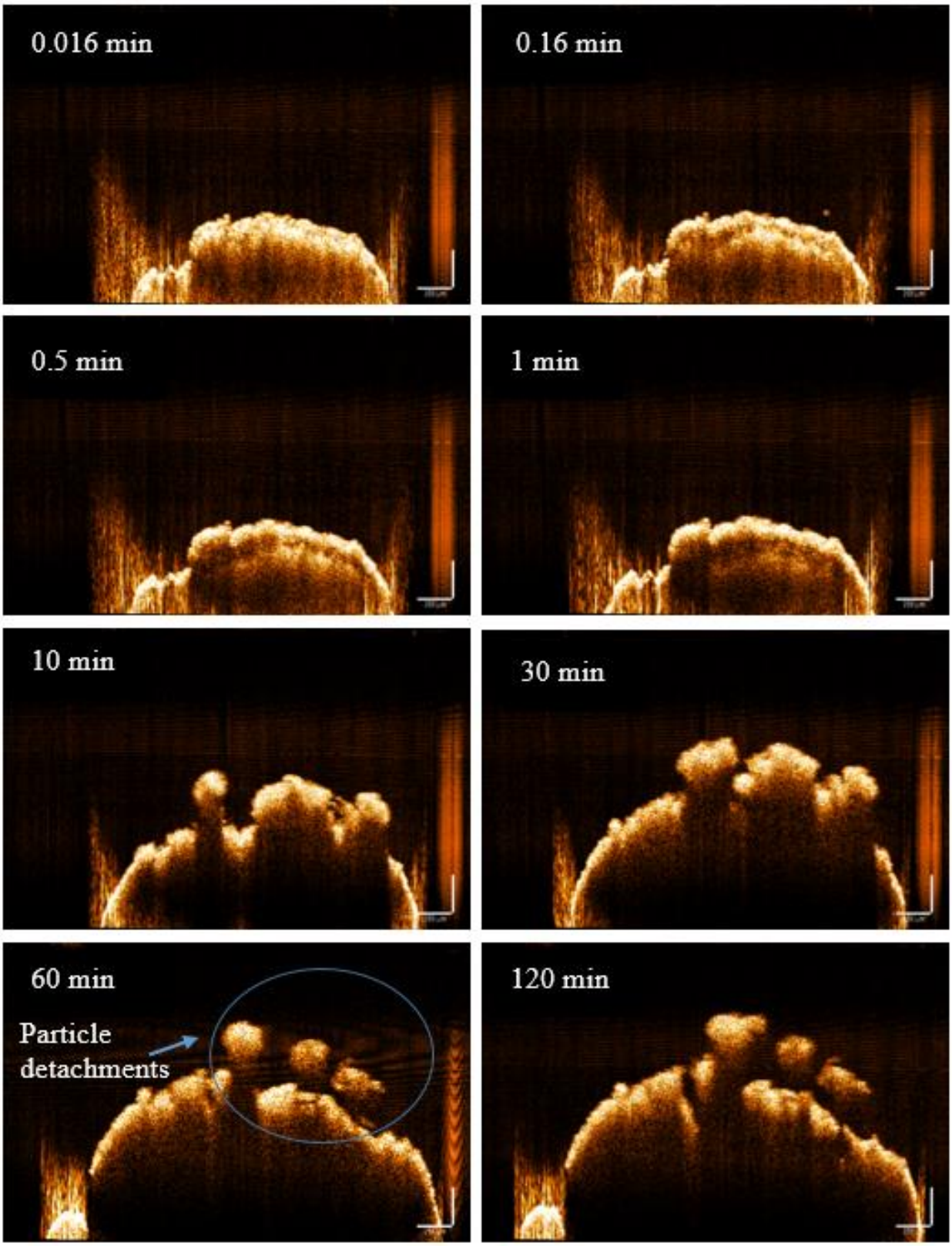

Figure 6.15: OCT images of the granule with 5 min granulation time at different times. Scale bar = 250 µm

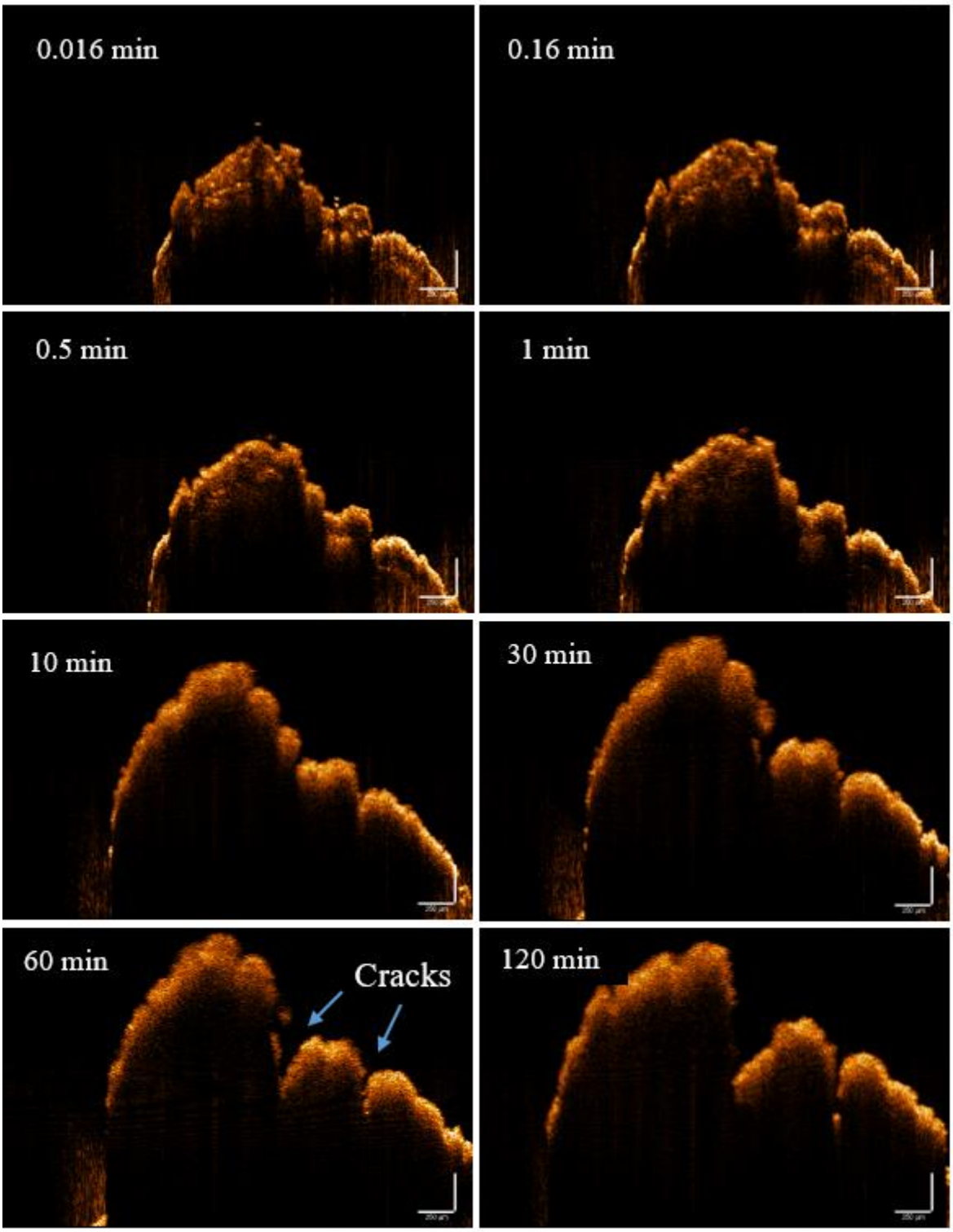

Figure 6.16: OCT images of the granule with 10 min granulation time at different times. Scale bar = 250 µm

The swelling characteristics of different granulation time granules were investigated by measuring the changing in the swelling rate upon long duration of water contact. Figures 6.17 & 6.18 show the full and the first 5 min swelling rate profiles of different granulation time granules. During the first 40 min of the experiment, the swelling rate of 10 min granule was the fastest, hence the porosity was lower than 2.5 min granule. This is possible due to some of surface cracks within 10 min granule (Figure 6.16).

Furthermore, after 40 min, the granule produced after 2.5 min shows the highest swelling rate which may due to the continued liquid movement towards the interior large pores of this granule. These pores allow a relatively fast movement of liquid towards the interior granule particles. The swelling occurred rapidly but abruptly ceased within 50 min, which is relatively short time compared to the swelling duration observed in other granules. 5 min granules with lowest porosity began a slow swelling as discussed earlier due to the expected slow penetration rate, and as the time of liquid penetration increased, this denser granule continued swelling for longer duration (140 min).

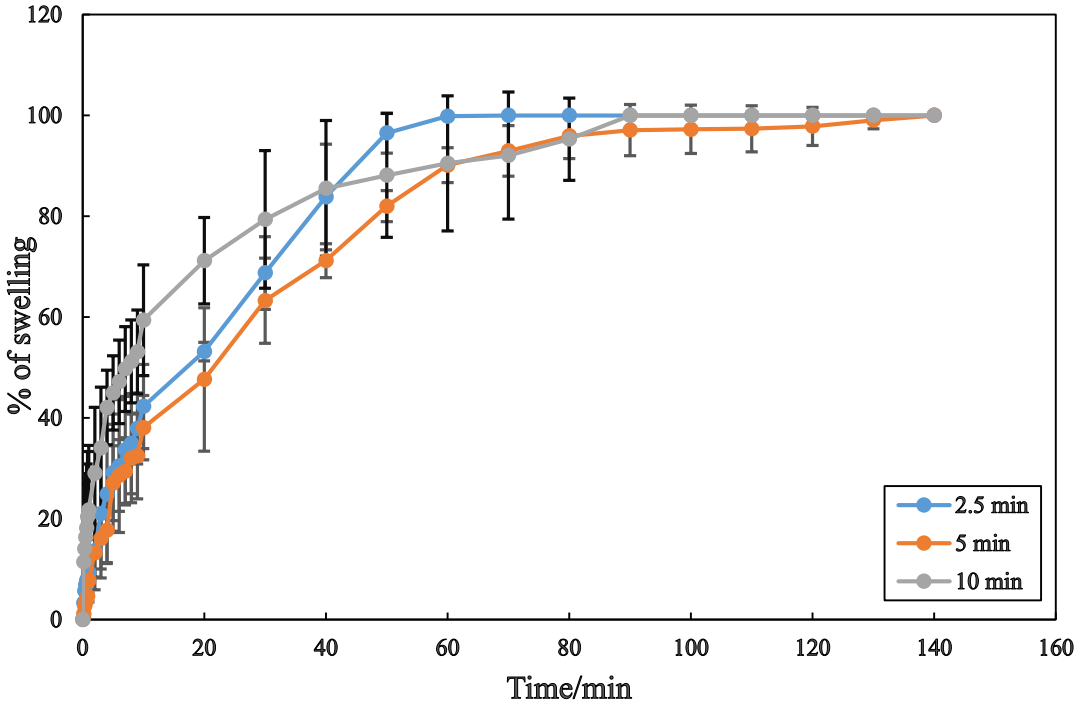

Figure 6.17: Swelling rate of different granulation time granules. Error bars represent standard deviation for three measurements

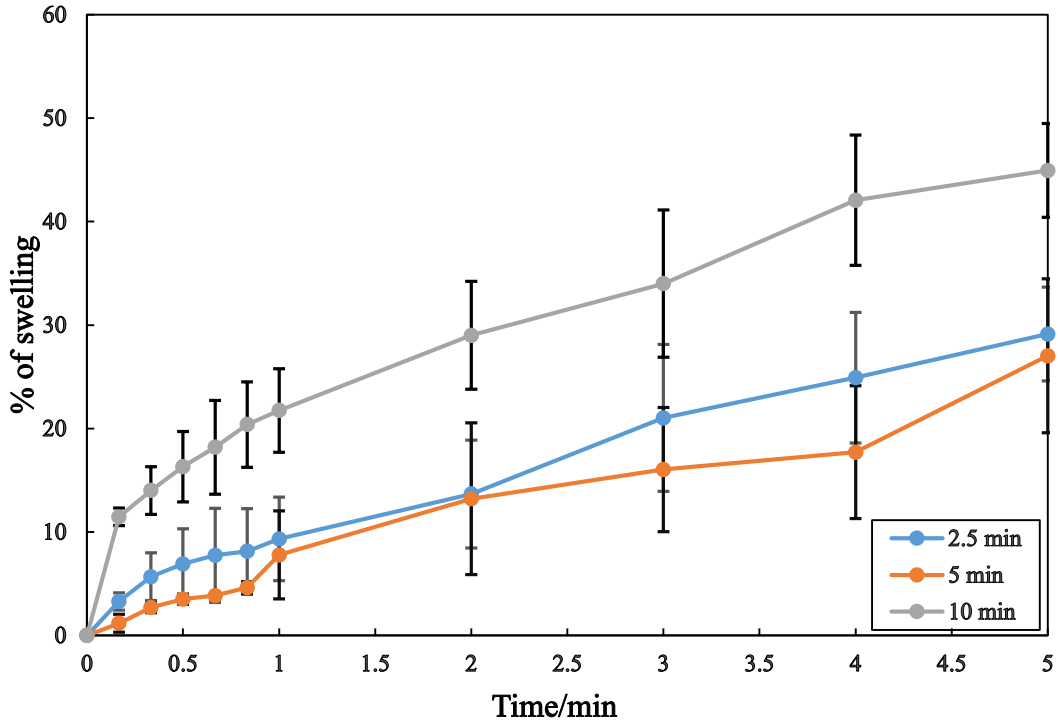

Figure 6.18: Swelling rate of the different granulation time granules at the initial 5 min. Error bars represent standard deviation for three measurements.

In addition to what was discussed previously, the granule porosity is the most important factor in determining the granule swelling rate. The variation in granule porosity is clearly reflected in the granule swelling, as illustrated in Figure 6.19. A granule with a porosity of 62 % swells rapidly probably due to the fast water penetration step. However, this rapid swelling ended (within approximately 10 min). On the other hand, the swelling rate of the 25 % porosity granule was the slowest and this swelling continued until the nearly end of the test. It is believed this is due to slow liquid penetration into granule particles, leading this granule to continue swelling for approximately 140 min due to the difficulty of water penetration into granule particles. Most interestingly, the 32 % porosity granule swells faster compared to the 38 % and 39 % granules. It is likely that this reflects the effect of granule surface cracks and other large internal pores created during the longer granulation time.

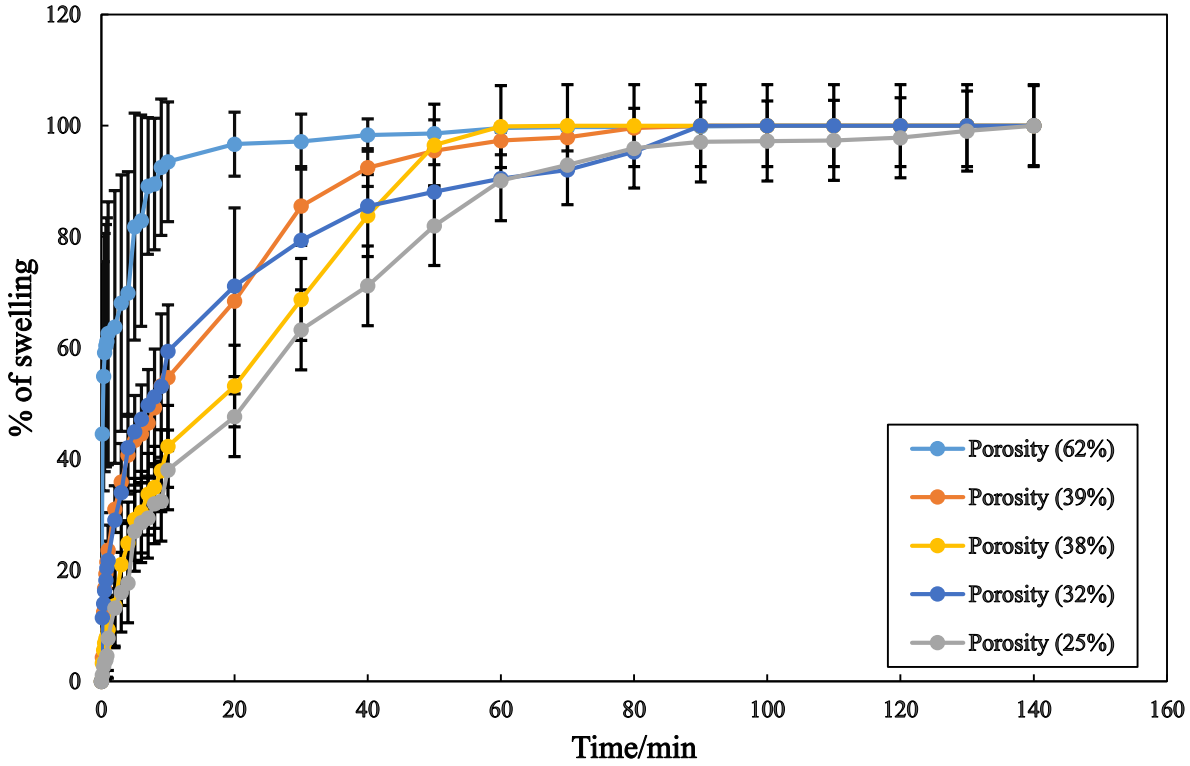

Figure 6.19: The swelling rate of the granules with different porosity. Error bars represent standard deviation for three measurements.

6.2.3 Comparison of disintegration and dissolution performance

In general, the granule swelling has a clear effect on the granule dissolution performance and Figure 6.20 shows a relationship between the granule swelling and dissolution performance. However, they do not correlate perfectly, especially in the first 30 min of the test. To quantitatively compare and comment on statistically significant similarities or differences in the relationship between the granule disintegration and dissolution performance, a t-test was performed to obtain the probability value (p-value).

In statistics, the p-value is a measure of the strength of evidence against the null hypothesis (here the effect of disintegration on the granule dissolution performance). It is used to determine the statistical significance of an observed effect or the results of a statistical test. The p-value represents the probability of obtaining results as extreme as or more extreme than the observed data, assuming that the null hypothesis is true. The p-value is a number between 0 and 1. Typically, a p-value less than a predetermined significance level (commonly 0.05) is considered statistically significant. This means that if the p-value is less than 0.05, there is strong evidence against the null hypothesis, and the observed effect is unlikely to have occurred by chance. In this work, the p-value was 0.0094 which represents the weak relationship between disintegration and dissolution performance. This is probably due to the surface cracks which effect the swelling and the surface aspirin particles which gives a higher dissolution within the initial stage of the dissolution. However, a high porosity granule (62 %) shows a better relationship which is possibly due to the instantaneous liquid penetration resulting in swelling and dissolution occurring quickly (Figure 6.21).

On the other hand, low porosity granules (25 %) show less of a relationship, particularly in the in the initial stage of the test. This is probably because of the slow initial swelling accompanied with initial high dissolution due to the dissolution of the surface aspirin particles. Granules produced after 2.5 min, which have a porosity 38 %, show a lower correlation compared to the other granules. This is probably because some early large detachments occurred during the disintegration (shown in Figure 6.14) which influences the granule swelling and dissolution behaviour, and resulting non-steady performance.

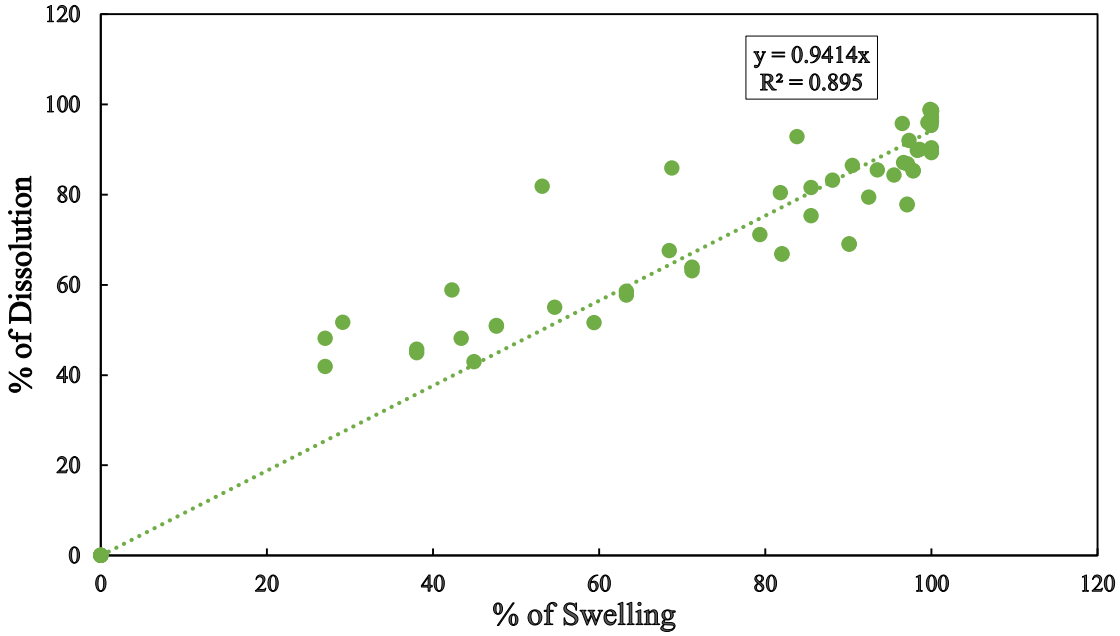

Figure 6.20: The overall relationship between the swelling and dissolution performance

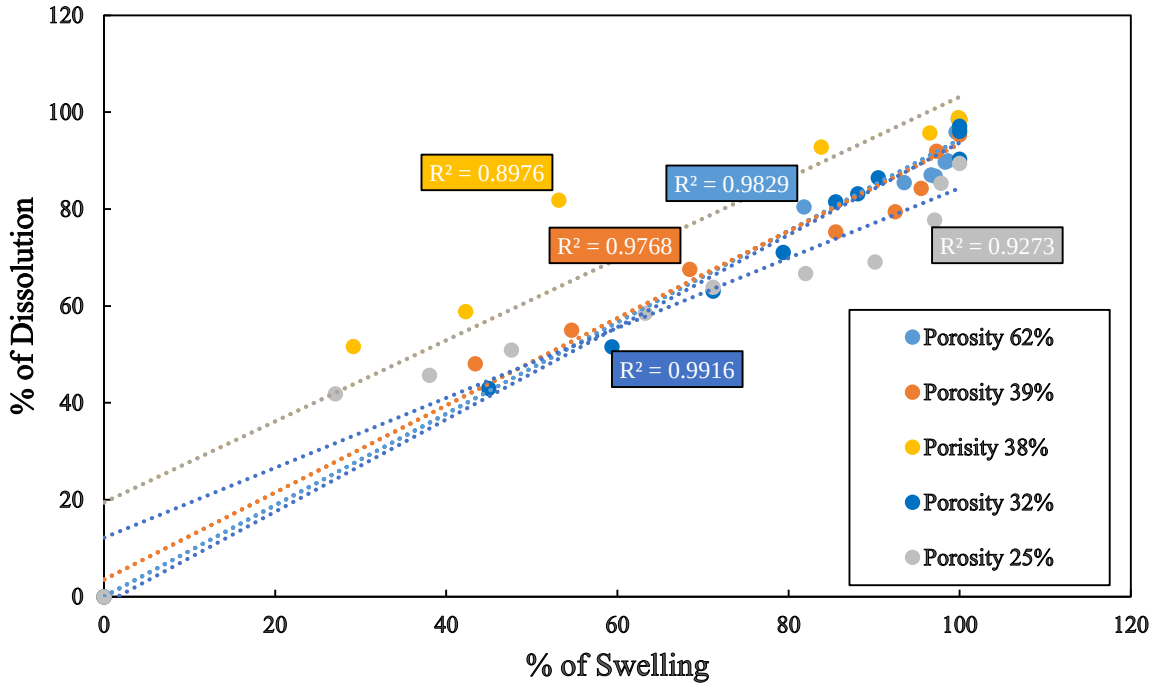

Figure 6.21: The relationship between the swelling and dissolution performance of the different porosity granules

6.2.4 Conclusions

The microscale studies were designed to study the swelling and disintegration of a single granule upon contact with water. The granule size and swelling behaviour were both quantified and tracked over time using digital imaging and an OCT technique. Single granule swelling rate was mainly influenced by granule porosity, with more porous granules displaying faster swelling kinetics compared to denser granules which exhibited slower and longer swelling behaviour. Granules with different L/S mass ratio show a high variation in swelling rate compared to the different granulation time. Longer granulation time granules swelled faster, which is interesting. This is likely due to the effect of some cracks along the granule surface and potentially within the granule itself. Liquid penetration into the granule structure was believed to be affected by granule porosity and the granule dissolution was correlated with the swelling characteristics. This demonstrated the importance of how the swelling kinetics influence the amount of active ingredient released from the microstructure during dissolution.

CHAPTER 7: Conclusions and Recommendations

7.1 Conclusions

The overarching aim of this thesis was to investigate the link between three main areas; granulation conditions, granule structure and granule performance. This was achieved by manufacturing granules with different microstructures and analyzing their performance.

To investigate the relationship between process conditions and granule microstructure, the liquid to solid mass ratio and granulation time were identified as the most influential parameters. These parameters were intentionally chosen and manipulated while keeping the granule formulation constant. The granule microstructure was carefully analyzed by employing various advanced characterization techniques, with a particular focus on quantifying porosity. The findings revealed a strong dependence of microstructure on the liquid to solid mass ratio. Furthermore, the results demonstrated that longer granulation times resulted in increased granule porosity, as evidenced by the presence of voids and cracks observed through 3D imaging.

An experimental methodology was designed for studying the relationship between granulation conditions and granule structure. High shear wet granulation at low liquid to solid mass ratios and short granulation times resulted in porous and fragile granules. Compared to the effect of granulation time, liquid to solid ratios showed a greater influence on the porosity of granules. Increasing the liquid to solid ratio by 0.2 was found to sharply reduce granule porosity to almost 50 %. This reiterated the importance of sufficient liquid binder around the granule particles to facilitate the particles binding during wet granulation. Although the influence of granulation time on granule porosity was less than the liquid to solid mass ratio, optimizing the granulation time is essential to ensure complete binding of granule particles. Extended granulation times caused granule porosity to increase and produce cracks along their surface. In addition to measuring the granule porosity, advanced characterization on the internal granule structure was performed where large void spaces with cracks were seen for more porous granules.

Following the investigation on the impact of process parameters to product structure, the performance of these granules was then explored through dissolution studies. Higher porosity granules have a faster dissolution when compared to selecting longer granulation times and

high liquid to solid mass ratios. It is likely that the higher porosity granules experienced accelerated liquid uptake into the granule pores, which resulted in faster dissolution of the drug into the dissolution liquid. In order to examine the link between product and performance, a series of experiments were conducted to explore how different granule porosities affect the release of the active ingredient. A convenient online sampling technique was employed to monitor the changing concentration profiles. The findings revealed that granules with lower porosities exhibited a slower dissolution rate when compared to those with higher porosities. These results suggest that the dissolution mechanism of the granules depends on their porosity, with either a diffusion-controlled dissolution process or a de-aggregation to finer particles followed by dissolution of the active ingredient in solution.

Further links between the granule structure to performance were then investigated through developing microscale experiments for a deeper insight into the granule performance through analysis of the disintegration mechanisms. By examining a single granule subjected to a well-controlled flow over time, quantified evolving size profiles and swelling rates along with tracking surface features through advanced tomography were achieved. Importantly, the results complemented previous findings on granule dissolution studies as more porous granules prompted faster swelling kinetics due to rapid liquid penetration into the granule which led to loosening of the particulate structure. Denser granules displayed slower and longer swelling behaviour accompanied by formation of voids and cracks. These differences in the disintegration characteristics show an obvious influence on the drug release profile.

The most important conclusion from this specific work is that granulation time and L/S mass ratio are well established critical process parameters affecting the granule structure. This specific research not only sheds light on the relationship between granulation process parameters, such as L/S ratio and granulation time, but also uncovers their direct impact on granule performance, specifically in terms of granule disintegration and dissolution during high shear wet granulation.

This specific work has facilitated the understanding of how these parameters affects granule structure and identified the link between the granule structure and dissolution particularly the single granule swelling and break-up.

Additionally, this study highlights the importance of considering granule disintegration and dissolution in high shear wet granulation. These factors directly impact drug release from the granule, thereby influencing the drug's pharmacokinetics and therapeutic efficacy. With this

newfound knowledge, formulation scientists can design granules that exhibit optimal disintegration profiles, ensuring efficient drug release and absorption within the body.

In conclusion, the novel insight obtained from this study bridges a crucial gap in our understanding of granulation processes. By unravelling the intricate relationship between L/S ratio, granulation time, and granule behaviour, this research opens up exciting opportunities for optimization, customization, and improved performance of granular materials. As researchers and industry professionals continue to leverage this knowledge, we can expect to witness transformative advancements in formulation development, manufacturing processes, and ultimately, the quality and efficacy of a wide range of products.

7.2 Recommendations

Below are some suggestions for future work to improve our understanding of the relationship between the granulation process and granule performance.

- Two main process parameters (L/S mass ratio and granulation time) in high shear wet granulation that influence the granule structure have been studied in this work. Further parameters can be investigated in the future, including;

    - The recommended impeller speeds for studying the effect on granule structures are 200, 400, and 600 rpm.
    - The quantity of material that used in this work was 200 g, but it is also suggested to explore other quantities, such as 100 g and 400 g.
    - In this study, the water addition method employed was injection. However, alternative methods such as peristaltic pump and spray injection can also be considered for water addition.

- MCC was used as an excipient in this work. However, other commonly used excipients such as lactose monohydrate and hydroxylpropyl methylcellulose should also be investigated.
- In future work, super disintegrants such as sodium starch glycolate (SSG) can be added to MCC to study the effect of process parameters on the disintegration efficiency.
- It is recommended that the drug release performance is modelled and used to develop the experimental model.
- The design of the flow-cell used in this study contains only one lid and O-ring area. It is advised that an additional window be placed to the flow cell's base. This allows the granule to be visualised using a camera placed beneath the flow-cell.
- One of the challenges of this project was the testing of the flow cell, which required numerous adjustments until clear images were obtained. In addition to measuring the swelling rate of the granule, it is suggested that this flow-cell can be utilised in the future to assess the water penetration rate and absorption capacity of various granule structures.

- It is recommended that this modified flow cell can be used to validate the theoretical data obtained from future swelling models.
- It is strongly advised to proceed with the tableting of the porous granules to assess the dissolution and swelling behaviour of the resulting compressed tablets. The impact of different tablet compression techniques on granule and tablet porosity should be studied, with particular focus on understanding the influence of compression on tablet disintegration. This investigation will provide essential knowledge for optimizing tablet formulation and enhancing drug release characteristics.
- It is highly advised to utilize the experimental data from this study to develop a model equation that establishes a connection between granule porosity and drug release. By modelling the relationship between granule disintegration and dissolution, it is possible to formulate an equation that quantitatively describes this association.

References

Allen, T. (2013) 'Sampling of Powders', in *Particle size measurement*. Springer US (Powder Technology Series), pp. 1–33.

Ansari, M. A. and Stepanek, F. (2008) 'The effect of granule microstructure on dissolution rate', *Powder Technology*, 181(2), pp. 104–114. doi: 10.1016/j.powtec.2006.12.012.

Azarmi, S., Roa, W. and Löbenberg, R. (2007) 'Current perspectives in dissolution testing of conventional and novel dosage forms', *International Journal of Pharmaceutics*, 328(1), pp. 12–21. doi: 10.1016/j.ijpharm.2006.10.001.

Badawy, S. I. F. *et al.* (2012) 'Mechanistic basis for the effects of process parameters on quality attributes in high shear wet granulation.', *International Journal of Pharmaceutics*, 439(1–2), pp. 324–33. doi: 10.1016/j.ijpharm.2012.09.011.

Baishya, H. (2017) 'Application of mathematical models in drug release kinetics of carbidopa and levodopa ER tablets', *Journal of Developing Drugs*, 06(02), pp. 1–8. doi: 10.4172/2329-6631.1000171.

Bouwman, A. M. *et al.* (2005) 'The effect of the amount of binder liquid on the granulation mechanisms and structure of microcrystalline cellulose granules prepared by high shear granulation', *International Journal of Pharmaceutics*, 290(1–2), pp. 129–136. doi: 10.1016/j.ijpharm.2004.11.024.

Cameron, I. T. *et al.* (2005) 'Process systems modelling and applications in granulation: A review', *Chemical Engineering Science*, 60(14), pp. 3723–3750. doi: 10.1016/j.ces.2005.02.004.

Chang, F. *et al.* (2014) 'Preparation and characterization of modified starch granules with high hydrophobicity and flowability', *Food Chemistry*. Elsevier Ltd, 152, pp. 177–183. doi: 10.1016/j.foodchem.2013.11.140.

Chirkot, T. (2002) 'Scale-up and endpoint issues of pharmaceutical wet granulation in a V-type low shear granulator', *Drug Development and Industrial Pharmacy*, 28(7), pp. 871–888. doi: 10.1081/DDC-120005633.

Chitu, T. M., Oulahna, D. and Hemati, M. (2011) 'Rheology, granule growth and granule strength: Application to the wet granulation of lactose-MCC mixtures', *Powder Technology*. Elsevier B.V., 208(2), pp. 441–453. doi: 10.1016/j.powtec.2010.08.041.

Chu, K. R. *et al.* (2012) 'Effect of particle size on the dissolution behaviors of poorly water-soluble drugs', *Archives of Pharmacal Research*, 35(7), pp. 1187–1195. doi: 10.1007/s12272-012-0709-3.

Collins, J. *et al*. (2007) 'Characterizing the evolution of porosity during controlled drug release' *Applied Magnetic Resonance,* 32, pp. 185-204.

Desai, P. M., Liew, C. V. and Heng, P. W. S. (2016) 'Review of Disintegrants and the Disintegration Phenomena', *Journal of Pharmaceutical Sciences*. Elsevier Ltd, 105(9), pp. 2545–2555. doi: 10.1016/j.xphs.2015.12.019.

Diersch, H. J. G. *et al.* (2010) 'Modeling unsaturated flow in absorbent swelling porous media: Part 1. theory', *Transport in Porous Media*, 83(3), pp. 437–464. doi: 10.1007/s11242-009-9454-6.

Van Den Dries, K. *et al.* (2003) 'Granule breakage phenomena in a high shear mixer; influence of process and formulation variables and consequences on granule homogeneity', *Powder Technology*, 133(1–3), pp. 228–236. doi: 10.1016/S0032-5910(03)00106-2.

Eshtiaghi, N., Arhatari, B. and Hapgood, K. P. (2009) 'Producing hollow granules from hydrophobic powders in high-shear mixer granulators', *Advanced Powder Technology*. The Society of Powder Technology Japan., 20(6), pp. 558–566. doi: 10.1016/j.apt.2009.08.006.

Farag Badawy, S. I., Lee, T. J. and Menning, M. M. (2000) 'Effect of drug substance particle size on the characteristics of granulation manufactured in a high-shear mixer', *AAPS PharmSciTech*, 1(4), p. 7. doi: 10.1208/pt010433.

Farber, L., Tardos, G. and Michaels, J. N. (2003) 'Use of X-ray tomography to study the porosity and morphology of granules', 132, pp. 57–63. doi: 10.1016/S0032-5910(03)00043-3.

Faure, A., York, P. and Rowe, R. C. (2001) 'Process control and scale-up of pharmaceutical wet granulation processes: A review', *European Journal of Pharmaceutics and Biopharmaceutics*, 52(3), pp. 269–277. doi: 10.1016/S0939-6411(01)00184-9.

Flore, K., Schoenherr, M. and Feise, H. (2009) 'Aspects of granulation in the chemical industry', *Powder Technology*, pp. 327–331. doi: 10.1016/j.powtec.2008.04.010.

Gao, J. Z. H. *et al.* (2002) 'Fluid bed granulation of a poorly water soluble, low density, micronized drug: Comparison with high shear granulation', *International Journal of Pharmaceutics*, 237(1–2), pp. 1–14. doi: 10.1016/S0378-5173(01)00982-6.

Giesche, H. (2006) 'Mercury Porosimetry: A General (Practical) Overview', *Particle & Particle Systems Characterization*. WILEY-VCH Verlag, 23(1), pp. 9–19. doi: 10.1002/ppsc.200601009.

Grassi, M., Colombo, I. and Lapasin, R. (2000) 'Drug release from an ensemble of swellable crosslinked polymer particles', *Journal of Controlled Release*, 68(1), pp. 97–113. doi: 10.1016/S0168-3659(00)00241-8.

Hansuld, E. M. and Briens, L. (2014) 'A review of monitoring methods for pharmaceutical wet granulation', *International Journal of Pharmaceutics*. Elsevier B.V., 472(1–2), pp. 192–201. doi: 10.1016/j.ijpharm.2014.06.027.

Hapgood, K. P., Litster, J. D. and Smith, R. (2003) 'Nucleation regime map for liquid bound granules', *AIChE Journal*. Wiley Online Library, 49(2), pp. 350–361.

Hayata, Y. (2002) 'NII-Electronic Library Service', *Chemical Pharmaceutical Bulletin*, (43), p. 2091. Available at: http://www.mendeley.com/research/geology-volcanic-history-eruptive-style-yakedake-volcano-group-central-japan/.

Hemati, M. *et al.* (2003) 'Fluidized bed coating and granulation: Influence of process-related variables and physicochemical properties on the growth kinetics', *Powder Technology*, 130(1–3), pp. 18–34. doi: 10.1016/S0032-5910(02)00221-8.

Iveson, S. M., Wauters, P. A. L., *et al.* (2001) 'Growth regime map for liquid-bound granules: Further development and experimental validation', *Powder Technology*, 117(1–2), pp. 83–97. doi: 10.1016/S0032-5910(01)00317-5.

Iveson, Simon M., Litster, J. D., *et al.* (2001) 'Nucleation, growth and breakage phenomena in agitated wet granulation processes: A review', *Powder Technology*, 117(1–2), pp. 3–39. doi: 10.1016/S0032-5910(01)00313-8.

Iveson, Simon M, Litster, J. D., *et al.* (2001) 'Nucleation , growth and breakage phenomena in agitated wet granulation processes : a review'.

Iveson, S. M., Litster, J. D. and Ennis, B. J. (1996) 'Fundamental studies of granule consolidation part 1: Effects of binder content and binder viscosity', *Powder Technology*, 88(1), pp. 15–20. doi: 10.1016/0032-5910(96)03096-3.

Karehill, P. G. and Nyström, C. (1990) 'Studies on direct compression of tablets XXI. Investigation of bonding mechanisms of some directly compressed materials by strength characterization in media with different dielectric constants (relative permittivity)', *International Journal of Pharmaceutics*, 61(3), pp. 251–260. doi: 10.1016/0378-5173(90)90216-Q.

Kipper, M. J. and Narasimhan, B. (2005) 'Molecular description of erosion phenomena in biodegradable polymers', *Macromolecules*, 38(5), pp. 1989–1999. doi: 10.1021/ma047661r.

Knight, P. C. (2001) 'Structuring agglomerated products for improved performance', *Powder Technology*, 119(1), pp. 14–25. doi: 10.1016/S0032-5910(01)00400-4.

Kothekar, V. (2012) 'Basic UV-Vis Theory, Concepts and Applications Basic UV-Vis Theory, Concepts and Applications', *Protocol*, pp. 1–28.

Krishnaiah, Y. S. . (2010) 'Pharmaceutical Technologies for Enhancing Oral Bioavailability of Poorly Soluble Drugs', *Journal of Bioequivalence & Bioavailability*, 02(02), pp. 28–36. doi: 10.4172/jbb.1000027.

Kumar, A. *et al.* (no date) 'DEVELOPMENT OF REGIME MAP FOR STEADY - STATE HIGH SHEAR WET TWIN - SCREW GRANULATION'.

Li, J. *et al.* (2011) 'The effect of the physical states of binders on high-shear wet granulation and granule properties: A mechanistic approach toward understanding high-shear wet granulation process. part II. granulation and granule properties', *Journal of Pharmaceutical Sciences*. Elsevier Masson SAS, 100(1), pp. 294–310. doi: 10.1002/jps.22261.

Litster, J. (2016a) *Design and processing of particulate products*. First edti, *Design and Processing of Particulate Products*. First edti. Cambridge UK: Jim Lister. doi: 10.1017/CBO9781139017558.

Litster, J. (2016b) *Particle Characterization and Particle Property Distributions, Design and Processing of Particulate Products*. doi: 10.1017/cbo9781139017558.003.

Litster, J. and Ennis, B. (2004) '*The science and engineering of granulation processes*' (Vol. 15). Springer Science & Business Media.

Liu, B. *et al.* (2021) 'A review of high shear wet granulation for better process understanding, control and product development', *Powder Technology*. Elsevier B.V., 381, pp. 204–223. doi: 10.1016/j.powtec.2020.11.051.

Liu, J. *et al.* (2014) 'Experimental investigation on pore structure characterization of concrete exposed to water and chlorides', *Materials*, 6(9), pp. 6646–6659. doi: 10.3390/ma7096646.

Liu, L. X. *et al.* (2000) 'Coalescence of deformable granules in wet granulation processes', *AIChE Journal*, 46(3), pp. 529–539. doi: 10.1002/aic.690460312.

Lowenthal, W. (1972) 'Disintegration of tablets', *Journal of Pharmaceutical Sciences*. Elsevier Masson SAS, 61(11), pp. 1695–1711. doi: 10.1002/jps.2600611102.

Maclean, N. *et al.* (2021) 'Exploring the performance-controlling tablet disintegration mechanisms for direct compression formulations', *International Journal of Pharmaceutics*. Elsevier B.V., 599. doi: 10.1016/j.ijpharm.2021.120221.

Mangwandi, C. *et al.* (2011) 'Effect of batch size on mechanical properties of granules in high shear granulation', *Powder Technology*. Elsevier B.V., 206(1–2), pp. 44–52. doi: 10.1016/j.powtec.2010.05.025.

Markl, D. *et al.* (2017) 'Non-destructive Determination of Disintegration Time and Dissolution in Immediate Release Tablets by Terahertz Transmission Measurements', *Pharmaceutical Research*. Pharmaceutical Research, 34(5), pp. 1012–1022. doi: 10.1007/s11095-017-2108-4.

Markl, D. and Zeitler, J. A. (2017) 'A Review of Disintegration Mechanisms and Measurement Techniques', *Pharmaceutical Research*. Pharmaceutical Research, 34(5), pp. 890–917. doi: 10.1007/s11095-017-2129-z.

Meng, W. *et al.* (2019) 'Continuous high-shear granulation: Mechanistic understanding of the influence of process parameters on critical quality attributes via elucidating the internal

physical and chemical microstructure', *Advanced Powder Technology*, (xxxx). doi: 10.1016/j.apt.2019.04.028.

Micromeritics (2015) 'Accupyc II - Gas Displacement Pycnometry System', p. 9.

Moura, M. J., Ferreira, P. J. and Figueiredo, M. M. (2005) 'Mercury intrusion porosimetry in pulp and paper technology', *Powder Technology*, 160(2), pp. 61–66. doi: 10.1016/j.powtec.2005.08.033.

Nordström, J. and Alderborn, G. (2015) 'The granule porosity controls the loss of compactibility for both dry- and wet-processed cellulose granules but at different rate', *Journal of Pharmaceutical Sciences*, 104(6), pp. 2029–2039. doi: 10.1002/jps.24439.

Oka, S. *et al.* (2015) 'The effects of improper mixing and preferential wetting of active and excipient ingredients on content uniformity in high shear wet granulation', *Powder Technology*, 278, pp. 266–277. doi: 10.1016/j.powtec.2015.03.018.

Panalytical, M. (2013) 'Overview of Important Particle Characterization Techniques', pp. 1–10. Available at: https://www.azom.com/article.aspx?ArticleID=9937.

Patel, S., Kaushal, A. M. and Bansal, A. K. (2007) 'Effect of particle size and compression force on compaction behavior and derived mathematical parameters of compressibility', *Pharmaceutical Research*, 24(1), pp. 111–124. doi: 10.1007/s11095-006-9129-8.

Pathare, P. B. *et al.* (2011) 'Effect of high shear granulation process parameters on the production of granola cereal aggregates', *Biosystems Engineering*, 110(4), pp. 473–481. doi: 10.1016/j.biosystemseng.2011.10.004.

Perfetti, G. *et al.* (2010) 'X-ray micro tomography and image analysis as complementary methods for morphological characterization and coating thickness measurement of coated particles', *Advanced Powder Technology*. The Society of Powder Technology Japan, 21(6), pp. 663–675. doi: 10.1016/j.apt.2010.08.002.

Quodbach, J. *et al.* (2014) 'Tablet disintegration studied by high-resolution real-time magnetic resonance imaging', *Journal of Pharmaceutical Sciences*. Elsevier Masson SAS, 103(1), pp. 249–255. doi: 10.1002/jps.23789.

Quodbach, J. and Kleinebudde, P. (2016) 'A critical review on tablet disintegration', *Pharmaceutical Development and Technology*, 21(6), pp. 763–774. doi: 10.3109/10837450.2015.1045618.

Rahmanian, N. *et al.* (2009) 'Characterisation of granule structure and strength made in a high shear granulator', *Powder Technology*. Elsevier B.V., 192(2), pp. 184–194. doi: 10.1016/j.powtec.2008.12.016.

Rahmanian, N., Naji, A. and Ghadiri, M. (2011) 'Effects of process parameters on granules properties produced in a high shear granulator', *Chemical Engineering Research and Design*, 89(5), pp. 512–518. doi: 10.1016/j.cherd.2010.10.021.

Rajniak, P. *et al.* (2007) 'Experimental study of wet granulation in fluidized bed: Impact of the binder properties on the granule morphology', *International Journal of Pharmaceutics*, 334(1–2), pp. 92–102. doi: 10.1016/j.ijpharm.2006.10.040.

Rankell, A. S. *et al.* (1964) 'Continuous production of tablet granulations in a fluidized bed II. Operation and performance of equipment', *Journal of Pharmaceutical Sciences*. Elsevier Masson SAS, 53(3), pp. 320–324. doi: 10.1002/jps.2600530316.

Rhodes, M.J. ed., (2008) '*Introduction to particle technology*'. John Wiley & Sons.

Rija, S. and Kolios, M. C. (2020) 'Assessment of cell death using dynamic light scattering with M-mode optical coherence tomography imaging', (February 2020), p. 25. doi: 10.1117/12.2545364.

Ritala, M. *et al.* (1988) 'Influence of liquid bonding strength on power consumption during granulation in a high shear mixer', *Drug Development and Industrial Pharmacy*, 14(8), pp. 1041–1060. doi: 10.3109/03639048809151919.

Ryzak, M. and Bieganowski, A. (2011) 'Methodological aspects of determining soil particle-size distribution using the laser diffraction method', *Journal of Plant Nutrition and Soil Science*, 174(4), pp. 624–633. doi: 10.1002/jpln.201000255.

Sackett, C. K. and Narasimhan, B. (2011) 'Mathematical modeling of polymer erosion: Consequences for drug delivery', *International Journal of Pharmaceutics*. Elsevier B.V., 418(1), pp. 104–114. doi: 10.1016/j.ijpharm.2010.11.048.

Sakr, W. F. *et al.* (2012) 'Upgrading wet granulation monitoring from hand squeeze test to mixing torque rheometry', *Saudi Pharmaceutical Journal*. King Saud University, 20(1), pp. 9–19. doi: 10.1016/j.jsps.2011.04.007.

Scurati, A., Feke, D. L. and Manas-Zloczower, I. (2005) 'Analysis of the kinetics of agglomerate erosion in simple shear flows', *Chemical Engineering Science*, 60(23), pp. 6564–6573. doi: 10.1016/j.ces.2005.05.059.

Seager, R. J. *et al.* (2018) 'Solid dissolution in a fluid solvent is characterized by the interplay of surface area-dependent diffusion and physical fragmentation', *Scientific Reports*. Springer US, 8(1), pp. 1–17. doi: 10.1038/s41598-018-25821-x.

Seem, T. C. *et al.* (2015) 'Twin screw granulation - A literature review', *Powder Technology*. Elsevier B.V., 276, pp. 89–102. doi: 10.1016/j.powtec.2015.01.075.

Shi, L., Feng, Y. and Sun, C. C. (2011) 'Massing in high shear wet granulation can simultaneously improve powder flow and deteriorate powder compaction: A double-edged sword', *European Journal of Pharmaceutical Sciences*. Elsevier B.V., 43(1–2), pp. 50–56. doi: 10.1016/j.ejps.2011.03.009.

Siepmann, J. and Peppas, N. A. (2011) 'Higuchi equation: Derivation, applications, use and misuse', *International Journal of Pharmaceutics*. Elsevier B.V., 418(1), pp. 6–12. doi: 10.1016/j.ijpharm.2011.03.051.

Siepmann, J. and Siepmann, F. (2013) 'Mathematical modeling of drug dissolution', *International Journal of Pharmaceutics*. Elsevier B.V., 453(1), pp. 12–24. doi: 10.1016/j.ijpharm.2013.04.044.

Sinko, P. J. (2013) 'Coarse dispersions', *Martin's Physical Pharmacy and Pharmaceutical Sciences: Physical Chemical and Biopharmaceutical Principles in the Pharmaceutical Sciences: Sixth Edition*, pp. 410–441.

Smith, B. T. (2016) 'Remington Education: Physical Pharmacy', *Physical Pharmacy*, pp. 31–50. Available at: https://www.pharmpress.com/files/docs/remington-education-physical-pharmacy-sample-chapter-3.pdf%0Awww.pharmpress.com.

Smrčka, D., Dohnal, J. and Štěpánek, F. (2016) 'Dissolution and disintegration kinetics of high-

active pharmaceutical granules produced at laboratory and manufacturing scale', *European Journal of Pharmaceutics and Biopharmaceutics*, 106, pp. 107–116. doi: 10.1016/j.ejpb.2016.04.005.

Sondej, F. *et al.* (2015) 'Investigation of coating layer morphology by micro-computed X-ray tomography', *Powder Technology*. Elsevier B.V., 273, pp. 165–175. doi: 10.1016/j.powtec.2014.12.050.

Soundaranathan, M. *et al.* (2020) 'Quantification of swelling characteristics of pharmaceutical particles', *International Journal of Pharmaceutics*. Elsevier B.V., 590(September), p. 119903. doi: 10.1016/j.ijpharm.2020.119903.

Swarbrick, J. *et al.* (2005) 'Handbook of Pharmaceutical Granulation Technology', *Handbook of Pharmaceutical Granulation Technology*. doi: 10.1201/9780849354953.

Sweijen, T. *et al.* (2017) 'Grain-scale modelling of swelling granular materials; application to super absorbent polymers', *Powder Technology*. The Author(s), 318, pp. 411–422. doi: 10.1016/j.powtec.2017.06.015.

Tardos, G. I., Khan, M. I. and Mort, P. R. (1997) 'Critical parameters and limiting conditions in binder granulation of fine powders', *Powder Technology*, 94(3), pp. 245–258. doi: 10.1016/S0032-5910(97)03321-4.

Thapa, P. *et al.* (2019) 'Effects of granulation process variables on the physical properties of dosage forms by combination of experimental design and principal component analysis', *Asian Journal of Pharmaceutical Sciences*. Elsevier B.V., 14(3), pp. 287–304. doi: 10.1016/j.ajps.2018.08.006.

Tu, W. Da, Ingram, A. and Seville, J. (2013) 'Regime map development for continuous twin screw granulation', *Chemical Engineering Science*. Elsevier, 87, pp. 315–326. doi: 10.1016/j.ces.2012.08.015.

van den Ban, S. and Goodwin, D. J. (2017) 'The Impact of Granule Density on Tabletting and Pharmaceutical Product Performance', *Pharmaceutical Research*. Pharmaceutical Research, 34(5), pp. 1002–1011. doi: 10.1007/s11095-017-2115-5.

Vonk, P. *et al.* (1997) 'Growth mechanisms of high-shear pelletisation', *International Journal*

of Pharmaceutics, 157(1), pp. 93–102. doi: 10.1016/S0378-5173(97)00232-9.

Wade, J. B., Martin, G. P. and Long, D. F. (2015) 'An assessment of powder pycnometry as a means of determining granule porosity', *Pharmaceutical Development and Technology*. Taylor & Francis, 20(3), pp. 257–265. doi: 10.3109/10837450.2013.860550.

Wang, J. and Flanagan, D. R. (1999) 'General solution for diffusion-controlled dissolution of spherical particles. 1. Theory', *Journal of Pharmaceutical Sciences*, 88(7), pp. 731–738. doi: 10.1021/js980236p.

Weatherley, S. *et al.* (2013) 'Hot-melt granulation in a twin screw extruder: Effects of processing on formulations with caffeine and ibuprofen', *Journal of Pharmaceutical Sciences*, 102(12), pp. 4330–4336. doi: 10.1002/jps.23739.

Yassin, S. *et al.* (2015) 'The Disintegration Process in Microcrystalline Cellulose Based Tablets, Part 1: Influence of Temperature, Porosity and Superdisintegrants', *Journal of Pharmaceutical Sciences*. Elsevier Masson SAS, 104(10), pp. 3440–3450. doi: 10.1002/jps.24544.

Appendix

Appendix A

MCC and ground aspirin size fractions were measured in a Malvern mastersizer 3000.

Table A.1: Volume density of each size classes for MCC

Size Classes (μm)	Volume Density (%)
0.011	0
0.012	0
0.014	0
0.016	0
0.018	0
0.020	0
0.022	0
0.026	0
0.030	0
0.034	0
0.038	0
0.043	0
0.049	0
0.056	0
0.063	0
0.072	0
0.082	0
0.093	0
0.106	0
0.121	0
0.137	0
0.155	0
0.178	0
0.201	0
0.228	0
0.259	0
0.294	0
0.334	0
0.380	0
0.432	0
0.490	0
0.558	0
0.634	0
0.719	0
0.818	0
0.929	0

1.055	0
1.199	0
1.363	0
1.548	0
1.759	0
1.999	0
2.271	0
2.580	0
2.932	0
3.330	0
3.784	0.0001
4.299	0.009
4.885	0.097
5.550	0.162
6.306	0.250
7.165	0.374
8.140	0.540
9.249	0.749
10.51	1.003
11.94	1.300
13.56	1.636
15.41	2.005
17.51	2.405
19.89	2.830
22.60	3.281
25.68	3.757
29.18	4.260
33.15	4.787
37.66	5.333
42.79	5.884
48.61	6.416
55.24	6.895
62.76	7.280
71.30	7.528
81.01	7.598
92.05	7.466
104.58	7.121
118.82	6.572
134.99	5.844
153.38	4.978
174.26	4.027
197.99	3.055
224.95	2.134
255.58	1.334
290.38	0.712
329.92	0.288
374.84	0.024
425.88	0.001

483.87	0
549.76	0
624.62	0
709.67	0
806.30	0
916.09	0
1040.83	0
1182.55	0
1343.57	0
1526.52	0
1734.38	0
1970.53	0
2238.85	0
2543.70	0
2890.06	0
3283.58	0

Table A.2: Volume density of each size classes for aspirin

Size Classes (μm)	Volume Density (%)
0.011	0
0.012	0
0.013	0
0.015	0
0.017	0
0.020	0
0.022	0
0.026	0
0.029	0
0.033	0
0.038	0
0.043	0
0.049	0
0.056	0
0.063	0
0.072	0
0.082	0
0.093	0
0.106	0
0.120	0
0.136	0
0.155	0
0.176	0
0.200	0.0004
0.228	0.0072
0.259	0.073
0.294	0.087

0.334	0.093
0.380	0.098
0.432	0.101
0.490	0.103
0.557	0.105
0.633	0.107
0.719	0.110
0.817	0.115
0.929	0.124
1.05	0.137
1.20	0.158
1.36	0.186
1.54	0.225
1.75	0.274
1.99	0.337
2.27	0.415
2.58	0.508
2.93	0.620
3.33	0.752
3.78	0.904
4.29	1.07
4.88	1.26
5.55	1.47
6.30	1.69
7.16	1.92
8.14	2.16
9.24	2.40
10.50	2.63
11.93	2.86
13.56	3.07
15.41	3.28
17.50	3.48
19.89	3.67
22.60	3.85
25.68	4.02
29.17	4.19
33.14	4.35
37.66	4.50
42.79	4.64
48.61	4.77
55.23	4.87
62.76	4.95
71.31	4.98
81.01	4.96
92.04	4.88
104.58	4.73
118.82	4.51
134.99	4.21

153.38	3.823
174.26	3.332
197.99	2.756
224.95	2.123
255.58	1.481
290.38	0.885
329.92	0.319
374.84	0.025
425.88	0.003
483.87	0
549.76	0
624.62	0
709.67	0
806.30	0
916.09	0
1040.83	0
1182.55	0
1343.55	0
1526.52	0
1734.38	0
1970.53	0
2238.85	0
2543.70	0
2890.06	0
3283.58	0

Appendix B granule porosity data

Table B.1: Pycnometry porosity data

Granule	Granulation time	True density g/cm³	Envelope density g/cm³	Porosity	% porosity	Mean	St deviation
0.8 L/S	5 min	1.53	0.66	0.56	56.72		
0.8 L/S	5 min	1.52	0.71	0.52	52.86	53.60	2.82
0.8 L/S	5 min	1.54	0.75	0.51	51.22		
1.0 L/S	5 min	1.50	1.11	0.26	26.17		
1.0 L/S	5 min	1.52	1.18	0.22	22.29	22.16	4.07
1.0 L/S	5 min	1.49	1.22	0.18	18.02		
1.2 L/S	5 min	1.50	1.30	0.13	13.48		
1.2 L/S	5 min	1.50	1.21	0.18	18.97	18.32	4.55
1.2 L/S	5 min	1.50	1.16	0.22	22.51		
1.2 L/S	2.5 min	1.51	1.16	0.22	22.94		
1.2L/S	2.5 min	1.46	1.05	0.28	28.27	26.30	2.92
1.2 L/S	2.5 min	1.47	1.06	0.27	27.70		
1.2 L/S	10 min	1.47	1.20	0.18	18.55		
1.2 L/S	10 min	1.46	1.16	0.20	20.88	19.74	1.16
1.2 L/S	10 min	1.47	1.18	0.19	19.79		

Table B.2: MIP porosity data

Granule	Granulation time	Porosity	Mean	St deviation
0.8 L/S	5 min	62.76		
		63.02	62.45	0.77
		61.56		
1.0 L/S	5 min	38.21		
		39.99	39.94	1.26
		41.62		
1.2 L/S	5 min	26.55		
		24.53	25.67	1.03
		25.94		
1.2 L/S	2.5 min	41.09		
		41.41	40.65	1.04
		39.45		
1.2 L/S	10 min	32.19		
		30.24	31.35	0.99
		31.60		

Table B.3: XRCT porosity data

Granule	Granulation time	Porosity	Mean	St deviation
0.8 L/S	5 min	61.58		
		61.57	62.32	1.29
		63.81		
1.0 L/S	5 min	40.17		
		39.72	39.53	0.74
		38.72		
1.2 L/S	5 min	25.06		
		24.95	25.17	0.29
		25.51		
1.2 L/S	2.5 min	38.99		
		37.02	38.15	1.01
		38.44		
1.2 L/S	10 min	33.05		
		31.36	32.35	0.88
		32.64		

Appendix C Aspirin release data

Table C.1: Aspirin release data of different L/S ratio granules (First 5 min)

Time/min	0.8 L/S granules	St deviation	1.0 L/S granules	St deviation	1.2 L/S granules	St deviation
0	0	0	0	0	0	0
0.16	54.13	13.01	20.92	1.13	19.84	2.88
0.33	58.15	9.58	21.70	0.35	19.84	2.88
0.5	67.64	2.15	22.46	1.75	20.25	2.34
0.66	73.71	5.02	25.25	3.76	21.78	2.31
0.83	73.90	2.89	26.04	2.20	21.27	1.78
1	73.80	5.47	27.32	2.59	21.52	1.78
1.16	75.57	4.28	28.86	2.56	23.81	1.18
1.33	80.26	6.04	29.10	4.01	23.04	4.98
1.5	80.65	4.33	29.63	2.39	24.34	0.11
1.66	80.61	1.28	32.67	5.28	25.09	1.17
1.83	80.62	0.90	36.30	2.84	24.84	2.80
2	82.18	2.68	36.83	1.67	24.34	1.20
2.16	83.43	3.61	38.91	1.24	25.61	3.33
2.33	83.68	3.21	39.40	1.31	25.10	2.80
2.5	83.39	0.57	39.43	1.38	26.37	1.70
2.66	83.37	3.21	39.92	0.41	25.34	3.86
2.83	83.24	3.46	40.18	1.24	26.12	1.70
3	82.55	1.85	42.19	3.43	29.19	5.89
3.16	82.32	1.07	39.10	5.14	29.15	1.62
3.33	82.89	1.07	39.37	4.01	29.15	1.62
3.5	82.13	1.67	41.15	4.93	34.49	0.10
3.66	82.26	0.51	40.67	3.17	37.26	4.14
3.83	80.39	1.26	42.71	3.06	37.52	5.21
4	82.64	2.01	43.74	3.87	38.77	11.12
4.16	80.90	1.84	45.82	1.81	38.54	6.29
4.33	80.99	1.88	45.57	1.41	41.2	9.48
4.5	80.00	2.65	45.31	2.23	39.83	4.12
4.66	80.32	3.19	45.82	1.81	39.05	7.90
4.83	80.82	2.94	46.32	2.95	39.07	6.84
5	80.45	2.05	48.10	3.48	40.58	8.95

Table C.2: Aspirin release data of different L/S ratio granules (5 hrs)

Time/min	0.8 L/S granules	St deviation	1.0 L/S granules	St deviation	1.2 L/S granules	St deviation
5	80.45	2.05	48.10	3.48	40.58	8.95
10	85.46	3.70	55.01	5.70	44.94	1.34
15	87.10	5.19	62.45	5.71	47.48	0.21
20	87.10	5.19	67.57	6.65	50.83	2.50
25	86.04	3.28	74.28	3.21	55.40	0.97
30	86.78	5.24	75.29	5.23	57.70	0.46
35	88.61	5.09	78.94	2.50	61.51	1.08
40	89.75	6.03	79.45	1.68	63.81	0.51
45	89.49	6.47	81.49	2.97	65.86	0.48
50	89.99	7.03	84.28	4.17	66.87	2.08
55	92.29	5.54	88.36	6.39	67.92	0.05
60	95.93	0.41	91.95	6.40	68.95	0.59
90	98.63	1.59	95.32	4.36	77.88	3.97
120	98.64	1.60	96.36	3.25	85.23	1.99
150	98.48	1.98	98.43	1.57	89.27	3.29
180	98.43	2.71	99.73	0.45	90.82	3.29
210	99.68	0.54	100	0	97.43	2.87
240	99.37	1.08	100	0	98.96	0
270	99.37	1.08	100	0	100	0
300	100	0	100	0	100	0

Table C.3: Aspirin release data of different granulation time granules (First 5 min)

Time/min	2.5 min granules	St deviation	5 min granules	St deviation	10 min granules	St deviation
0	0	0	0	0	0	0
0.16	27.48	1.42	19.87	2.88	18.75	2.88
0.33	28.32	4.50	19.87	2.88	18.45	3.68
0.5	29.45	5.71	20.26	2.34	18.69	4.02
0.66	29.01	6.26	21.78	2.31	20.25	1.66
0.83	30.01	5.61	21.40	1.78	20.10	4.96
1	30.04	5.34	21.40	1.78	22.21	2.34
1.16	32.65	5.48	24.82	1.18	22.02	3.04
1.33	30.72	5.50	22.89	4.98	22.71	4.26
1.5	31.13	7.40	24.83	0.11	22.24	4.69
1.66	32.19	6.04	25.58	1.17	23.42	4.91
1.83	31.12	5.11	24.43	2.80	24.17	5.50
2	33.95	9.58	24.06	1.20	24.19	6.76
2.16	34.58	8.31	24.81	3.33	25.89	5.28
2.33	35.05	8.93	24.43	2.80	24.85	6.27
2.5	36.89	7.27	25.96	1.70	25.89	5.89
2.66	37.68	11.15	25.18	3.86	27.56	4.75
2.83	37.49	10.18	25.96	1.70	27.76	5.09
3	38.16	10.52	30.58	5.89	28.22	5.20
3.16	38.58	6.58	30.52	1.62	29.45	4.62
3.33	38.80	6.71	30.52	1.62	29.68	4.84
3.5	40.93	9.13	37.75	0.10	31.58	6.47
3.66	41.33	10.19	40.76	4.14	31.32	6.93
3.83	40.79	8.15	40.75	5.21	32.60	6.04
4	50.77	16.45	41.08	11.12	32.93	4.51
4.16	50.18	13.83	40.74	6.29	35.13	5.14
4.33	53.05	14.95	42.23	9.48	34.48	5.14
4.5	51.95	13.53	41.52	4.12	35.36	4.27
4.66	48.20	11.98	40.34	7.90	35.89	3.36
4.83	52.08	11.91	39.59	6.84	38.38	9.01
5	53.42	8.41	41.86	8.95	42.97	10.91

Table C.4: Aspirin release from different granulation time granules (5 hrs)

Time/min	2.5 min granules	St deviation	5 min granules	St deviation	10 min granules	St deviation
5	53.42	5.59	41.86	8.95	42.97	10.91
10	60.58	4.54	47.24	1.34	51.60	4.54
15	73.21	4.62	50.29	0.21	58.16	5.82
20	83.32	0.64	52.21	2.50	63.11	5.45
25	82.67	2.29	57.14	0.97	68.16	5.69
30	87.37	3.57	59.03	0.46	71.09	5.77
35	89.97	2.80	62.44	1.08	77.54	8.83
40	94.25	2.24	64.34	0.51	81.51	4.74
45	94.88	1.01	65.86	0.48	82.69	4.44
50	94.89	1.56	66.99	2.08	83.19	4.55
55	95.31	1.20	66.25	0.05	85.68	4.24
60	98.06	2.80	66.63	0.59	86.47	5.64
90	97.62	2.60	75.78	3.97	90.32	6.49
120	99.34	0.64	85.64	1.99	96.08	1.70
150	99.57	0.74	90.15	3.29	97.13	3.65
180	99.57	0.37	90.15	3.29	97.83	2.49
210	100	0.00	97.96	2.87	97.60	2.87
240	100	0.00	100	0	99.53	0.80
270	100	0.00	100	0	100	0
300	100	0.00	100	0	100	0

Appendix D Single granule swelling

Table D.1: The swelling rate of different L/S ratio granules

Time/min	0.8 L/S granules	St deviation	1.0 L/S granules	St deviation	1.2 L/S granules	St deviation
0	0	0	0	0	0	0
0.16	44.55	14.21	4.32	2.87	1.17	0.86
0.33	54.89	20.64	12.49	6.81	2.69	0.48
0.5	59.16	21.42	16.76	4.71	3.51	0.49
0.66	60.40	21.80	19.34	5.16	3.83	0.31
0.83	61.20	22.20	21.50	3.73	4.61	0.59
1	62.64	23.65	23.61	4.49	7.77	4.25
2	63.75	24.54	31.00	4.21	13.21	7.33
3	68.06	23.06	35.85	6.95	16.03	6.01
4	69.88	21.84	40.70	6.99	17.70	6.41
5	81.81	20.40	43.37	8.05	27.02	7.43
6	82.89	19.03	44.53	8.79	28.57	7.12
7	89.13	12.30	46.50	9.60	29.39	6.65
8	89.49	11.84	49.23	10.58	31.98	8.81
9	92.51	12.27	53.21	12.91	32.43	8.57
10	93.49	10.76	54.63	13.08	38.04	6.37
20	96.66	5.77	68.46	16.75	47.62	14.20
30	97.13	4.96	85.52	7.08	63.26	8.44
40	98.30	2.93	92.45	3.40	71.17	3.35
50	98.58	2.44	95.50	2.55	81.99	3.05
60	99.58	0.72	97.30	2.53	90.10	3.45
70	99.71	0.48	97.87	2.41	92.93	5.01
80	99.71	0.48	99.58	0.69	95.93	4.52
90	99.83	0.28	99.98	0.01	97.07	5.05
100	100	0	100	0	97.22	4.80
110	100	0	100	0	97.35	4.58
120	100	0	100	0	97.81	3.77
130	100	0	100	0	99.02	1.68
140	100	0	100	0	100	0

Table D.2: The swelling rate of different granulation time granules

Time/min	2.5 min granules	St deviation	5 min granules	St deviation	10 min granules	St deviation
0	0	0	0	0	0	0
0.16	3.28	0.84	1.17	0.86	11.46	14.56
0.33	5.67	2.30	2.69	0.48	14.01	13.43
0.5	6.90	3.40	3.51	0.49	16.31	12.62
0.66	7.73	4.53	3.83	0.31	18.18	12.68
0.83	8.12	4.13	4.61	0.59	20.38	12.91
1	9.32	4.04	7.77	4.25	21.74	12.78
2	13.67	5.21	13.21	7.33	29.01	13.06
3	21.02	12.78	16.03	6.01	34.01	12.10
4	24.91	13.82	17.70	6.41	42.06	7.38
5	29.12	11.63	27.02	7.43	44.94	7.37
6	30.45	13.17	28.57	7.12	47.15	8.26
7	33.67	10.61	29.39	6.65	49.70	8.40
8	34.89	9.95	31.98	8.81	51.19	8.21
9	37.90	7.02	32.43	8.51	53.08	8.33
10	42.27	8.35	38.04	6.37	59.37	11.01
20	53.14	1.85	47.62	14.20	71.17	8.57
30	68.73	7.22	63.26	8.44	79.36	13.69
40	83.83	10.47	71.17	3.35	85.51	13.46
50	96.49	3.98	81.99	3.05	88.10	12.27
60	99.83	0.28	90.10	3.45	90.49	13.41
70	100	0	92.93	5.01	92.04	12.59
80	100	0	95.93	4.52	95.28	8.16
90	100	0	97.07	5.05	100	0
100	100	0	97.22	4.80	100	0
110	100	0	97.35	4.58	100	0
120	100	0	97.81	3.77	100	0
130	100	0	99.02	1.68	100	0
140	100	0	100	0	100	0